# Higher order QCD radiative corrections to processes at the Large Hadron Collider

by

**Anurag Tripathi**

**Harish Chandra Research Institute, Allahabad**

A Thesis submitted to the
Board of Studies in Physical Science Discipline
in partial fulfillment of requirements
for the degree of

**DOCTOR OF PHILOSOPHY**
**of**
**Homi Bhabha National Institute**

August, 2009

# Certificate

This is to certify that the Ph.D. thesis titled **Higher order QCD radiative corrections to processes at the Large Hadron Collider** submitted by Anurag Tripathi for the award of the degree of Doctor of Philosophy is a record of bona fide research work done under my supervision. It is further certified that the thesis represents independent work by the candidate and collaboration was necessitated by the nature and scope of the problems dealt with.

Date: August 2009

**Prof. V. Ravindran**

Thesis Adviser

# Declaration

This thesis is a presentation of my original research work. Whenever contributions of others are involved, every effort is made to indicate this clearly, with due reference to the literature and acknowledgement of collaborative research and discussions.

The work is original and has not been submitted earlier as a whole or in part for a degree or diploma at this or any other Institution or University.

This work was done under guidance of Professor V. Ravindran, at Harish Chandra Research Institute, Allahabad.

Date: August 2009

**Anurag Tripathi**

Ph.D. Candidate

**To my wife Neelima**

# Acknowledgments

Completion of my thesis gives me a satisfaction and makes me eager to look further. Every piece of work done by an individual is a result of direct or indirect support and help of many others. Who else would be most important of them if not Ravi -my supervisor? I hardly ever thanked him and Bhuvna for anything, now also I will not as I never thanked my parents for anything.

Without the collaboration of Prakash Mathews and M.C. Kumar the projects carried out during my Ph.D. would not have finished. I am thankful to them for their extremely useful collaboration. Simplicity of my collaborators is adorable.

I learned a lot from my teachers at HRI and would like to express my gratitude towards them.

I would also like to acknowledge the use of High Performance Scientific Computing facility at the Harish-Chandra Research Institute, Allahabad, India.

I spent a good amount of time discussing physics and life in general with my friend Sanil. I am thankful to nature for giving me such a friend. I am fortunate to have Umashankar and Payal as my friends who have been a big support, and Andreas who is an immense source of knowledge and a good human being.

Life makes sense and is beautiful because of my parents, brother Rinku, sister Pinki, loving wife Neelima, mother and father-in-law, Ankur, Ruchika, Divya and Neha. I remain in debt for their love and support.

# Synopsis

The standard model has been extremely successful in explaining the phenomena occurring at very small length scales or equivalently at high energies. In this model $SU(2) \times U(1)$ is broken spontaneously by introducing a fundamental scalar field. The remnant of symmetry breaking is a scalar Higgs boson which remains elusive to this date. The nature of symmetry breaking is not yet clear; it is not known whether symmetry breaking occurs through a fundamental field or through some other mechanism. The upcoming Large Hadron Collider (LHC) has, as its one of main aims, the discovery of mechanism of spontaneous symmetry breaking. Even if the symmetry breaking occurs the way the SM predicts, there remain issues which need to be addressed. One of the problems arises because of the large hierarchy between the electroweak scale ($\sim$ TeV) and the Planck scale $M_{Pl}$ ($\sim 10^{19}$) GeV. As Higgs boson is a scalar particle its mass gets quadratic radiative corrections. If the SM is assumed to be valid upto the Planck scale, the Higgs mass gets corrections of the order $M_{Pl}$. This amounts to a large amount of fine-tuning in the bare Higgs mass so that the physical mass is at the electroweak scale. This is the fine-tuning or naturalness problem.

There were many proposals to cure this problem, one of the most popular being the Supersymmetric scenario. Another interesting idea was proposed by Arkani-Hamed, Dimopolous and Dvali in 1998 which created lot of activity in this field. The proposal is to introduce extra spatial dimensions, and assume that the Plank scale $M_s$ in extradimensional world is of the order of electroweak scale, that is there is only one fundamental scale in the theory, thereby removing the hierarchy between the two scales. The effective Planck scale in 4-dimensions still remains $M_{Pl}$. This is how hierarchy problem can be solved. In this model the SM fields are localized on a 3-brane and gravity naturally propagates in all dimensions. Gravity appears as Kaluza-Klein excitations and couples to the SM fields and produces deviations to the predictions of SM. This exciting possibility of extra dimensions can be tested through the effects of gravity on the SM fields.

There are other interesting possibilities as well which do not address the problems of the SM but are interesting in their own right. One such possibility is of the scale invariant degrees of freedom coupling to the SM fields at low energies. In this model, proposed recently by Georgi, it is assumed that at very high energies the SM field couple weakly to a hidden sector through exchange of heavy particles. This sector is proposed to have an infrared fixed point. Near the fixed point the fields in the hidden sector become scale invariant and hence are called unparticles. These unparticles can couple to the SM fields to give observable deviations from the SM predictions.

The upcoming LHC will achieve high energies never achieved before in any collider. Signals of new physics could be observed through the deviations they produce in the SM predictions. There are many important channels which can be used as a probe, such as, di-lepton, di-jet productions, or production of photon pairs. Photon pairs serve as an important probe in new physics searches as this is a clean channel with no difficulties associated with reconstruction. We have used this channel as a tool in search studies of new physics at the LHC.

As LHC is a hadron collider, QCD plays an extremely important role in any physics study. Not only QCD gives large backgrounds to signals it also gives important contributions through radiative corrections as the strong coupling constant is not very small. The other feature of theoretical predictions at the LHC is their sensitivity to factorization scale $\mu_F$ which is largely arbitrary. At leading order $\mu_F$ enters through the parton distribution functions. As the LHC detectors ATLAS and CMS will measure the photon production rates very precisely it is important to have an accurate prediction from theory side. Inclusion of next-to-leading order QCD corrections brings down the sensitivity to $\mu_F$ , these corrections are important. With these aims we have studied production of photon pairs at the LHC in large extra dimension model by Arkani-Hamed, Dimopoulos and Dvali and in unparticle model.

The final state photons are subject to various kinematical cuts used by ATLAS and CMS detectors. Also many kinematical distributions need to be evaluated to compare against the experimental data. For these requirements Monte Carlo methods prove to be very powerful. To this effect, we used the semi-numerical method of *two cutoff phase space slicing* for our next-to-leading order computation.

A next-to-leading order computation involves, in addition to born contributions, virtual corrections and contributions from real emission processes. A soft gluon in a loop or in final state gives rise to soft divergences. Similarly two collinear massless partons give collinear singularities. We used dimensional regularization with $n = 4+\epsilon$ to separate these singularities as poles in $\epsilon$. The complicated tensor integrals appearing in virtual diagrams were simplified using Passarino-Veltman reduction. Although the soft singularities cancel between virtual and real emission contributions, the collinear singularities do not cancel completely and are absorbed into bare parton distribution functions. We arrange for the cancellation/ absorption of these singularities analytically in $\overline{MS}$ scheme using the two cutoff phase space slicing method.

This method introduces two small dimensionless parameters $\delta_s$ and $\delta_c$ to divide the phase-space into *soft* and *hard* regions. The part of phase-space where the energy of the gluon is soft is defined as *soft* and the region complementary to it is *hard*. For small values of $\delta_s$ the matrix elements can be simplified and integrated over the soft region to give a $\delta_s$ dependent, order $\alpha_s$, 2-body contribution $d\sigma_S(\delta_s, \epsilon)$. This contains the poles in $\epsilon$ arising from the soft singularities. The hard region can be further divided into collinear and non-collinear regions using another small dimensionless slicing parameter $\delta_c$. The part of phase-space in which the final state parton is collinear to the incoming parton is defined as collinear region and gives an order $\alpha_s$ contribution $d\sigma_{HC}(\delta_s, \delta_c, \epsilon)$. The hard non-collinear 3-body contribution denoted by $d\sigma_{\overline{HC}}(\delta_s, \delta_s)$ is free of any QCD singularities and can be evaluated numerically using Monte Carlo integration. The collinear singularities appearing in $d\sigma_{HC}(\delta_s, \delta_c, \epsilon)$ are removed by mass factorization in $\overline{MS}$ scheme by adding appropriate counter terms to give $d\sigma_{HC+CT}(\delta_s, \delta_c, \epsilon)$. The sum of 2-body and 3-body contributions is independent of the slicing parameters $\delta_s$ and $\delta_c$.

In addition to the above divergences, QED singularities appear in final state in real emission contributions when a fermion becomes collinear to one of the final state photons. These singularities can be removed by absorbing them into fragmentation functions. Fragmentation functions arise because of the processes where the final state photons are produced through the fragmentation of partons into photons. However the fragmentation functions are not known to a good accuracy. An alternative to avoid the final state QED singularity and simultaneously suppress the fragmentation photons in an infrared safe manner is to use the smooth cone isolation prescription advocated by Frixione. We used this isolation criterion to completely remove the fragmentation contributions.

We developed a Monte Carlo based code on the two cutoff slicing method to implement the experimental cuts and the smooth cone isolation criterion. The code uses Monte Carlo integrator *VEGAS* to do the phase space integrals numerically. This code was subject to various crucial test to check its reliability. To this end, it was found that the sum of 2-body and 3-body contributions were fairly stable under variations of slicing parameters $\delta_s$ and $\delta_c$. Also the SM results were reproduced to check the correctness of the code and our matrix elements. Using our code various important kinematical distributions such as invariant mass, rapidity, $p_T$, etc., distributions were obtained. These distributions are important as these will be measured at the LHC. We found that the QCD corrections give significant enhancement over the leading order predictions in all the kinematical distributions. By our computations we were able to show a significant reduction in the sensitivity to the factorization scale $\mu_F$, which makes the new theoretical predictions quite precise.

# List of Publications

1. Unparticle physics in diphoton production at the CERN LHC.
   Authors: M. C. Kumar, Prakash Mathews, V. Ravindran and Anurag Tripathi.
   **Ref: Phys. Lett. B 672 (2009) 45. Arxiv : 0811.1670 [hep-ph]**.

2. Diphoton signals in theories with large extra dimensions to NLO QCD at hadron colliders.
   Authors: M. C. Kumar, Prakash Mathews, V. Ravindran and Anurag Tripathi.
   **Ref: Phys. Lett. B 672 (2009) 45. Arxiv : 0811.1670 [hep-ph]**.

3. Unparticles in diphoton production to next-to-leading order in QCD at the LHC
   Authors: M. C. Kumar, Prakash Mathews, V. Ravindran and Anurag Tripathi.
   **Ref: Phys. Rev. D 79 (2009) 075012. Arxiv : 0804.4054 [hep-ph]**

# Contents


## I Introduction 1

**1 Introduction** **3**

**2 Models** **7**

2.1 ADD model . . . . . . . . . . 7

2.2 Unparticle Physics . . . . . . . . . . 11

**3 QCD** **17**

3.1 QCD Lagrangian . . . . . . . . . . 17

3.2 Renormalization Group . . . . . . . . . . 19

3.3 Parton Model and Factorization . . . . . . . . . . 21

3.4 Scale uncertainties . . . . . . . . . . 24

## II Isolated Direct Photon Pair Production at the Large Hadron Collider 27

**4 Isolated direct photon pair production at NLO** **29**

4.1 Isolated direct photons . . . . . . . . . . 29

4.2 Leading Order . . . . . . . . . . 31

4.3 Next-to-leading order . . . . . . . . . . 33

4.3.1 Virtual . . . . . . . . . . 33

4.3.2 Real Emission . . . . . . . . . . 39

4.4 Phase Space . . . . . . . . . . 51

4.4.1 Conversion factor . . . . . . . . . . 55

**5 Results and Conclusions** **57**

5.1 $PP \to \gamma\gamma$ with scalar unparticles . . . 58
5.2 $PP \to \gamma\gamma$ in ADD and unparticle model . . . 60
5.2.1 Large extra dimension model . . . 61
5.2.2 Tensor unparticles . . . 63

**6 Summary and conclusions** **81**

**7 Appendix** **83**
7.1 Feynman rules and diagrams . . . 83
7.2 Area of a unit sphere in $n$ dimensions . . . 90
7.3 Dilogarithm and its properties . . . 91
7.4 Gamma function $\Gamma(x)$ . . . 92
7.5 Casimir invariants of SU(N) algebra . . . 93
7.6 Integrals . . . 93

# List of Figures


2.1 Integration contour used in the integral in eq. 2.2 . . . . . . . . . . . . . . 13

3.1 evolution of strong coupling constant with scale . . . . . . . . . . . . . . . . 21

3.2 Leading order parton distribution functions . . . . . . . . . . . . . . . . . . . 23

3.3 Next-to-leading order parton distribution functions . . . . . . . . . . . . . . 24

5.1 The function $\chi_u^2$ showing its variation with the scaling dimension $d_u$ of the unparticle operator. . . . . . . . . . . . . . . . . . . . . . . . . . . . . . . . 59

5.2 Spin-0 unparticles: Invariant mass distribution for the choice $\Lambda_u = 1$ TeV and $\lambda_s = 0.9$. We imposed an angular cut $|\cos\ \theta_\gamma| < 0.8$ on the photons to suppress the SM background. Left panel: The contribution of the various sub processes with $d_u = 1.01$. Right panel: Variation with $d_u$. . . . . . . . 65

5.3 Spin-0 unparticles: Invariant mass distribution is plotted for various values of the coupling $\lambda_s$ for spin-0 with $\Lambda_u = 1$ TeV and $d_u = 1.01$, with an angular cut on the photons $|\cos\theta_\gamma| < 0.8$. . . . . . . . . . . . . . . . . . . . 66

5.4 Spin-0 unparticles: Angular distributions $d\sigma/d\cos\ \theta^*$ of the photons for spin-0 with $\Lambda_u = 1$ TeV and $d_u = 1.01$. We have taken couplings $\lambda_s = 0.6, 0.4$ integrating Q in the range 600 GeV $< Q < 0.9\Lambda_u$. . . . . . . . . . . 67

5.5 Spin-0 unparticles: Left Panel:$d\sigma/dY$ of the di-photon system. Right panel: $d\sigma/dy^\gamma$ of photons. $\Lambda_u = 1$ TeV and $d_u = 1.01$. We have taken the couplings to be $\lambda_s = 0.6, 0.4$ with Q in the region 600 GeV $< Q < 0.9\Lambda_u$. . 68

5.6 ADD: Stability of the order $\alpha_s$ contribution to the SM cross section against the variation of the slicing parameter $\delta_s$ (top), with $\delta_c = 10^{-5}$ fixed, in the invariant mass distribution of the di-photon. Below is shown the variation of the sum of 2-body and 3-body contributions over the range of $\delta_s$ considered and contrasted against the one at $\delta_s = 10^{-3}$. . . . . . . . . . . . 69

5.7 ADD: Stability of the order $\alpha_s$ contribution to the SM+ADD cross section against the variation of the slicing parameter $\delta_s$ (top), with $\delta_c = 10^{-5}$ fixed, in the invariant mass distribution of the di-photon with $M_S = 2$ TeV and $d = 3$. Below is shown the variation of the sum of 2-body and 3-body contributions over the range of $\delta_s$ considered and contrasted against the one at $\delta_s = 10^{-3}$. . . . . . . . . . . . . . . . . . . . . . . . . . . . 70

5.8 ADD: Invariant mass distribution of the di-photon production in the ADD model at the LHC. Both SM and the signal (SM+ADD) are presented at LO and NLO for $M_S = 2$ TeV and $d = 3$ in the left panel. Further the dependence of the cross sections on the scale $M_S$ in right panel has been shown to NLO in QCD. . . . . . . . . . . . . . . . . . . . . . . . . . . 71

5.9 ADD: Invariant mass distribution of the di-photon production in the ADD model at the LHC. The dependence of the cross sections on the number $d$ of extra dimensions is presented in the left panel and on the cut-off scale $\Lambda$ for the summation over virtual KK modes in the right panel to NLO in QCD. . . . . . . . . . . . . . . . . . . . . . . . . . . . . . . . . . . 72

5.10 ADD: Transverse momentum rapidity $d\sigma/dY$ (left) and $d\sigma/dQ_T$ (right) distributions of the di-photon production are presented in the ADD model with $M_S = 2$ TeV, $d = 3$ and by integrating over $Q$ in the range $600 < Q < 1100$ GeV. . . . . . . . . . . . . . . . . . . . . . . . . . . . . 73

5.11 ADD: Rapidity $d\sigma/dy^\gamma$ (left) and angular distributions $d\sigma/d\cos\theta^*$ (right) of the photons are presented in the ADD model with $M_S = 2$ and $d = 3$. Both of these distributions are obtained by integrating over the invariant mass of the di-photon in the range $600 < Q < 1100$ GeV. . . . . . . . . 74

5.12 ADD: Factorization scale dependency of the LO and NLO cross sections in the ADD model with $M_S = 2$ TeV and $d = 3$ for a scale variation of $Q/2 < \mu_F < 3Q/2$. For both the rapidity (left) and angular (right) distributions of the di-photon production, we have integrated over the invariant mass in the range $600 < Q < 1100$ GeV. . . . . . . . . . . . . . . . . . . . . . 75

5.13 Spin-2 unparticles: Plots showing stability of $d\sigma/dQ$ for the SM (left panel) and the SM+ UP (right panel) against $\delta_s$ variation with the choice of $\delta_c = 10^{-5}$. . . . . . . . . . . . . . . . . . . . . . . . . . . . . . . . 76

5.14 Spin-2 unparticles: Subprocess contributions in the SM and unparticle model in the invariant mass distribution at NLO for $400 < Q < 900$ GeV. . 77

5.15 Spin-2 unparticles: Plots showing invariant mass (left panel) and rapidity (right panel) distributions of the diphoton system with $d_u = 3.01$, $\Lambda_u = 1$ TeV and $\lambda_t = 0.9$. For rapidity distribution $Q$ is integrated in the range 600 GeV $< Q < 0.9\Lambda_u$. . . . . . . . . . . . . . . . . . . . . . . . . . 78

5.16 Spin-2 unparticles: Dependence on isolation parameters $E_T^{iso}$ (left panel) and $n$ (right panel) is shown in invariant mass distribution for the range $400 < Q < 900$ GeV. . . . . . . . . . 79

5.17 Spin-2 unparticles: Invariant mass distribution of the diphoton system (left panel) for $d_u > 4$ (conformal invariance) is contrasted with the $3 < d_u < 4$ (scale invariance). To LO in QCD and for $\Lambda_u = 2$ TeV (right panel), we have plotted the invariant mass distribution of the diphoton system for $d_u > 4$. . . . . . . . . . 80

7.1 Spin-0 unparticle vertices. . . . . . . . . . 83

7.2 Coupling of gravity (spin-2 unparticles) to SM fields. The functions $C_{\mu\nu,\rho\sigma}$, $D_{\mu\nu,\rho\sigma}(k_1, k_2)$, $E_{\mu\nu,\rho\sigma}(k_1, k_2)$, $F_{\mu\nu,\rho\sigma\lambda}(k_1, k_2, k_3)$, $G_{\mu\nu,\rho\sigma\lambda\delta}$ which appear in the Feynman rules are defined in the section 2.1 in the text. . . . . . . . . 85

7.3 Leading order diagram in SM. The diagram with the momenta of final state photons interchanged (which is not shown here) also contributes . . . . . . 86

7.4 Order $\alpha_s$ virtual diagrams in SM. The diagram with the momenta of final state photons interchanged (which is not shown here) also contribute. . . . 86

7.5 Order $\alpha_s$ real emission Feynman diagrams in SM. The diagram with the momenta of final state photons interchanged (which are not shown here) also contribute. . . . . . . . . . 87

7.6 LO gravity (spin-2 unparticle) mediated diagrams. . . . . . . . . . 88

7.7 Order $\alpha_s$ gravity (spin-2 unparticle) mediated virtual correction Feynman diagrams. . . . . . . . . . 88

7.8 Gravity (spin-2 unparticle) mediated real emission diagrams which contribute at NLO. . . . . . . . . . 89

7.9 Scalar diagrams. All the momenta are going into the diagrams . . . . . . . 94

# Part I

# Introduction

# Chapter 1

# Introduction

The standard model (SM) is one of the biggest achievements of $20^{\text{th}}$ century theoretical physics. It is a quantum field theory which encompasses three of the four forces of nature. Gravity is left out of this model. It is based on the direct product group $SU(3) \times SU(2) \times U(1)$. The $SU(2) \times U(1)$ component, also refered to as Glashow-Salam-Weinberg (GSW) model, describes the electromagnetic and weak forces of nature. The strong forces are described by $SU(3)$ gauge theory. The standard model has passed stringent quantitative experimental tests over the years and describes a plethora of phenomena in elementary physics that it has got the stature of *standard* model. The Higgs mechanism in SM through which the electroweak symmetry is spontaneously broken predicts a fundamental scalar particle, the Higgs boson [1],[2],[3], which remains elusive to this date, and a considerable effort would be devoted to discover this particle at the Large Hadron Collider (LHC). Despite its success, the SM leaves out many questions unanswered. Also it is plagued with fine-tuning and hierarchy problem which is related to Higgs boson as mass of a scalar particle is not protected by any symmetry against large radiative corrections. This will be briefly discussed in the next chapter. There we will see that this points towards some new physics beyond the standard model.

There are various new physics scenarios which address the fine-tuning and hierarchy problem. Supersymmetry and extra dimension models are among the popular new physics scenarios. Possibility of extra spatial dimensions in addition to the 3-spatial dimensions which we see offers a possible solution to hierarchy problem. In this thesis we will consider the proposal by Arkani-Hamed, Dimopolous and Dvali (ADD) [4, 5] that nature may have large extra dimensions which are compactified and have remained hidden. In addition to the models which propose to solve problems associated with the SM, there are also other interesting possibilities which have been explored. One such idea came from Georgi [6, 7, 9] recently where he introduced the idea of unparticles. This was motivated by early works of Banks and Zaks [10]. This model is based on the possibility of scale invariant degrees of freedom coupling weakly to SM fields at low energies. The scale invariance affords a great deal of simplification theoretically and can have phenomenological implications that can be tested in experiments.

The LHC is proton proton collider which will operate at a centre of mass energy of 14 TeV. Experiments at the LHC should shed light on the mechanism of electroweak symmetry breaking. It will search the Higgs boson, and measure its mass, production cross-sections, and branching ratios. Apart from its Higgs searches, experiments at the LHC will also be aimed to find signals of any new physics beyond the SM. There are many channels available at the LHC which can explore the signatures of new physics. These include, among other important channels, production of jet pairs, dileptons, diphoton. Diphoton production is a clean channel with no ambiguities associated with jet reconstruction etc. The ATLAS and CMS detectors at the LHC can carry out precise measurements of the energy and momentum of photons. This process has been extensively studied because of its importance in light mass Higgs boson searches. The standard model Higgs boson mass is bounded from above by precision electroweak measurements, $m_H \lesssim 192 - 230 GeV$ at 95% C.L [11, 12, 13]. The LHC will completely cover the low mass region preferred by precision electroweak fits as well as much higher masses. For $m_H < 140 GeV$, the most important mode involves production via gluon fusion, $gg \to H$, followed by decay into two photons, $H \to \gamma\gamma$ [14], [15]. However this mode has a very large continuum $\gamma\gamma$ background [16]. This background process $PP \to \gamma\gamma X$ proceeds at lowest order via the quark annihilation subprocess $q\bar{q} \to \gamma\gamma$. The next-to-leading order corrections to this subprocess have been incorporated into a number of Monte Carlo programs [17, 18, 19, 20, 21, 22, 23, 24, 25]. Beside this important motivation, this process deserves interest by its own. The production of such pairs of photons has been experimentally studied in a large domain of energies, from fixed targets [26, 27] to colliders [28, 29, 30]. A wide variety of observables has been measured, such as distributions of invariant mass, azimuthal angle and transverse momentum of the pairs of photons, inclusive transverse momentum distributions of each photon, which offer the opportunity to test our understanding of this process. We will use this relatively clean and extensively studied process in this thesis. Many studies have been carried out in the extra dimension models using these channels [31, 32, 33, 34, 35, 36, 37, 38, 39, 40] Next-to-leading order studies in dilepton channel were carried out in gravity models in [35, 36]. In [37] effects on diphoton production were studied for large extra dimension model ADD at the hadron colliders. This study was carried out at leading order in the strong coupling constant. As we discuss below, a leading order result at hadron colliders can at best serve as a first approximation due to the theoretical scale uncertainties it has. Also it is not appropriate to take a constant $K$ factor ($K$ factor is defined as the ratio of NLO cross section to LO cross section) as it depends on the value of kinematical invariants and also on the kinematical cuts. A calculation involving higher order radiative QCD effects improves the leading order results not only because it gives higher order terms but more importantly because it reduces the sensitivity to the factorization and renormalization scales. The reason why factorization scale enters in leading order calculation can be understood as follows. At the hadron colliders the incoming states which undergo scattering in a collision are partons ie., quarks and gluons. These partons emit other partons before they undergo a hard scattering. In an inclusive study we observe only the two photons in the final state and carry out a summation over all other final states. However, typically, there is no integration over the incoming quarks and gluons when we compute parton level cross sections. As the initial states which emit quarks and gluons are not integrated over, the collinear divergences which appear in the calculation do not get canceled with those appearing at virtual level. The configurations where two massless partons become parallel to each other give collinear divergences. These will be discussed in detail in later chapters. These divergences are removed by the procedure of mass factorization where these are absorbed into bare parton distribution functions (pdf) at a scale $\mu_F$ called the factorization scale. This introduces an arbitrary scale $\mu_F$ called factorization scale into the parton distribution functions. A leading order prediction is highly sensitive to the choice of $\mu_F$ and can at best be treated as a crude approximation of the quantity. As higher order QCD contributions are included in the calculation, the dependence on $\mu_F$ gets milder thereby improving theoretical predictions. This has been our main motivation to carry out a full next-to-leading order study. These corrections also give increments to leading order predictions as order $\alpha_s$ pieces are included. We also note here that the factorization scale $\mu_F$ does not appear in next-to-leading order calculations for $e^+e^-$ initial states and this is an issue when one or both of the colliding particles are hadrons such as at electron proton collider or hadron colliders.

In this thesis we will consider production of isolated direct photon pairs as probes to new physics. By direct photons it is meant that these do not result from the decay of $\pi^0, \eta, \omega$ at large transverse momentum. As discussed above leading order predictions are very sensitive to the choice of factorization and renormalization scales, and a next-to-leading order study considerably reduces these uncertainties. The aim of this thesis is to obtain precise predictions for diphoton production in ADD and unparticle models by carrying out a full next to leading order calculation. To facilitate comparison with experiments we will obtain many kinematical distributions using the experimental cuts. Many of the early and fully inclusive next-to-leading order studies were carried out analytically. However this is an inefficient method if many kinematic distributions are to be evaluated as it requires repetition of entire calculation. Moreover it is difficult to implement experimental and calorimetric constraints in a fully analytical study. For some observables it is difficult to calculate the appropriate Jacobian for the transformation from partonic to hadronic variables. In the above circumstances it is more appropriate to use semi-analytical methods based on Monte Carlo techniques. Two very useful techniques which are based on these methods are two cutoff phase space slicing method and dipole subtraction method. We have developed a Monte Carlo code based on two cutoff phase space slicing method. This code generates random partonic momentum configurations consistent with energy momentum and carries out phase space integrations numerically. Using this code , we can evaluate many kinematical distributions simultaneously and also easily implement various experimental kinematical constraints at the parton level.

This thesis proceeds as follows. In chapter 2 the ADD model and Unparticle model are briefly discussed and the Feynman rules are presented. In chapter 3 we summarize some basic facts of QCD which will be helpful for the following chapters. In chapter 4 we give in detail full next-to-leading order computation of isolated direct diphoton production and present the matrix elements. Here we employ the two cutoff phase space slicing method to separate the singular regions from the finite regions and carry out mass factorization. In chapter 5 we present various kinematical distributions obtained using our Monte Carlo code. We show significant reduction in scale uncertainty when higher order QCD corrections are included in the calculation.

# Chapter 2

# Models

## 2.1 ADD model

The standard model provides description of phenomena in particle physics to a very good accuracy. However it does not give answer to many questions, such as why there are three generations of quarks and leptons, what is the mechanism of symmetry breaking etc. There are reasons to belive that this may not be the complete story. One of the useful ideas to extend the standard model originates from the following observation. The three independent gauge couplings of $SU(3) \times SU(2) \times U(1)$ get very close to each other when they are extrapolated to very high energies using renormalization group evolution. The coupling constants of non-abelian part decrease with increase in energy because of the phenomenon of asymptotic freedom. The abelian coupling constant increases at higher energy scales. The running of the coupling constants is very slow as the RG flow is only logarithmic in nature. Thus the couplings come close to each other at very high energies. Making some modification in the $\beta$ function (using supersymmetry), unification of the couplings can be achieved at the energies of the order of $10^{16}$ GeV. A physical meaning to the unification of the three couplings can be given if the $SU(3) \times SU(2) \times U(1)$ is embedded into a larger symmetry group such as $SU(5)$ [41] , and spontaneously breaking the larger symmetry at $10^{16}$ GeV. Close to this scale is the Planck scale which is of the order of $10^{19}$ GeV. One can imagine that the Planck scale is somehow related to the scale of Grand Unification as the gravitational attraction between particles gets comparable to the gauge force around this scale.

The large difference between the weak scale and the Planck scale gives rise to problems associated with the Higgs boson mass. In SM the $SU(2) \times U(1)$ symmetry is broken spontaneously by introduction of a fundamental scalar Higgs field. The Higgs boson mass term should be of the size

$$-\mu_H^2 \sim -(100 GeV)^2 \tag{2.1}$$

The problem is that the bare Higgs boson mass at the cutoff scale $\Lambda$ should naturally be of the order $-\Lambda^2$, and it gets additive radiative corrections under RG evolution. In order that we get $-(100GeV)^2$ at the electroweak scale the bare mass should be very finely tuned to arrange for huge cancellations so that the mass$^2$ is 34 orders of magnitude smaller than its natural value. This fine tuning is required due to the large hierarchy between the electroweak scale and the Planck scale.

The Higgs boson mass can be made much smaller than the underlying mass scale of the fundamental interactions by introducing additional symmetries. The symmetry would then protect it from getting large radiative corrections. One such attractive idea is introduction of supersymmetry. There are other proposals also to address the hierarchy problem by introducing extra dimensions. These derive their motivation from string theory which can be consistently defined only if extra dimensions are introduced. In 1998 Arkani-Hamed, Dimopolous and Dvali (ADD) [4, 5] introduced very interesting idea of allowing only gravity to propagate in all dimensions and confining the SM fields to a 3-brane. A yet another proposal came from Randall and Sundrum [42, 43] who suggested a single extra dimension in an Anti-de-Sitter ($ADS_5$) metric. In the following the ADD model is described briefly.

If spacetime is $4+d$ dimensional, where $d$ is the number of extra spatial dimensions which are compactified over some scale $R$, then the fundamental scale, $M_S$, is different from the Planck scale $M_{Pl}$ in 4-dimensions. The fundamental scale can be close to the electroweak scale so that there is really only one scale in the theory. This removes the hierarchy between the electroweak scale and the Planck scale. Then the 4-dimensional Planck scale $M_{\rm Pl}$ is no longer the relevant scale but is related to the fundamental scale $M_S$ as follows [44]:

$$M_{Pl}^2 \sim M_S^{d+2} R^d. \tag{2.2}$$

If there are extra spatial dimensions the field lines will leak into them and the inverse square law of electromagnetic and gravitational force will get modified. But the inverse square law of electromagnetic force has been tested to very high precision in experiments and no deviations have been found. One can keep this intact by confining the SM fields to a 3-brane. The gravity of course propagates in all the dimensions as it is dynamics of spacetime itself. Tests of gravitational force are extremely difficult as this force is very weak. The accuracy to which this law has been tested in experiments does not rule out possibility of having large compactified extra dimensions. According to Eq. (2.2), deviations from the usual Newtonian gravitational force law can be expected at distances smaller than $R \sim 2 \times 10^{-17+32/d}$cm [44]. For $d \geq 2$, large extra dimensions are consistent with the current experiments since gravitational forces currently are only well probed at distances about 40 $\mu m$ [45] (However for $d = 2$, there are constraints arising from, e.g., supernova cooling [46], which require $M_S \gtrsim 14$TeV if $d = 2$). Recently, there are also some new constraints $M_S \gtrsim 1$TeV [47] from direct search at the Tevatron.

We will follow Han, Lykken and Zhang (HLZ) [48, 49] and compactify the extra dimensions on a d-torii, with all the compactification scales set to be equal to $R$. The effect of extra dimensions on SM fields is felt through their coupling to massive Kaluza Klein gravitons. The SM fields couple to Kaluza Klein (KK) gravitons through the energy momentum tensor $T^{\mu\nu}$.

$$\mathcal{L} = -\frac{\kappa}{2}\sum_{\vec{n}=0}^{\infty} T^{\mu\nu}(x)h^{\vec{n}}_{\mu\nu}(x) \tag{2.3}$$

where $\kappa = \sqrt{16\pi}/M_{Pl}$ and the massive KK gravitons are labeled by a d-dimensional vector of positive integers, $\vec{n} = (n_1, n_2, \ldots, n_d)$. Convention for the signature is $(+,-,-,-)$. The zero mode corresponds to the usual 4-dimension massless graviton. For a given KK level $\vec{n}$, there are, one spin-2 state, $(n-1)$ spin-1 states, and $n(n-1)/2$ spin-0 states, and they are all mass degenerate:

$$m^2_{\vec{n}} = \frac{4\pi\vec{n}^2}{R}. \tag{2.4}$$

Following HLZ we define the relation among the gravitational coupling, the volume of the extra dimensions, and the fundamental scale as

$$\kappa^2 R^d = 8\pi(4\pi)^{d/2}\Gamma(d/2)M_S^{-(d+2)}. \tag{2.5}$$

The propagator for the massive spin-2 KK states $h^{\vec{n}}_{\mu\nu}$ is

$$i\Delta^h_{\{\mu\nu,\vec{n}\},\{\rho\sigma,\vec{m}\}}\,(k) \;=\; \frac{i\delta_{\vec{n},-\vec{m}}\;B_{\mu\nu,\rho\sigma}(k)}{k^2 - m^2_{\vec{n}} + i\varepsilon}\;, \tag{2.6}$$

where

$$\begin{aligned} B_{\mu\nu,\rho\sigma}(k) \;=\; & \left(\eta_{\mu\rho} - \frac{k_\mu k_\rho}{m^2_{\vec{n}}}\right)\left(\eta_{\nu\sigma} - \frac{k_\nu k_\sigma}{m^2_{\vec{n}}}\right) + \left(\eta_{\mu\sigma} - \frac{k_\mu k_\sigma}{m^2_{\vec{n}}}\right)\left(\eta_{\nu\rho} - \frac{k_\nu k_\rho}{m^2_{\vec{n}}}\right) \\ & -\frac{2}{3}\left(\eta_{\mu\nu} - \frac{k_\mu k_\nu}{m^2_{\vec{n}}}\right)\left(\eta_{\rho\sigma} - \frac{k_\rho k_\sigma}{m^2_{\vec{n}}}\right)\;. \end{aligned} \tag{2.7}$$

In this thesis we will consider effects of only spin-2 KK gravitons which enter through the propagator. To this end we note that the mass separation between excitations is of $\mathcal{O}(1/R)$ which is much smaller than other physical scales involved in the problem for small number of extra dimensions. The mass splittings become comparable with the experimental energy resolution for large number of extra dimensions. The effects are difficult to observe if the number of extra dimensions are large as not many KK modes can be produced. We are thus interested in the lower side say $d \leq 6$ where enormous number of accessible KK modes can compensate the $1/M^2_{Pl}$ factor in the scattering amplitude [49]. It is convenient to go from discrete $\vec{n}$ to the continuum limit. The number of states in the mass interval $dm^2_{\vec{n}}$ can be written as

$$\delta\vec{n}^2 \simeq \rho(m_{\vec{n}})dm^2_{\vec{n}}, \tag{2.8}$$

where the density of states is given by

$$\rho(m_{\vec{n}}) = \frac{R^d\ m_{\vec{n}}^{d-2}}{(4\pi)^{d/2}\ \Gamma(d/2)}. \tag{2.9}$$

With this we can sum over KK states to find the effective propagator:

$$\mathcal{D}_{\rm eff}(s) \ = \ \sum_{\vec{n}} \frac{i}{s - m_{\vec{n}}^2 + i\varepsilon} \ = \int_0^\infty dm_{\vec{n}}^2\ \rho(m_{\vec{n}}) \frac{i}{s - m_{\vec{n}}^2 + i\varepsilon} \ , \tag{2.10}$$

which may be singular near a real KK state production. Note that we have kept the $i\varepsilon$ term as the timelike momentum in the propagator can become onshell that is equal to $m_{\vec{n}}^2$. We can isolate this using the principle part

$$\frac{1}{s - m^2 + i\varepsilon} \ = \ P\left(\frac{1}{s - m^2}\right) - i\pi\delta(s - m^2) \ , \tag{2.11}$$

Substituting this and the expression for density of states we find the effective propagator,

$$\mathcal{D}_{\rm eff}(s) \ = \ \frac{s^{d/2-1}}{\Gamma(d/2)} \frac{R^d}{(4\pi)^{d/2}} \left[\pi + 2iI(\Lambda/\sqrt{s})\right] \ , \tag{2.12}$$

where

$$I(\Lambda/\sqrt{s}) \ = \ P\int_0^{\Lambda/\sqrt{s}} dy\ \frac{y^{d-1}}{1 - y^2} \ . \tag{2.13}$$

We have introduced an explicit ultraviolet cutoff $\Lambda$ in the integral. It may be noted that a point $y = 1$ has been removed from the integration path.

The resonant production of a single KK mode with $m_{\vec{n}}^2 = s$ gives the real part proportional to $\pi$. The imaginary part comes from the summation over many non resonant states. The integral $I$ above gives (with $\Lambda = M_S$) [48]

$$\begin{aligned} I(M_S/\sqrt{s}) \ &= \ -\sum_{k=1}^{d/2-1} \frac{1}{2k}\left(\frac{M_S}{\sqrt{s}}\right)^{2k} - \frac{1}{2}\log\left(\frac{M_S^2}{s} - 1\right) \qquad d = \text{even}, \\ &= \ -\sum_{k=1}^{(d-1)/2} \frac{1}{2k-1}\left(\frac{M_S}{\sqrt{s}}\right)^{2k-1} + \frac{1}{2}\log\left(\frac{M_S + \sqrt{s}}{M_S - \sqrt{s}}\right) \qquad d = \text{odd}. \end{aligned} \tag{2.14}$$

Having given the propagator we give next the vertex Feynman rules to carry out the computations. In Fig. 7.2 (Appendix) the vertices coupling SM fields to gravitons are shown. The functions appearing in the rules are defined as follows.

$$C_{\mu\nu,\rho\sigma} \ = \ \eta_{\mu\rho}\eta_{\nu\sigma} + \eta_{\mu\sigma}\eta_{\nu\rho} - \eta_{\mu\nu}\eta_{\rho\sigma} \ , \tag{2.15}$$

$$D_{\mu\nu,\rho\sigma}(k_1,k_2) = \eta_{\mu\nu}k_{1\sigma}k_{2\rho} - \Big[\eta_{\mu\sigma}k_{1\nu}k_{2\rho} + \eta_{\mu\rho}k_{1\sigma}k_{2\nu} - \eta_{\rho\sigma}k_{1\mu}k_{2\nu} + (\mu\leftrightarrow\nu)\Big] , \tag{2.16}$$

$$\begin{aligned} E_{\mu\nu,\rho\sigma}(k_1,k_2) &= \eta_{\mu\nu}(k_{1\rho}k_{1\sigma} + k_{2\rho}k_{2\sigma} + k_{1\rho}k_{2\sigma}) \\ &\quad -\Big[\eta_{\nu\sigma}k_{1\mu}k_{1\rho} + \eta_{\nu\rho}k_{2\mu}k_{2\sigma} + (\mu\leftrightarrow\nu)\Big] , \end{aligned} \tag{2.17}$$

$$\begin{aligned} F_{\mu\nu,\rho\sigma\lambda}(k_1,k_2,k_3) &= \eta_{\mu\rho}\eta_{\sigma\lambda}(k_2-k_3)_\nu + \eta_{\mu\sigma}\eta_{\rho\lambda}(k_3-k_1)_\nu \\ &\quad +\eta_{\mu\lambda}\eta_{\rho\sigma}(k_1-k_2)_\nu + (\mu\leftrightarrow\nu) , \end{aligned} \tag{2.18}$$

$$\begin{aligned} G_{\mu\nu,\rho\sigma\lambda\delta} &= \eta_{\mu\nu}(\eta_{\rho\sigma}\eta_{\lambda\delta} - \eta_{\rho\delta}\eta_{\sigma\lambda}) + \Big(\eta_{\mu\rho}\eta_{\nu\delta}\eta_{\lambda\sigma} + \eta_{\mu\lambda}\eta_{\nu\sigma}\eta_{\rho\delta} \\ &\quad -\eta_{\mu\rho}\eta_{\nu\sigma}\eta_{\lambda\delta} - \eta_{\mu\lambda}\eta_{\nu\delta}\eta_{\rho\sigma} + (\mu\leftrightarrow\nu)\Big) . \end{aligned} \tag{2.19}$$

All of them are symmetric in $\mu \leftrightarrow \nu$. The parameter $\xi$ appearing in the rules is a gauge fixing parameter [48]. The fact that $\xi$ does not appear in the final results would serve as a check on the computation.

## 2.2 Unparticle Physics

Georgi recently proposed an interesting possibility of scale invariant degrees of freedom coupling to SM fields at low energies [6, 7]. (For a correspondence between HEIDI and unparticle see [9].) Let us describe the scheme proposed by him briefly. The theory at very high energy has two sectors, one is the SM and the other we will call Banks-Zaks (BZ) sector following Georgi. It is proposed that the two sectors couple to each other very weakly via exchange of very heavy particles. A crucial assumption is made regarding the BZ sector in infrared. It is assumed that the BZ sector has a non trivial fixed point in infrared. A consequence of which is that at low energies the BZ sector becomes scale invariant. The property of scale invariance affords huge simplifications and does not require detailed understanding of the BZ sector at very high energies. The phenomenology can be carried out if we take an effective field theory approach. If the two sectors interact weakly via exchange of particles with a large mass $M$, then below this mass scale there are nonrenormalizable couplings involving both standard model fields and Banks-Zaks fields suppressed by powers of $M$. The couplings have the generic form

$$\frac{1}{M^k}\mathcal{O}_{SM}\mathcal{O}_{BZ}, \tag{2.20}$$

where $\mathcal{O}_{SM}$ is an operator constructed out of SM fields and has a mass dimension $d_{SM}$. The operator $\mathcal{O}_{BZ}$ is similarly constructed out of the BZ fields and has a mass dimension

$d_{BZ}$. As we go further down in energy using RG flow, scale invariance emerges below some energy scale $\Lambda_u$. Here the fields are termed as unparticles and the interactions (2.20) match onto interactions of the form

$$C_U \frac{\Lambda_u^{d_{BZ}-d_u}}{M^k} \mathcal{O}_{SM} \mathcal{O}_U, \tag{2.21}$$

where $d_u$ is the scaling dimension of the unparticle operator $\mathcal{O}_U$ and $C_U$ is a coefficient function. Using these effective interactions phenomenology can be carried out.

Let us now derive the propagator [7, 8] for scalar unparticle. If operator $\mathcal{O}_U$ is scale invariant and has a scaling dimension $d_u$, then

$$\langle 0|\mathcal{O}_U(\lambda x)\mathcal{O}_U^\dagger(\lambda x')|0\rangle = \lambda^{2d_u}\langle 0|\mathcal{O}_U(x)\mathcal{O}_U^\dagger(x')|0\rangle. \tag{2.22}$$

Inserting a complete set of states $|P\rangle$ with 4-momentum $P^\mu$ we can write

$$\langle 0|\mathcal{O}_U(x)\mathcal{O}_U^\dagger(x')|0\rangle = \sum_P \langle 0|\mathcal{O}_U(x)|P\rangle\langle P|\mathcal{O}_U^\dagger(x')|0\rangle. \tag{2.23}$$

Using translational invariance we can express the above equation as

$$\begin{aligned}
\langle 0|\mathcal{O}_U(x)\mathcal{O}_U^\dagger(x')|0\rangle &= \sum_P \langle 0|\mathcal{O}_U(0)|P\rangle\langle P|\mathcal{O}_U^\dagger(0)|0\rangle e^{-iP\cdot(x-x')} \\
&= \sum_P |\langle 0|\mathcal{O}_U(0)|P\rangle|^2 e^{-iP\cdot(x-x')} \\
&= \int \frac{d^4q}{(2\pi)^4}\rho(q)\,|\langle 0|\mathcal{O}_U(0)|q\rangle|^2 e^{-iq\cdot(x-x')},
\end{aligned} \tag{2.24}$$

where the spectral density is defined as

$$\rho(q)\,|\langle 0|\mathcal{O}_U(0)|q\rangle|^2 = \int d^4x e^{iq.x}\langle 0|\mathcal{O}_U(x)\mathcal{O}_U^\dagger(0)|0\rangle. \tag{2.25}$$

In this we have put $x' = 0$ without any loss of generality. On general grounds we can argue that the rhs. is Lorentz invariant. Also $q^0 > 0$ as it is energy of state $|q\rangle$ so that it is proportional to $\theta(q^0)$. Thus we can write

$$\rho(q)\,|\langle 0|\mathcal{O}_U(0)|q\rangle|^2 = \theta(q^0)\theta(q^2)f(q^2), \tag{2.26}$$

where $f(q^2)$ is some Lorentz invariant function. We can fix the spectral density using scale invariance apart from an overall factor,

$$\rho(\lambda q)\,|\langle 0|\mathcal{O}_U(0)|\lambda q\rangle|^2 = \rho(q)\,|\langle 0|\mathcal{O}_U(0)|q\rangle|^2 (\lambda^2)^{d_u-2}. \tag{2.27}$$

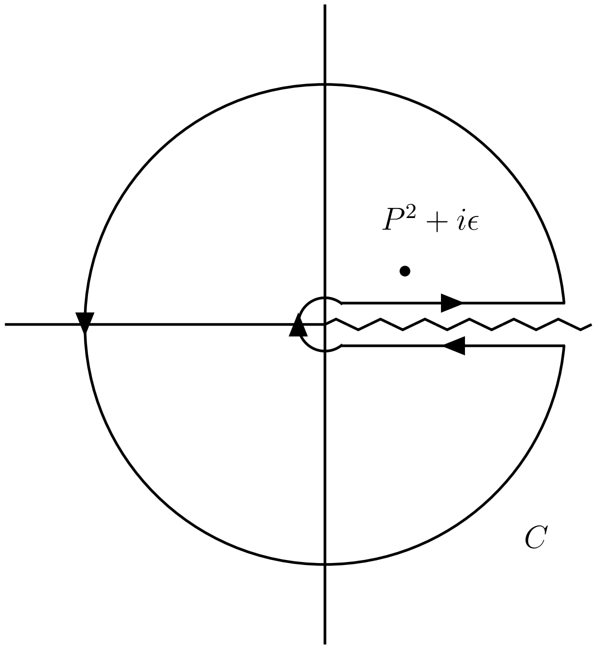


Figure 2.1: Integration contour used in the integral in eq. 2.2 .

Using this we can readily write

$$\rho(q^2)\left|\langle 0|\mathcal{O}_U(0)|q\rangle\right|^2 = A_{du}(\mathcal{O}_U)\theta(q^0)\theta(q^2)(q^2)^{d_u-2}. \tag{2.28}$$

Following Georgi [6] we will take

$$A_{d_u}(\mathcal{O}_U) = \frac{16\pi^{5/2}}{(2\pi)^{2d_u}}\frac{\Gamma(d_u+1/2)}{\Gamma(d_u-1)\Gamma(2d_u)}. \tag{2.29}$$

Using Kallen-Lehmann spectral decomposition we can write the Fourier transform of two point function of unparticle operators as

$$\int d^4xe^{iP.x}\langle 0|T(\mathcal{O}_U(x)\mathcal{O}_U(0)|0\rangle = i\frac{A_{d_u}(\mathcal{O}_U)}{2\pi}\int_0^\infty dM^2\frac{(M^2)^{d_u-2}}{P^2-M^2+i\epsilon}. \tag{2.30}$$

To see peculiarity arising from having scale invariance with fractional $d_u$ we need to evaluate the integral

$$I = \int_0^\infty dM^2\frac{(M^2)^{d_u-2}}{M^2-(P^2+i\epsilon)}$$

Let us evaluate the following integral in the complex plane

$$I' = \int_C dz\frac{z^{d-2}}{z-(P^2+i\epsilon)}.$$

$i\epsilon$ prescription shifts pole off the real axis to $P^2 + i\epsilon$. We close the contour as shown in Fig. 2.2. Also note that $z^{d-2}$ is multivalued so we need to introduce a branch cut. We note that there is a simple pole inside at $P^2 + i\epsilon$, so $I' = 2\pi i(P^2 + i\epsilon)^{d-2}$. With this we have

$$\begin{aligned} I' &= \int_0^\infty dx \frac{x^{d-2} - x^{d-2} e^{2\pi i(d-2)}}{x - (P^2 + i\epsilon)} \\ &= -2i \int_0^\infty dx \frac{x^{d-2}}{x - (P^2 + i\epsilon)} \sin(d\pi)\ e^{i\pi(d-2)}, \end{aligned}$$

so we have

$$\int_0^\infty dx \frac{x^{d-2}}{x - (P^2 + i\epsilon)} = -\pi \frac{[e^{-i\pi}(P^2 + i\epsilon)]^{d-2}}{\sin(d\pi)}. \tag{2.31}$$

Note that the factor of $\sin(d\pi)$ arises because of discontinuity across the branch cut which is due to fractional scaling dimension. Changing $x$ to $M^2$ we obtain

$$\int_0^\infty dM^2 \frac{(M^2)^{d-2}}{P^2 - M^2 + i\epsilon} = \pi \frac{[e^{-i\pi}(P^2 + i\epsilon)]^{d-2}}{\sin(d\pi)}. \tag{2.32}$$

With this we can finally write the propagator for unparticles as

$$\int d^4x e^{iP.x} \langle 0|T(\mathcal{O}_U(x)\mathcal{O}_U(0)|0\rangle = \frac{iA_{d_u}(\mathcal{O}_U)}{2} \frac{[e^{-i\pi}(P^2 + i\epsilon)]^{d-2}}{\sin(d_u\pi)}. \tag{2.33}$$

The unparticle operators could be of scalar, vector, tensor or fermionic type [50]. Here we will restrict ourselves to scalar and tensor unparticles coupled to SM fields given by

$$\frac{\lambda_s}{\Lambda_u^{d_u-1}} \overline{\psi}\psi\mathcal{O}_U,\ \frac{-\lambda_s}{4\Lambda_u^{d_u}} F_{\mu\nu}F^{\mu\nu}\mathcal{O}_U,\ \frac{\lambda_t}{\Lambda_u^{d_u}} T_{\mu\nu}\ \mathcal{O}_U^{\mu\nu}\ , \tag{2.34}$$

where $\lambda_{s,t}$ are the dimensionless coupling constants. The unparticle tensor operator $O_U^{\mu\nu}$ is traceless and symmetric and has a scaling dimension $d_u$. $T_{\mu\nu}$ is the energy momentum tensor of the SM. Scale invariance restricts the scaling dimension of tensor unparticle operator to $d_u \geq 3$ [51]. Conformal invariance on the other hand leads to a constraint $d_u \geq 4$ on the second rank tensor operators. Scale and conformal symmetries can only guide us on fixing the tensor structures of the propagator leaving the overall normalization undetermined. Unlike the conformal invariance, the scale invariance does not fix the relative coefficients of the tensors appearing in the tensor propagator [51]. We use the following tensor propagator for our phenomenological study:

$$\begin{aligned} \int d^4x\ e^{ik\cdot x} \langle 0|TO_U^{\mu\nu}(x)O_U^{\alpha\beta}(0)|0\rangle &= -iC_T \frac{\Gamma(2-d_u)}{4^{d_u-1}\Gamma(d_u+2)}(-k^2)^{d_u-2} \\ &\times [d_u(d_u-1)(\eta_{\mu\alpha}\eta_{\nu\beta} + \mu \leftrightarrow \nu) + \ldots] \end{aligned} \tag{2.35}$$

We will choose $C_T$ =1. The terms given by ellipses do not contribute to the diphoton production. The terms in the ellipses depend on tensors, proportional to $\eta^{\mu\nu}$, $k^\mu$ and $k^\nu$. The exact tensorial form of course depends on the symmetry (scale or conformal). These terms do not contribute to physical processes thanks to the conservation and traceless nature of the SM energy momentum tensor. Hence the symmetry restriction enters only through the scaling dimension $d_u$ (the overall undetermined constant could be different for the scale and conformal invariant propagators). Hence we can safely use the above propagator Eq. (2.35) with $d_u \geq 3$ ($\geq 4$) for scale (conformal) invariant analysis. As larger $d_u$ values give smaller unparticle contributions, we would demand only scale invariance which allows smaller values of $d_u$. In addition, as the SM energy momentum tensor is a conserved quantity, it does not require any operator mixing under SM renormalization. As the unparticles couple to the SM energy momentum tensor we can use the vertex Feynman rules given in Fig. 7.2 after appropriate modification of the factor $\kappa^2\mathcal{D}(s)$, see Eq. (5.8).

# Chapter 3

# QCD

## 3.1 QCD Lagrangian

The standard model has been very successful in describing the processes occurring at high energies. Its SU(3) component called the Quantum Chromodynamics (QCD) has by now matured as the correct description of the strong force. In the present chapter we will introduce QCD very briefly to set some of the notations and ideas. The later chapters would rely on some of the preparations made here. QCD is a $SU(3)$ gauge theory that describes interactions of quarks and gluons which are elementary particles carrying $SU(3)$ quantum numbers. The quarks (fermions) transform under the 3-dimensional fundamental representation. The $SU(3)$ charges are called color and thus quarks come in three different colors. The gluons (bosons) which are carriers of strong forces transform under the 8-dimensional adjoint representation.

In quantum field theory n-point Green functions are one of the most important quantities as S-Matrix can be expressed using these. A $n$-point Green function constructed out of operators containing quark fields $\Psi = \{\psi_i\}$,$i = 1, 2, 3$ and gluon fields $A^a_\mu$, $a = 1, \ldots, 8$ has the following generic form in path integral language.

$$
\begin{aligned}
< 0|T\mathcal{O}_1(x_1)\ldots\mathcal{O}_n(x_n)|0 > &= \frac{\int \mathcal{D}[\Phi]e^{iS_{QCD}[\Phi]}\mathcal{O}_1(x_1)\ldots\mathcal{O}_n(x_n)}{\int \mathcal{D}[\Phi]e^{iS_{QCD}[\Phi]}}, \qquad (3.1)\\
[\Phi] &= \left\{A^a_\mu, \Psi, \overline{\Psi}, c, \overline{c}\right\} \qquad (3.2)
\end{aligned}
$$

where $S_{QCD} = \int d^4x\mathcal{L}_{QCD}$. The field $c(x)$ denotes the ghost fields which appear due to gauge fixing procedure. The Lagrangian $\mathcal{L}_{QCD}$ in covariant gauge is given by (quarks are treated as massless)

$$
\mathcal{L}_{QCD} = -\frac{1}{4}F^a_{\mu\nu}F^{a\mu\nu} - \frac{1}{2\zeta}(\partial^\mu A^a_\mu)(\partial^\nu A^{a\nu}) + \overline{\Psi}i\not{\mathcal{D}}\Psi + \overline{c}^a(-\partial^\mu\mathcal{D}^{ac}_\mu)c^c \qquad (3.3)
$$

The field strength $F^a_{\mu\nu}$ is defined by

$$F^a_{\mu\nu} = \partial_\mu A^a_\nu - \partial_\nu A^a_\mu + g_s f^{abc} A^b_\mu A^c_\nu, \tag{3.4}$$

$f^{abc}$ are the structure constants of $SU(3)$ group. The covariant derivative appearing in $\mathcal{L}_{QCD}$ is given by

$$\mathcal{D}^{ab}_\mu = \partial_\mu \delta^{ab} - i g_s A^c_\mu (t^c)^{ab}, \tag{3.5}$$

$c$ and $\overline{c}$ are ghost fields, $\zeta$ is the gauge fixing parameter and $g_s$ is the dimensionless strong coupling constant.

One could go ahead and derive the Feynman rules for computations. But any calculation beyond tree level would involve loop integrals and these are generally ultraviolet divergent. A systematic way to deal with these singularities is to analytically continue the theory to $n = 4 + \epsilon$ space-time dimensions so that the divergences appear as poles in $\epsilon$. Further, the fields and couplings are redefined such that the Green's functions are finite in the limit $\epsilon \to 0$. This procedure is called renormalization. Let us call the unrenormalized fields appearing in $\mathcal{L}_{QCD}$ as bare fields and denote them with a hat, and denote the renormalized fields without a hat. The bare quantities are defined in terms of renormalized fields as follows

$$\begin{aligned}
\hat{\Psi} &= Z_\Psi^{\frac{1}{2}}(\mu_R) \;\; \Psi(\mu_R), \\
\hat{A}^a_\mu &= Z_A^{\frac{1}{2}}(\mu_R) \;\; A^a_\mu(\mu_R), \\
\hat{c}^a &= Z_c^{\frac{1}{2}}(\mu_R) \;\; c^a(\mu_R), \\
\hat{g}_s &= Z_g(\mu_R) \;\; (\mu_R)^{-\epsilon/2} \;\; g_s(\mu_R), \\
\hat{\zeta} &= Z_\zeta(\mu_R) \;\; \zeta(\mu_R).
\end{aligned} \tag{3.6}$$

In the renormalization constants, $Z\,'s$, the ultraviolet poles are absorbed to make the Green functions finite. The scale $\mu_R$ is the scale at which the divergences are subtracted in the renormalized theory. The coupling constant $\hat{g}_s$ has a mass dimension $-\epsilon/2$ in $4+\epsilon$ dimensions, hence a factor of $(\mu_R)^{-\epsilon/2}$ has been factored out so that the renormalized coupling $g_s(\mu_R)$ is dimensionless. The gauge parameter $\zeta$ remains dimensionless. The freedom in absorbing a finite piece in addition to the poles in $Z\,'s$ is fixed by defining the scheme of renormalization. In this thesis $\overline{MS}$ scheme will be used where in addition to the poles a finite piece $\ln 4\pi - \gamma_E$ is also absorbed into $Z's$. Here $\gamma_E$ is Euler's constant and has a numerical value $\gamma_E = 0.5772$.

With the redefinition of fields the $\mathcal{L}_{QCD}$ can be written as

$$\mathcal{L}_{QCD} = -\frac{1}{4} F^a_{\mu\nu} F^{a\mu\nu} - \frac{1}{2\zeta}(\partial^\mu A^a_\mu)(\partial^\nu A^{a\nu}) + \overline{\Psi} i \not{\mathcal{D}} \Psi + \overline{c}^a(-\partial^\mu \mathcal{D}^{ac}_\mu) c^c$$

$$
\begin{aligned}
&-\frac{1}{4}\left(Z_A-1\right)\left(\partial^\mu A^a_\nu-\partial^\nu A^a_\mu\right)^2 \\
&-\frac{1}{4}\left(Z_A^2 Z_g^2-1\right) g_s^2(\mu_R)\ \mu_R^{-\epsilon}\left(f^{abc}A^b_\mu A^c_\nu\right)\left(f^{ade}A^d_\mu A^e_\nu\right) \\
&-\left(Z_g Z_A^{3/2}-1\right) g_s(\mu_R)\mu_R^{-\epsilon/2} f^{abc}\partial_\mu A^a_\nu\ A^b_\mu A^c_\nu \\
&-\frac{1}{2\zeta}\left(Z_\zeta^{-1}Z_A-1\right)\partial^\mu A^a_\mu \partial^\nu A^a_\nu \\
&+\left(Z_\psi-1\right)\left(\overline{\Psi} i\partial\!\!\!/\ \Psi\right) \\
&+\left(Z_\psi Z_A^{1/2} Z_g-1\right) g_s(\mu_R)\ \mu_R^{-\epsilon/2}\ \overline{\Psi}\gamma^\mu A^a_\mu t^a \Psi \\
&+\left(Z_c-1\right)\bar{c}^a\left(-\partial^2\right)\delta^{ac}c^c \\
&-\left(Z_c Z_g Z_A^{1/2}-1\right) g_s(\mu_R)\ \mu_R^{-\epsilon/2}\ \bar{c}^a f^{abc}\partial^\mu A^b_\mu c^c. \qquad (3.7)
\end{aligned}
$$

Gauge symmetry relates various counterterms and not all of them are independent.

## 3.2 Renormalization Group

The unrenormalized coupling constant $\hat{g}_s$ does not depend on the renormalization scale $\mu_R$. Using this fact the evolution of the renormalized coupling $g_s(\mu_R)$ can be evaluated. Defining $a_s = g_s^2/16\pi^2$ we can write

$$
\hat{a}_s = Z_g^2 a_s(\mu_R)\left(\mu_R^2\right)^{-\epsilon/2}. \qquad (3.8)
$$

Differentiating both sides w.r.t $\mu_R^2$ we get

$$
\beta(a_s) = \mu_R^2 \frac{da_s}{d\mu_R^2} = \frac{\epsilon}{2}a_s - a_s \mu_R^2 \frac{d\ln Z_g^2}{d\mu_R^2}. \qquad (3.9)
$$

In $\overline{MS}$ scheme $\beta$ function does not depend explicitly on $\mu_R$ and is a function of $g_s(\mu_R)$. In this scheme $Z_g$ has the following simple form

$$
Z_g = 1 + a_s\frac{z_1}{\epsilon} + a_s^2\left(\frac{z_2}{\epsilon^2}+\frac{z_3}{\epsilon^3}\right)+\ldots. \qquad (3.10)
$$

The coefficients $z_i$ do not depend on $\mu_R$. Using the above two equations the $\beta$ function can be written as

$$
\beta(a_s) = \frac{\epsilon}{2}a_s - a_s^2\beta_0 - a_s^3\beta_1 - a_s^4\beta_2 - \ldots \qquad (3.11)
$$

with

$$\begin{aligned}\beta_0 &= \frac{11}{3}C_A - \frac{4}{3}n_f T_f, \\ \beta_1 &= \frac{34}{3}C_A^2 - \frac{4}{3}n_f T_f(3C_F + 5C_A),\end{aligned} \tag{3.12}$$

where

$$C_A = 3, \qquad C_F = \frac{4}{3}, \tag{3.13}$$

are Casimir invariants in adjoint and fundamental representations respectively of SU(3). $n_f$ denotes the number of active flavors. We note that $\beta_0$ is positive ( if $n_f < 16.5$ ) in real world with six quark flavors. This gives rise to the celebrated phenomenon of asymptotic freedom [52, 53], that is, the strong coupling constant decreases at higher energies. It is customary to define a dimensionful parameter $\Lambda$ by the definition

$$\ln\frac{Q^2}{\Lambda^2} = -\int_{a_s(Q^2)}^{\infty}\frac{da_s}{\beta(a_s)}. \tag{3.14}$$

Retaining only the lowest order term with coefficient $\beta_0$ and solving we obtain in $n = 4$

$$a_s\left(Q^2\right) = \frac{1}{\beta_0\ln\dfrac{Q^2}{\Lambda^2}}. \tag{3.15}$$

A next-to-leading order definition of $\Lambda$ is obtained by retaining upto $\beta_1$ term. Solving the above equation and expanding in inverse powers of $\ln(Q^2/\Lambda^2)$ we obtain

$$a_s(Q^2) = \frac{1}{\beta_0\ln\dfrac{Q^2}{\Lambda^2}}\left[1 - \frac{(\beta_1/\beta_0)\ \ln\ln\dfrac{Q^2}{\Lambda^2}}{\beta_0\ln\dfrac{Q^2}{\Lambda^2}}\right]. \tag{3.16}$$

Here, following the standard practice, a term of order $1/\ln^2(Q^2/\Lambda^2)$ has been absorbed into the definition of $\Lambda$. Once $a_s$ is measured experimentally at some energy scale $Q$ the above equations can be solved to determine $\Lambda$ which can then be used to determine $a_s$ at any other energy scale. We note that the sign of $\beta$ function is crucial in determining the behavior of the strong coupling with change in scale. In Fig. 3.2 we have plotted $\alpha_s = 4\pi a_s$ as a function of scale.

Returning back to $\Lambda$ we note that it depends on the number of active quark flavours. Henceforth we will use $\Lambda(4)$ and $\Lambda(5)$ for 4 and 5 flavors respectively. The coupling constant should be a continuous function of scale, this provides with the matching conditions as the fermion mass thresholds are crossed. Experimentally determined $\alpha_s(M_Z) = 0.118$ at the Z-Boson mass of 91.19 $GeV$ in (3.16) gives $\Lambda(5) = 226MeV$. Using this we can determine the value of $\alpha_s$ at the bottom mass, 4.20 GeV which gives $\alpha_s(M_b) = 0.225$. Now we can solve (3.16) with $n = 4$ and $\alpha_s(M_b) = 0.225$ and obtain $\Lambda(4) = 326$MeV.

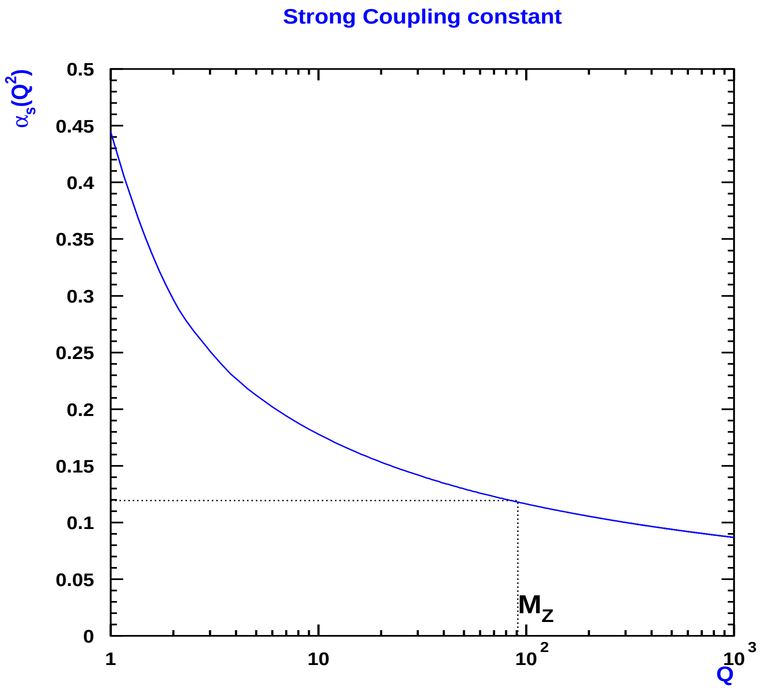


Figure 3.1: evolution of strong coupling constant with scale

## 3.3 Parton Model and Factorization

A hadron is a low energy state made of quarks and gluons. In parton model the scattering of hadrons is due entirely to the scattering of individual constituents. The probability distribution functions $f_{a/H}(x)$ give probability of finding a parton $a$ within the hadron $H$ carrying a fraction $x$ of hadron momentum. Using this, crosssection can be written as

$$\sigma^{LO} = \int_0^1 dx_1 \int_0^1 dx_2 \sum_{ab} f^{LO}_{a/H_1}(x_1, \mu_F) \; f^{LO}_{b/H_2}(x_2, \mu_F) \; \hat{\sigma}^{LO}_{ab}(x_1, x_2, Q), \tag{3.17}$$

where $\hat{\sigma}^{LO}_{ab}$ is a leading order partonic crosssection for the hard scattering event at leading order. In the above expression we see that low momentum scale physics encoded in the factor $f^{LO}_{a/H_1}(x_1, \mu_F) \; f^{LO}_{b/H_2}(x_2, \mu_F)$ is separated from the short distance physics expressed in $\sigma^{LO}_{ab}(x_1, x_2, Q)$. This is the content of naive parton model [54]. Beyond leading order, high energy interactions of hadrons are described by QCD improved parton model and is based on the important property of factorization. This states that in certain processes the long distance physics can be separated from the short distance physics:

$$\sigma = \int_0^1 dx_1 \int_0^1 dx_2 \; f_{a/H_1}(x_1, \mu_F) \; f_{b/H_2}(x_2, \mu_F) \; \hat{\sigma}_{ab}(x_1, x_2, Q/\mu_R^2, \mu_F^2/\mu_R^2) \tag{3.18}$$

Here $\hat{\sigma}_{ab}$ denotes the short distance part of the partonic crosssection which involves large momentum transfers. This is calculable in perturbation theory because the strong coupling constant is small at large momenta due to asymptotic freedom. This factorization property of the cross section can be proved to all orders in perturbation theory [55]. Let us explain more clearly what is meant by $\hat{\sigma}_{ab}$. At higher orders in perturbation theory a parton can emit another parton at low transverse momentum before it enters into a hard scattering event. This is a long distance part which should be included in the parton distribution functions. This procedure is called factorization and is carried out at an arbitrary scale $\mu_F$ called factorization scale. The parton level crosssection obtained after factorization is what appears in (3.18). In the next chapter we will explicitly carry out this procedure.

The factorization scale $\mu_F$ is an arbitrary parameter. It can be thought of as a scale which separates the long and short distance physics. Thus a parton emitted with a small transverse momentum, less than the scale $\mu_F$ is considered part of the hadron structure and is absorbed in parton distribution. A parton emitted at large transverse momentum is part of the short distance crosssection. Although apriori $\mu_F$ is arbitrary we should choose this to be close to the hard scale $Q$ which characterizes parton parton interaction. This is important because powers of logarithms of $Q/\mu_F$ and $Q/\mu_R$ appear at every order in perturbation theory. If $\mu_F$ and $\mu_R$ are widely separated from $Q$ then these large logarithms appearing at every order in perturbation will invalidate a fixed order computation. That is why generally $\mu_F$ and $\mu_R$ are chosen in the range $Q/2 < \mu_F, \mu_R < 2Q$. Although we are completely free to choose $\mu_F$ and $\mu_R$ to be different from each other they are generally identified. We will also make this identification in the following chapters.

Although the pdfs cannot be calculated, their evolution with $\mu_F$ is completely determined by QCD and can be calculated perturbatively. This evolution is given by Dokshitzer-Gribov-Lipatov-Altarelli-Parisi (DGLAP) evolution equation [56, 57, 58, 59].

$$\mu_F^2 \frac{\partial f_{a/H}(x,\mu_F^2)}{\partial \mu_F^2} = a_s(\mu_F^2) \int_x^1 \frac{dz}{z} P_{ab}\left(\frac{x}{z}, a_s(\mu_F^2)\right) f_{b/H}(z,\mu_F^2) \tag{3.19}$$

Both the leading order [58] and $\mathcal{O}(\alpha_s)$ [60, 61, 62, 63, 64] contributions to DGLAP splitting functions have been calculated. The leading order splitting functions $P_{ab}(x,\epsilon)$ for $x \leq 1$ are given by

$$\begin{aligned}
P_{qq}(x,\epsilon) &= 4C_F\left[\frac{1+x^2}{(1-x)_+} + \frac{3}{2}\delta(1-x)\right] + \epsilon\ 2C_F(1-x), \\
P_{qg}(x,\epsilon) &= 4T_F\left[x^2 + \left(1-x^2\right)\right] + \epsilon\ 2x(1-x), \qquad , \\
P_{gq}(x,\epsilon) &= 4C_F\left[\frac{1+(1-x^2)}{x}\right] + \epsilon\ 2C_F x,
\end{aligned}$$

$$P_{gg}(x,\epsilon) = 8C_A\left[\frac{x}{(1-x)_+}+\frac{1-x}{x}+x(1-x)\right] + 4\delta(1-x)\frac{11C_A-4n_fT_F}{6} \qquad (3.20)$$

The *plus* -distributions are defined by the following equation

$$\int_a^1 dx\frac{f(x)}{(1-x)_+} = \int_a^1 dx\frac{f(x)-f(1)}{1-x} + f(1)\ln(1-a), \qquad (3.21)$$

where $f(x)$ is well behaved arbitrary function. In Figs. 3.2 and 3.3 leading order and

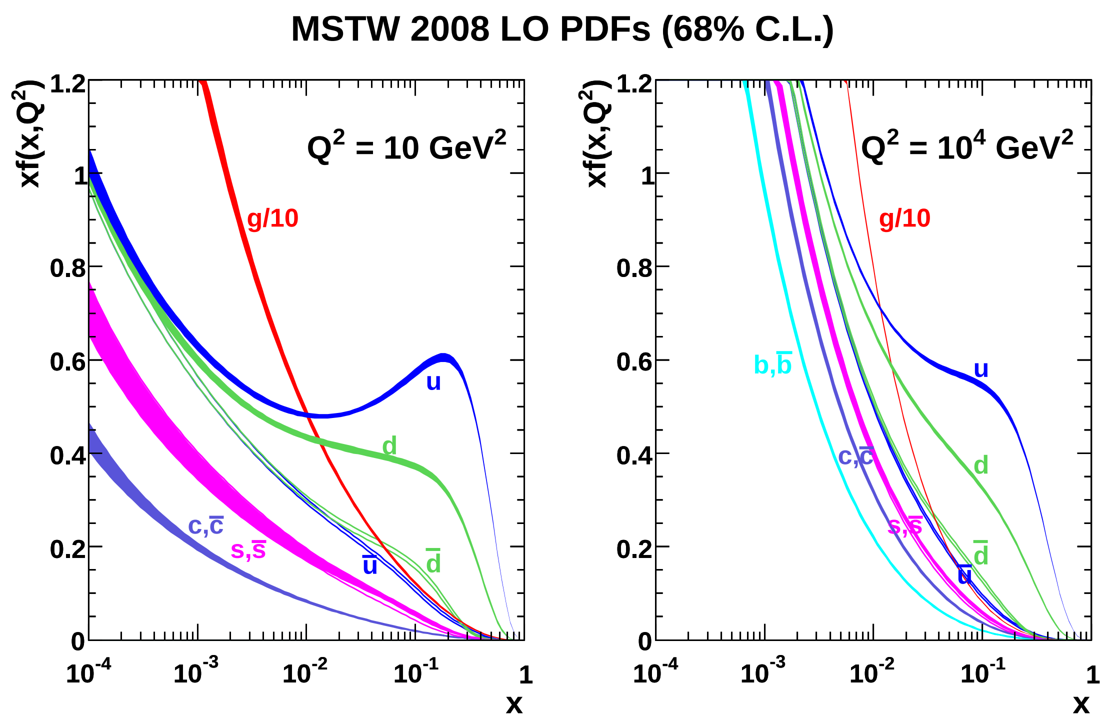


Figure 3.2: Leading order parton distribution functions

next-to-leading order distribution functions of various quarks and gluons in proton are shown at different energy scales [65]; these plots are taken from the site http://projects.hepforge.org/mstwpdf/plots/plots.html . We note from these figures that gluon distribution functions increase rapidly at lower values of $x$. Thus if a process probes very small values of $x$, gluon initiated processes may dominate over quark-antiquark initiated processes.

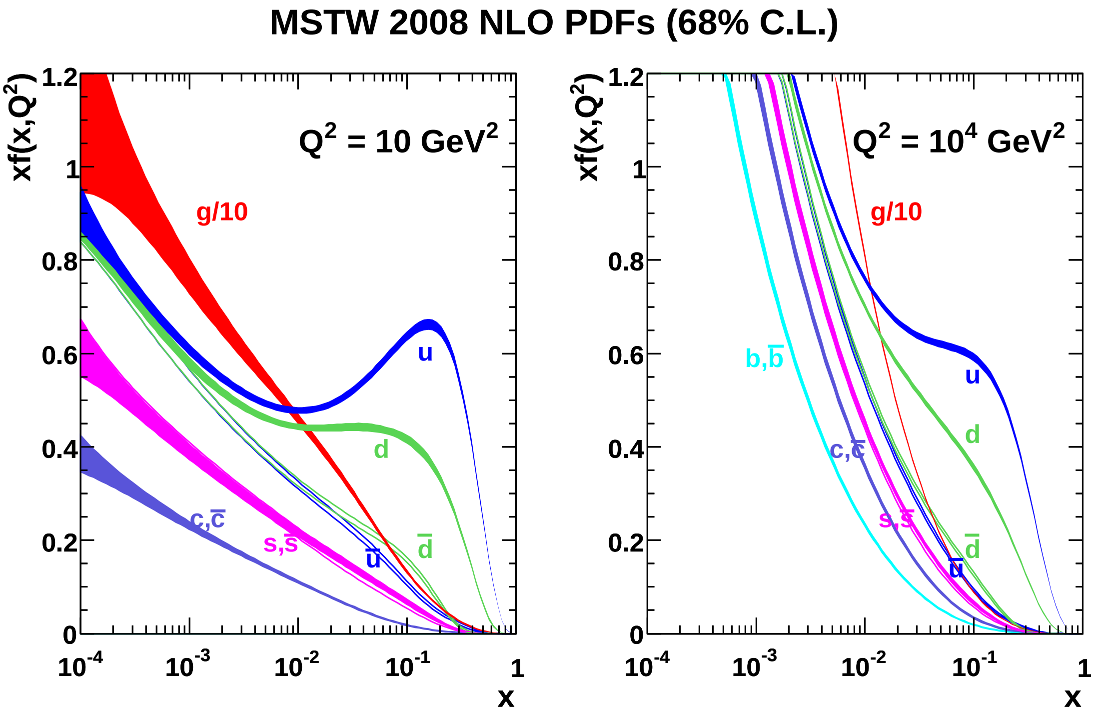


Figure 3.3: Next-to-leading order parton distribution functions

## 3.4 Scale uncertainties

A calculation beyond leading order in strong coupling involves Feynman diagrams which have infrared divergences. When the gluon momenta in loops or in real emission processes become soft that is vanishingly small soft divergences appear as poles in $\epsilon$. These soft divergences in virtual and real emission contributions cancel between each other giving a result free of soft divergences. Soft fermions do not give any divergences. There are additional QCD singularities called collinear singularities which appear at this order. When two massless partons become parallel to each other collinear divergences appear in loops as well as in real emission contributions. Again in dimensional regularization these appear as poles in $\epsilon$. These singularities, however do not cancel between each other if they appear in the initial state as there is typically no integration over the initial state partons [66, 67]. In order to get finite predictions mass factorization is carried out to remove these singularities. In this procedure, which is very similar to renormalization, the poles in $\epsilon$ are absorbed into bare parton distribution functions at some scale $\mu_F$ thereby defining scale dependent distribution functions. This scale is arbitrary and enters at leading order through parton distribution functions. Also the parton distribution functions depend on the scheme of factorization which fixes the amount of finite piece which is subtracted in addition to the poles. We will use parton distribution functions defined in $\overline{MS}$ scheme in this thesis. Thus we see that leading order predictions are very sensitive to the choice of factorization scales. As we include higher and higher order terms, the dependence on this scale gets progressively smaller. In addition to improvement in scale sensitivity NLO corrections may enhance or decrease the signals.

# Part II

# Isolated Direct Photon Pair Production at the Large Hadron Collider

# Chapter 4

# Isolated direct photon pair production at NLO

As has been discussed in the previous chapter, a computation at next-to-leading order in strong coupling constant is important not only because it contains higher order terms of the perturbation series but also because it reduces the sensitivity to the factorization scale. In the present chapter a next-to-leading order computation for the production of direct photon pairs in a hard scattering event at hadron colliders will be presented for the ADD model and the unparticle model . We will begin with a leading order computation and go on to discuss virtual corrections which appear at next-to-leading order. The singularities which appear in the loop corrections will be discussed. Next would follow presentation of contributions coming from real emission Feynman diagrams. Throughout dimensional regularization using $n = 4+\epsilon$ would be employed and $\overline{MS}$ scheme will be used to subtract the divergences. We will discuss in detail the semi-numerical *two cutoff phase space slicing method* on which our calculation is based.

## 4.1 Isolated direct photons

Photons arise from many sources in hadronic collisions. They are produced through decays of large transverse momentum $\pi^0, \eta, \omega$ etc., to photons and they may also be produced as direct photons. Direct photons are produced by two different mechanisms: either they take part directly in the hard subprocess, or they result from fragmentation of partons themselves produced at high transverse momentum in the subprocess. The process of fragmentation of partons (quarks and gluons) is a collinear phenomenon as the fragmentation photons are embedded in hadronic jets. The two mechanisms of direct photon production are closely related to each other. To understand this we note that the $qg$ initiated process (Fig. 7.5) has a final state QED singularity which can be removed by factoring it in the fragmentation function describing fragmentation photons.

The collider experiments do not measure inclusive photons. There are huge backgrounds from decays of high $p_T$ $\pi^0, \eta, \omega$ etc. Experimental isolation cuts are imposed to reject large background of secondary photons produced in the decays of these mesons. A widely used isolation criterion is the following. Only those events are selected which satisfy the following criterion. Inside a circle of radius $r$ centred at the photon in the rapidity and azimuthal angle plane, the total amount of transverse hadronic energy should be smaller than some fixed value $E_T^{max}$. The topic of the isolation of photons based on the above criterion is extensively discussed in theoretical literature [68, 69, 70, 71]. This isolation criterion in addition to rejecting secondary photons also rejects some of the fragmentation photons.

The fragmentation functions describing fragmentation photons are not known to a very good accuracy and it is desirable to have a way to avoid fragmentation photons. The most naive thing to do would be to veto the configurations in which a photon is very close to hadronic activity. This can be implemented by constructing a cone of some small fixed radius around photons and demanding that there be no hadronic activity within it. Experimentally such an event selection can be carried out easily, however such an observable is not infrared safe and cannot be calculated using QCD perturbation theory. This happens because nothing is allowed within the cone, not even the soft gluons. The soft gluon singularities cancel between real and virtual contributions; if we constrain the phase space of soft gluons this cancellation gets disturbed. An alternative would be to allow soft gluons in the cone but exclude the quarks. This would be fine as soft quarks do not give any singularity. But it is extremely difficult to determine experimentally the origin of jets. This makes this alternative unattractive. We can achieve our goal, of keeping only direct photons isolated from hadrons and at the same time the observable be infrared safe, following the *smooth cone isolation* prescription proposed by Frixione [72]. The idea is simple, we have to device a prescription that removes the fragmentation photons which are embedded in hadronic jets while allowing the soft gluons.

**Smooth cone isolation:** Let $z$–axis coincide with the hadron–hadron collision line, and $\theta$ and $\phi$ denote the polar and azimuthal angles respectively. It is more convenient to use pseudo-rapidity ($\eta$) in the context of hadron colliders instead of $\theta$, as they are additive under boosts. Draw concentric circles in the $\eta - \phi$ plane around each photon. Let the radius of the largest circle be $R_0$. We demand that the sum of hadronic transverse energy in any circle of radius $R < R_0$ be less than some specified amount $\mathcal{H}(R)$ which depends on the radius $R$. The function $\mathcal{H}(R)$ is decreasing with decreasing $R$. We would make the following choice for $\mathcal{H}(R)$:

$$\mathcal{H}(R) = \mathcal{E}_T^{iso} \left( \frac{1 - cosR}{1 - cosR_0} \right)^n , \tag{4.1}$$

where $\mathcal{E}_T^{iso}$ is some fixed amount of energy and the exponent $n$ can be taken to be any number greater than 1/2 [72]. One could in principle choose a very small value for $R_0$

but this would generate large logarithms at every order in perturbation theory thereby spoiling a fixed order computation. From the function it is clear that as we move closer to the photon lesser hadronic activity is allowed. Note that $\mathcal{H}(R) \to 0$ as $R \to 0$. Thus the soft gluons are allowed in the cone and the prescription is infrared safe. This also has the advantage of retaining the events which have larger hadronic activity slightly off the photon and we do not unnecessarily loose events. This smooth cone isolation prescription also suppresses QED collinear singularities which arise when the final state photons become collinear to the quark line which emits it. We will subject the photons to this isolation criterion when we obtain kinematical distributions.

A theoretical understanding of this process at NLO was initiated in [17]. A next-to-leading order study in standard model including fragmentation photons was presented in [23] in the context of light Higgs boson searches. In the following we will suppress the fragmentation photons by smooth cone isolation.

In what follows in the remainder of this chapter we will present the computation for the ADD model. Since the spin-2 unparticles couple to the SM energy momentum tensor the results presented for the ADD model are applicable for spin-2 unparticles as well with the modification of the factor $\kappa^2\mathcal{D}(s)$ (see Eqs. 2.3, 2.12) This modification of the coupling constant will be given in a later chapter when we discuss the numerical results.

## 4.2 Leading Order

The lowest order (in strong coupling) Feynman diagram for the process in the standard model is shown in Fig. 7.1. This is of order $\alpha_{em}$ and contributes at order $\alpha_{em}^2$. In addition, $q\overline{q}$ and $gg$ initiated $s$–channel diagrams with a KK graviton exchange also appear at this order as shown in Fig. 7.6. Note that $gg$ initiated process is present at this order. This happens because the SM fields couple via energy momentum tensor to the KK gravitons with equal strength. A parton level $2 \to 2$ process at the leading order is of the generic form

$$a(p_1) + b(p_2) \to \gamma(p_3) + \gamma(p_4). \tag{4.2}$$

where $a$ and $b$ are either quark and anti-quark or gluons. $p_1, p_2$ are momenta of incoming partons and $p_3, p_4$ are momenta of outgoing photons. The exact matrix elements in $n = 4 + \epsilon$ dimensions for $q\overline{q}$ and $gg$ initiated subprocesses are

$$\overline{|M^{(0)}|^2}_{q\overline{q},sm} = \frac{e_q^4}{N}\left[\frac{u}{t} + \frac{t}{u} + \epsilon\left(1 + \frac{u}{t} + \frac{t}{u}\right) + \frac{\epsilon^2}{4}\left(2 + \frac{u}{t} + \frac{t}{u}\right)\right], \tag{4.3}$$

$$\overline{|M^{(0)}|^2}_{q\overline{q},int} = -\kappa^2\mathcal{R}e\mathcal{D}(s)\ \frac{e_q^2}{8N}\left[4\left(t^2 + u^2\right) + \epsilon\left(3t^2 + 3u^2 + 2ut\right)\right], \tag{4.4}$$

$$\overline{|M^{(0)}|^2}_{q\bar{q},gr} = \frac{\kappa^4|\mathcal{D}(s)|^2}{16N}\Big[ut^3+tu^3+\frac{\epsilon}{4}\left(3tu^3+3t^3u+2u^2t^2\right)\Big], \tag{4.5}$$

$$\begin{aligned}\overline{|M^{(0)}|^2}_{gg,gr} &= \frac{\kappa^4|\mathcal{D}(s)|^2}{N^2-1}\Big[\frac{81}{128(3+\epsilon)^2}s^4+\frac{27}{64(3+\epsilon)}s^2\left(u^2+14tu+t^2\right)\\ &+\frac{5}{2(2+\epsilon)^2}s^2tu-\frac{1}{16(2+\epsilon)}s^2\left(7u^2+94tu+7t^2\right)\\ &+\frac{1}{128}\left(9t^4+28t^3u+54t^2u^2+28tu^3+9u^4\right)\Big],\end{aligned} \tag{4.6}$$

where $sm$, $gr$, $int$ represent contributions from SM, gravity, and interference of SM with gravity induced process respectively. Real part of $\mathcal{D}(s)$ is denoted by $\mathcal{R}e\mathcal{D}(s)$. The bar over the symbol $M^{(0)}$ represents that the matrix elements have been averaged over initial helicities and color, and summed over the final ones. Here $\mathcal{D}(s)$ is defined by $\mathcal{D}(s)=\mathcal{D}_{\text{eff}}(s)/i$ (see Eqs. 2.5, 2.12) and

$$\begin{aligned}\kappa^2\mathcal{D}(s) &= \kappa^2\sum_{\vec{n}}\frac{1}{s-m_{\vec{n}}^2+i\epsilon}\,,\\ &= \frac{8\pi}{M_S^4}\left(\frac{\sqrt{s}}{M_S}\right)^{(d-2)}\Big[-i\pi+2I(M_S/\sqrt{s})\Big]\,.\end{aligned} \tag{4.7}$$

$s,t,u$ are the usual Mandelstam invariants

$$s=(p_1+p_2)^2\,,\ t=(p_1-p_3)^2\,,\ u=(p_1-p_4)^2\,, \tag{4.8}$$

and $e_q$ is the charge of a quark or anti-quark and $\kappa$ is the coupling of gravity to SM fields. A factor of $1/2$ has been included for identical final state photons. These expression has been evaluated for quarks with $N$ and gluons with $N^2-1$ color degrees of freedom. We can use these matrix elements and integrate over the 2-body phase space to obtain parton level cross-section. This partonic cross-section can be convoluted with the parton distribution functions to obtain hadronic cross-sections.

$$\begin{aligned}d\sigma^{(0)}(x_1,x_2,\epsilon) &= dx_1dx_2\sum_i d\sigma^{(0)}_{q_i\bar{q}_i}(x_1,x_2,\epsilon)\left(f_{q_i}(x_1)f_{\bar{q}_i}(x_2)+x_1\leftrightarrow x_2\right)\\ &+dx_1dx_2d\sigma^{(0)}_{gg}(x_1,x_2,\epsilon)f_g(x_1)f_g(x_2).\end{aligned} \tag{4.9}$$

Here $d\sigma^{(0)}_{ab}$ denote leading order partonic cross-sections.

## 4.3 Next-to-leading order

### 4.3.1 Virtual

At NLO ie., at order $a_s$, gluonic corrections to the leading order Feynman diagrams need to be included. These are shown in Fig. 7.4. In general the integrals over loop momenta have both ultraviolet and infrared singularities, however, the process under consideration does not contain ultraviolet singularities as these cancel in the sum. This happens for the following reasons. The electromagnetic coupling $\alpha_{em}$ does not receive QCD corrections or equivalently Ward identities ensure cancellation of UV divergences. Secondly the gravitons couple to SM energy momentum tensor which is a conserved quantity and does not get renormalized.

The virtual Feynman graphs fall under three categories (see Figs. 7.4 and 7.7).

- Diagrams that have external leg corrections –fermion self energy and gluon self energy. The fermion self energy, and gluon self energy containing triple gluon vertex give loop integrals with two propagators and are denoted as $B_0$ or $B_\mu$. The one with 4-gluon vertex gives a tadpole, $A_0$. These symbols are explained below.

- Diagrams having vertex corrections. These give rise to integrals with three propagators and depending on the tensor structure they are labeled as $C_0$,$C_\mu$ etc. It will be useful to remember that the vertex correction is proportional to the leading order vertex for massless fermions and does not contain a $\sigma^{\mu\nu}(= i[\gamma^\mu, \gamma^\nu]/2)$ term which is present when the fermions are massive.

- Diagrams with four propagators. The loop corresponding loop integrals are labeled as $D_0, D_\mu$ etc.

Let us now define the tensor integrals which appear in the calculation

$$A_0(M_1) = \int \frac{d^n l}{(4\pi)^n} \frac{1}{D_1}, \tag{4.10}$$

$$B_{\{0,\mu,\mu\nu\}}(p_1, M_1, M_2) = \int \frac{d^n l}{(4\pi)^n} \frac{\{1, l_\mu, l_\mu l_\nu\}}{D_1 D_2}, \tag{4.11}$$

$$C_{\{0,\mu,\mu\nu,\mu\nu\rho\}}(p_1, p_2, M_1, M_2, M_3) = \int \frac{d^n l}{(4\pi)^n} \frac{\{1, l_\mu, l_\mu l_\nu, l_\mu l_\nu l_\rho\}}{D_1 D_2 D_3}, \tag{4.12}$$

$$D_{\{0,\mu,\mu\nu,\mu\nu\rho\}}(p_1, p_2, p_3, M_1, M_2, M_3, M_4) = \int \frac{d^n l}{(4\pi)^n} \frac{\{1, l_\mu, l_\mu l_\nu, l_\mu l_\nu l_\rho\}}{D_1 D_2 D_3 D_4}, \tag{4.13}$$

where the denominators are given by

$$
\begin{aligned}
D_1 &= l^2 - {M_1}^2 + i\epsilon, \\
D_2 &= (l+p_1)^2 - {M_2}^2 + i\epsilon, \\
D_3 &= (l+p_1+p_2)^2 - {M_3}^2 + i\epsilon, \\
D_4 &= (l+p_1+p_2+p_3)^2 - {M_4}^2 + i\epsilon.
\end{aligned}
\tag{4.14}
$$

For generality we have retained $M_i$'s but these are not present in our calculation. The tadpole $A_0$ vanishes in dimensional regularization for massless particles as there is no mass scale in the integral. Similarly $B_0$ vanishes as can be seen by shifting the loop momentum. Using the Lorentz symmetry we can write the above integrals as [73] :

$$
\begin{aligned}
B_\mu &= p_{1\mu} B_1, \\
B_{\mu\nu} &= p_{1\mu} p_{1\nu} + g_{\mu\nu} B_{22}, \\
C_\mu &= p_{1\mu} C_{11} + p_{2\mu} C_{12}, \\
C_{\mu,\nu} &= p_{1\mu} p_{1\nu} + p_{2\mu} p_{2\nu} C_{22} + \{p_1 p_2\}_{\mu\nu} C_{23} + g_{\mu\nu} C_{24}, \\
C_{\mu,\nu,\rho} &= p_{1\mu} p_{1\nu} p_{1\rho} C_{31} + p_{2\mu} p_{2\nu} p_{2\rho} C_{32} + \{p_1 p_1 p_2\}_{\mu\nu\rho} C_{33}, \\
&\qquad + \{p_1 p_2 p_2\}_{\mu\nu\rho} C_{34} + \{p_1 g\}_{\mu\nu\rho} C_{35} + \{p_2 g\}_{\mu\nu\rho} C_{36}, \\
D_\mu &= p_{1\mu} D_{11} + p_{2\mu} D_{12} + p_{3\mu} D_{13}, \\
D_{\mu\nu} &= p_{1\mu} p_{1\nu} D_{21} + p_{2\mu} p_{2\nu} D_{22} + p_{3\mu} p_{3\nu} D_{23} + \{p_1 p_2\}_{\mu\nu} D_{24} \\
&\quad + \{p_1 p_3\}_{\mu\nu} D_{25} + \{p_2 p_3\}_{\mu\nu} D_{26} + g_{\mu\nu} D_{27}, \\
D_{\mu\nu\rho} &= p_{1\mu} p_{1\nu} p_{1\rho} D_{31} + p_{2\mu} p_{2\nu} p_{2\rho} D_{32} + p_{3\mu} p_{3\nu} p_{3\rho} D_{33} + \{p_1 p_1 p_2\}_{\mu\nu\rho} D_{34} \\
&\quad + \{p_1 p_1 p_3\}_{\mu\nu\rho} D_{35} + \{p_1 p_2 p_2\}_{\mu\nu\rho} D_{36} + \{p_1 p_3 p_3\}_{\mu\nu\rho} D_{37} + \{p_2 p_2 p_3\}_{\mu\nu\rho} D_{38} \\
&\quad + \{p_2 p_3 p_3\}_{\mu\nu\rho} D_{39} + \{p_1 p_2 p_3\}_{\mu\nu\rho} D_{310} + \{p_1 g\}_{\mu\nu\rho} D_{311} \\
&\quad + \{p_2 g\}_{\mu\nu\rho} D_{312} + \{p_3 g\}_{\mu\nu\rho} D_{313},
\end{aligned}
\tag{4.15}
$$

where the scalar coefficients $B_i, B_{ij}, C_i, C_{ij}, D_i, D_{ij}, D_{ijk}$ are functions of invariants and the masses $M_i$ and we have used the notation

$$\{p_i p_j p_k\}_{\mu\nu\rho} \equiv \sum_{\sigma(i,j,k)} p_{\sigma(i)\mu} p_{\sigma(j)\nu} p_{\sigma(k)\rho} \ , \tag{4.16}$$

with $\sigma(i,j,k)$ denoting all different permutations of $(i,j,k)$, and

$$\{p_i g\}_{\mu\nu\rho} \equiv p_{i\mu} g_{\nu\rho} + p_{i\nu} g_{\mu\rho} + p_{i\rho} g_{\mu\nu}. \tag{4.17}$$

To keep the arguments general we will not specialize to $p_i^2 = 0$ while we discuss the integral reduction. Introduce $Q_i$ as follows

$$Q_1 = 0 \quad \text{and} \quad Q_i = \sum_{j=1}^{i-1} p_j \quad \text{for} \quad i > 1. \tag{4.18}$$

With this we can introduce

$$\begin{aligned} B_{\{0,\mu,\mu\nu\}}(k,l) &\equiv \int \frac{d^n l}{(4\pi)^n} \frac{\{1, l_\mu, l_\mu l_\nu\}}{D_k D_l}\Big|_{Q_k=0}, \\ C_{\{0,\mu,\mu\nu,\mu\nu\rho\}}(k,l,m) &\equiv \int \frac{d^n l}{(4\pi)^n} \frac{\{1, l_\mu, l_\mu l_\nu, l_\mu l_\nu l_\rho\}}{D_k D_l D_m}\Big|_{Q_k=0}. \end{aligned} \tag{4.19}$$

In the process of reducing to scalar integrals, the integrals $B_\mu$,$B_{\mu\nu}$ etc., will be contracted with the external momenta. This gives in the numerator of integrands factors of $l \cdot p_i$ which can be written as

$$\begin{aligned} 2l \cdot p_1 &= D_2 - D_1 + f_1 \ , \\ 2l \cdot p_2 &= D_3 - D_2 + f_2 \ , \\ 2l \cdot p_3 &= D_4 - D_3 + f_3 \ , \end{aligned} \tag{4.20}$$

where

$$f_i = (M_{i+1})^2 - (M_i)^2 - [(Q_{i+1})^2 - (Q_i)^2]. \tag{4.21}$$

To determine $B_1$ we contract both the sides in Eq. (4.11) with $p_1^\mu$. Substituting $p_1 \cdot l$ in $p_1^\mu B_\mu$ we obtain

$$B_1 = \int \frac{d^n l}{(4\pi)^n} \frac{1}{2} \frac{1}{{p_1}^2} \left[ \frac{1}{D_1} - \frac{1}{D_2} + \frac{f_1}{D_1 D_2} \right] \ . \tag{4.22}$$

In the second integral making a change of variable $l \to l - p_1$ gives

$$B_1 = \frac{1}{2p_1^2} \left[ f_1 B_0 + A_0(M_1) - A_0(M_2) \right] \ . \tag{4.23}$$

With this $B_\mu$ is completely determined in terms of scalar integrals. We note that scalar integrals of lower rank $A_0$ appear after reduction. Next we determine $B_{\mu\nu}$. Contracting $B_{\mu\nu}$ with $g_{\mu\nu}$ gives

$$p_1{}^2 B_{21} + n B_{22} = A_0 M_2 + M_1{}^2 B_0. \tag{4.24}$$

Contracting $B_{\mu\nu}$ with $p_1$,

$$\begin{aligned} p_1{}^\mu B_{\mu\nu} &= \int \frac{d^n l}{(4\pi)^n} \frac{1}{2} \frac{(D_2 - D_1 + f_1)\, l_\mu}{D_1 D_2} \\ &= \frac{p_{1\mu}}{2} A_0(M_2) + \frac{f_1}{2} B_\mu. \end{aligned}$$

Contracting with $p_1$ we can determine $B_{21}$

$$B_{21} = \frac{1}{p_1^2} \left\{ \frac{f_1 B_1 + A_0(M_2)}{2}. - B_{22} \right\} \tag{4.25}$$

Substituting $B_{21}$ in (4.24) determines $B_{22}$

$$B_{22} = \frac{1}{n-1} \left( M_1^2 B_0 - \frac{1}{2} [f_1 B_1 - A_0(M_2)] \right) . \tag{4.26}$$

Next we consider three point integral $C_\mu$ and determine the coefficients $C_{11}$ and $C_{12}$.

$$C_\mu = p_{1\mu} C_{11} + p_{2\mu} C_{12}. \tag{4.27}$$

Dotting this equation with $p_1$ and $p_2$ we get two equation which can be written in a matrix form as

$$\begin{aligned} \begin{pmatrix} p_1^\mu \\ p_2^\mu \end{pmatrix} C_\mu &= \begin{pmatrix} p_1^2 C_{11} + p_1 \cdot p_2 C_{12} \\ p_1 \cdot p_2 C_{11} + p_2^2 C_{12} \end{pmatrix} \\ &= \begin{pmatrix} p_1^2 & p_1 \cdot p_2 \\ p_1 \cdot p_2 & p_2^2 \end{pmatrix} \begin{pmatrix} C_{11} \\ C_{12} \end{pmatrix} = \begin{pmatrix} R_1 \\ R_2 \end{pmatrix}. \end{aligned} \tag{4.28}$$

We can determine $R_1$ and $R_2$ and use them to determine $C_{11}$ and $C_{12}$

$$R_1 = \int \frac{d^n l}{(4\pi)^n} \frac{1}{2} \frac{D_2 - D_1 + f_1}{D_1 D_2 D_3}. \tag{4.29}$$

Canceling the common factors in numerators and denominators in the various terms and shifting momenta we get

$$R_1 = \frac{1}{2} \left[ B_0(1,3) - B_0(2,3) + f_1 C_0 \right], \tag{4.30}$$

and similarly

$$R_2 = \frac{1}{2}\left[B_0(1,2) - B_0(1,3) + f_2 C_0\right]. \tag{4.31}$$

Following a similar procedure all other tensor integrals can be reduced. A compilation of the results can be found in [74]. Using the above integrals we can calculate the order $a_s$ squared matrix elements coming from virtual processes. The SM virtual diagrams are shown in Fig. 7.4. We see all 2-,3- and 4-point integrals appear. The virtual correction diagrams with a graviton propagator are shown in Fig. 7.7. Since the 3-gluon and 4-gluon vertices appear in Fig. 7.7h and Fig. 7.7(g) to correctly include the physical degrees of freedom the ghosts need to be included as shown in Fig. 7.7(e) and Fig. 7.7(f) .

The SM contribution at virtual level comes purely from $q\overline{q}$ initiated processes shown in Fig. 7.4 (a-d) and is given by

$$\begin{aligned}\overline{|M^V|^2}_{q\overline{q},sm} &= a_s(\mu_R^2) f(\epsilon,\mu_R^2,s) C_F \Bigg[\Upsilon(\epsilon)\ \overline{|M^{(0)}|^2}_{q\overline{q},sm} + 2\frac{e_q^4}{N}\Bigg\{(4\zeta(2)-7)\frac{u}{t} \\ &+\left(2+3\frac{u}{t}\right)\ln\frac{-t}{s} + \left(2+\frac{u}{t}+2\frac{t}{u}\right)\ln^2\frac{-t}{s} + t\leftrightarrow u\Bigg\}\Bigg],\end{aligned} \tag{4.32}$$

where

$$\Upsilon(\epsilon) = -\frac{16}{\epsilon^2}+\frac{12}{\epsilon}, \qquad f(\epsilon,\mu_R^2,s) = \frac{\Gamma\left(1+\frac{\epsilon}{2}\right)}{\Gamma(1+\epsilon)}\left(\frac{s}{4\pi\mu_R^2}\right)^{\frac{\epsilon}{2}} \tag{4.33}$$

There are two kinds of contributions that come from the interference of SM and gravity mediated processes; the $q\overline{q}$ initiated processes and $gg$ initiated processes. The $gg$ initiated box diagrams of Fig. 7.4(e) in SM interferes with the LO graviton mediated diagrams. The subscript $(int)$ indicates interference.

$$\begin{aligned}\overline{|M^V|^2}_{q\overline{q},int} &= a_s(\mu_R^2) f(\epsilon,\mu_R^2,s) C_F \Bigg[\Upsilon(\epsilon)\,\overline{|M^{(0)}|^2}_{q\overline{q},int} + \kappa^2 \mathcal{R}e\mathcal{D}(s)\frac{e_q^2}{2N}\Bigg\{(17-8\zeta(2))t^2 \\ &-(2tu+3u^2)\ln\frac{-t}{s} - \left(2tu+2t^2+u^2\right)\ln^2\frac{-t}{s} + t\leftrightarrow u\Bigg\} \\ &-\kappa^2\pi\mathcal{I}m\mathcal{D}(s)\frac{e_q^2}{2N}\Bigg\{3t^2+2tu+2(t^2+2tu+2u^2)\ln\frac{-u}{s} + t\leftrightarrow u\Bigg\}\Bigg]\end{aligned} \tag{4.34}$$

$$\begin{aligned}\overline{|M^V|^2}_{gg,int} &= a_s(\mu_R^2)\ e_q^2\kappa^2\ \frac{1}{N^2-1}\Bigg[s\ \mathcal{R}e\mathcal{D}(s)\ \Bigg\{u^2+(2tu+t^2)\ln\frac{-u}{s} \\ &+\left(u^2+\frac{1}{2}t^2+tu\right)\ln^2\frac{-u}{s}\Bigg\} + s\ \pi\mathcal{I}m\mathcal{D}(s)\ \Bigg\{u^2+2tu \\ &+(2u^2+2tu+t^2)\ln\frac{-u}{s}\Bigg\} + t\leftrightarrow u\Bigg].\end{aligned} \tag{4.35}$$

The contributions coming purely from gravity mediated diagrams are

$$\overline{|M^V|^2}_{q\overline{q},gr} = a_s(\mu_R^2) f(\epsilon, \mu_R^2, s) C_F \left[ \Upsilon(\epsilon)\, \overline{|M^{(0)}|^2}_{q\overline{q},gr} + 4(2\zeta(2) - 5) \overline{|M^{(0)}|^2}_{q\overline{q},gr} \right] \quad (4.36)$$

$$\begin{aligned} \overline{|M^V|^2}_{gg,gr} &= a_s(\mu_R^2) f(\epsilon, \mu_R^2, s) C_A \left[ \left\{ -\frac{16}{\epsilon^2} + \frac{4}{C_A \epsilon} \left( \frac{11}{3} C_A - \frac{4}{3} n_f T_F \right) \right\} \overline{|M^{(0)}|^2}_{gg,gr} \right. \\ &+ \left. \frac{1}{9} \left( 72\zeta(2) + 70 \frac{n_f T_F}{C_A} - 203 \right) \overline{|M^{(0)}|^2}_{gg,gr} \right], \end{aligned} \quad (4.37)$$

Here $\mu_R^2$ is the scale at which the theory is renormalized. The SM results are in agreement with the literature [75].

Let us analyze the results we have obtained above.

- We first observe that the $q\overline{q}$ and $gg$ initiated matrix element squares in pure gravity case are proportional to their leading order contributions. But this is spoiled for the SM $q\overline{q}$ initiated process due to the appearance of 4-point integrals.

- Next we see that all the $q\overline{q}$ initiated processes have the same singularity structure. They are all proportional to their respective born matrix element squares and are multiplied by the same common factor $a_s(\mu_R^2) C_F \Upsilon(\epsilon)$. The $gg$ initiated process is also proportional to its born contribution and $C_A$ appears in the coefficients. $C_F$ appears in $q\overline{q}$ case as fermions transform under fundamental representation of SU(N) and $C_A$ appears in $gg$ initiated process as gluons transform under the adjoint representation. More information on $C_F$ and $C_A$ can be found in the appendix. The reason for the universality in the singular pieces is that these are coming purely from QCD. The poles in $\Upsilon(\epsilon)$ arise due to soft and collinear singularities. As already mentioned there are no ultraviolet divergences here and the poles are purely of infrared origin. The soft singularities arise when gluon momentum in loop becomes vanishingly small. Similarly collinear singularity arises when two massless partons become collinear to each other. These singularities appear when two propagators go onshell simultaneously and the contour of the integral gets pinched between two poles. The soft and collinear singularities appear as poles in $\epsilon$ in dimensional regularization. The $1/\epsilon^2$ pole in $\Upsilon(\epsilon)$ arises because a gluon can be simultaneously soft and parallel to the parton which emits it. Thus it is a product of soft and collinear singularity.

- The interference of $gg$ initiated box diagrams in SM with leading order gravity mediated process does not contain any poles in $\epsilon$ and is completely finite. This is finite as the $gg$ box contribution ( sum of six diagrams ) is finite. That it should be finite is understandable as this is the first time a $gg$ initiated contribution appears and is like a leading order piece.

Using the above matrix elements, the virtual contribution to cross-section can be obtained by integrating over the phase space and multiplying with parton distribution functions.

$$\begin{aligned} d\sigma^{virt} &= a_s(\mu_R^2) dx_1 dx_2 f(\epsilon, \mu_R^2, s) \\ & \times \Bigg[ C_F \left( -\frac{16}{\epsilon^2} + \frac{12}{\epsilon} \right) \sum_i d\sigma^{(0)}_{q_i \overline{q}_i}(x_1, x_2, \epsilon) \left( f_{q_i}(x_1) f_{\overline{q}_i}(x_2) + x_1 \leftrightarrow x_2 \right) \\ & + C_A \left\{ -\frac{16}{\epsilon^2} + \frac{4}{C_A \epsilon} \left( \frac{11}{3} C_A - \frac{4}{3} n_f T_F \right) \right\} d\sigma^{(0)}_{gg}(x_1, x_2, \epsilon) \Big( f_g(x_1) f_g(x_2) \Big) \\ & + C_F \sum_i d\sigma^{V,fin}_{q_i \overline{q}_i}(x_1, x_2, \epsilon) \left( f_{q_i}(x_1) f_{\overline{q}_i}(x_2) + x_1 \leftrightarrow x_2 \right) \\ & + C_A \; d\sigma^{V,fin}_{gg}(x_1, x_2, \epsilon) (f_g(x_1) f_g(x_2)) \Bigg] \end{aligned} \tag{4.38}$$

where $d\sigma^{V,fin}_{q\overline{q}}(x_1, x_2, \epsilon)$ is the finite (in $\epsilon \to 0$ limit) coefficient of $a_s(\mu_R^2) f(\epsilon, \mu_R^2, s) C_F$ that appears in the above matrix element squares and integrated over 2-body phase space and similarly $d\sigma^{V,fin}_{gg}(x_1, x_2, \epsilon)$ is the finite coefficient of $a_s(\mu_R^2) f(\epsilon, \mu_R^2, s) C_A$ integrated over 2-body phase space.

### 4.3.2 Real Emission

We have seen in the previous subsection that the contributions coming from virtual processes are singular in 4-dimensions. According to the Bloch-Nordsick theorem [76] soft divergences cancel, when both the virtual and their corresponding bremsstrahlung diagrams are taken into account. For cancellation of soft singularity inclusion of soft bremsstrahlung, which gives states degenerate to leading order states, is required. One can choose some cutoff $\mathcal{E}$ for energy of real gluons (experimentally it translates to cutoff on jet energy) and include only the ones which have energies less than $\mathcal{E}$. However, then, the final result would depend on $\mathcal{E}$. Instead, it is more useful to integrate over the final state gluons completely. The remaining collinear singularities are removed by mass factorization. In this subsection we present the contributions coming from order $a_s$ processes where in addition to the two photons in the final state a parton is also emitted.

Eventually we will put several experimental cuts on the two photons to isolate them from the photons coming from hadron decays such as $\pi^0$ decays. Also we will obtain many kinematical distributions to facilitate comparison with experiments. These requirements make a Monte Carlo based method most apt for the computation. It facilitates an easy implementation of kinematical constraints and repetition of calculation for different distributions is not required. With these things in mind we have opted for a semi numerical approach based on the method of *two cutoff phase space slicing method* . This method [77] has already been used extensively to study various processes and has been nicely reviewed in [78].

The idea of the two cutoff phase space slicing method is simple. The matrix elements and phase space simplify in the soft and collinear limit, thus the phase space integrals can be easily carried out analytically to get the soft and collinear singularities. After the cancellation and mass factorization of these singularities the remaining finite pieces are integrated numerically using Monte Carlo. The region of phase space which is free of any singularities can again be integrated numerically and added to the above piece to get real emission contributions. Thus in this method two small dimensionless parameters $\delta_s$ and $\delta_c$ are introduced to divide the 3-body phase space into singular and non-singular regions. The parameter $\delta_s$ slices phase space into soft and hard regions. The soft region contains soft gluons. The hard region is further decomposed into collinear and non-collinear regions parts using $\delta_c$. This region contains collinear singularities. The hard non-collinear region which is free of any singularities can be directly integrated in 4-dimensions.

In the following we will describe the computation using phase space slicing method. First we will obtain real emission contribution to cross section in the soft limit and then in the collinear limit.

### Soft

The following momenta assignment for real emission diagrams will be used

$$a(p_1) + b(p_2) \to \gamma(p_3) + \gamma(p_4) + c(p_5). \tag{4.39}$$

The Lorentz scalars that appear can be written as $p_{ij} = (p_i + p_j)^2$ if both $i$ and $j$ are either incoming particles or outgoing particles. When one of them is incoming and the other is outgoing we use $p_{ij} = (p_i - p_j)^2$. The incoming parton momenta in the center of mass frame of incoming partons can be written using above definition of scalars, in $n$ dimensions, as

$$\begin{aligned} p_1 &= \frac{\sqrt{p_{12}}}{2}\,(1, 0, 0, \cdots, 0, 1)\,, \\ p_2 &= \frac{\sqrt{p_{12}}}{2}\,(1, 0, 0, \cdots, 0, -1)\,, \end{aligned} \tag{4.40}$$

The Feynman diagrams in Figs. 7.5(a), 7.5(b) give soft divergences when the final state gluons become soft. Similarly diagrams in Figs. 7.8(a), 7.8(b) and Figs. 7.8(i), 7.8(j) are divergent in the soft limit. Let us first consider $q\overline{q}$ initiated process and denote by $M_1$ the sum of diagrams Figs. 7.5(a) and 7.8(a), and by $M_2$ the sum of diagrams Figs. 7.5(b) and 7.8(b). In $M_1$ the gluon is attached to the fermion line carrying momentum $p_1$ and in $M_2$ to the fermion line with momentum $p_2$. Using $\delta_s$ soft region can be defined as the region of phase space where the final state gluon has an energy less than $\delta_s\sqrt{p_{12}}/2$ in the centre of mass frame of incoming partons. Let us now simplify the matrix elements in soft limit. In this limit the matrix elements take the following simple form

$$M_1^a \simeq M^{(0)}\left(p_1,p_2\to p_3,p_4\right)\left[T^a_{ji}\frac{p_1^\mu}{p_1\cdot p_5}\right]\mu_R^{-\frac{\epsilon}{2}} g_s\ \epsilon_\mu(p_5),$$

$$M_2^a \simeq M^{(0)}\left(p_1,p_2\to p_3,p_4\right)\left[-T^a_{ji}\frac{p_2^\mu}{p_2\cdot p_5}\right]\mu_R^{-\frac{\epsilon}{2}} g_s\ \epsilon_\mu(p_5). \tag{4.41}$$

Here $M^{(0)}$ denotes the born amplitude and $a$ is the color index carried by the soft gluon. The factors in the square brackets are the eikonal currents which factor out in the soft limit. The square of the sum of the above two matrix elements averaged and summed over initial and final state color and polarizations is

$$\overline{|M_1+M_2|^2}_{q\bar q} \simeq \frac{2p_1\cdot p_2}{p_1\cdot p_5\ p_2\cdot p_5}\ C_F\mu_R^{-\epsilon}g_s^2\ \overline{|M^{(0)}|^2}_{q\bar q}\left(p_1,p_2\to p_3,p_4\right). \tag{4.42}$$

Similarly for the $gg$ initiated real emission process we denote by $M_1$ the diagram Fig. 7.8(i) and by $M_2$ the diagram Fig. 7.8(j). In the soft limit

$$\overline{|M_1+M_2|^2}_{gg} \simeq \frac{2p_1\cdot p_2}{p_1\cdot p_5\ p_2\cdot p_5}\ C_A\mu_R^{-\epsilon}g_s^2\ \overline{|M^{(0)}|^2}_{gg}\left(p_1,p_2\to p_3,p_4\right). \tag{4.43}$$

The soft singularities get revealed when the phase space integration over the eikonal factors is carried out. Let us now simplify the phase space in this limit. The three body phase space

$$d\Gamma_3 = \prod_{i=3}^{5}\frac{d^{n-1}p_i}{(2\pi)^{n-1}}\frac{1}{2E_i}(2\pi)^n\delta^n(p_1+p_2-p_3-p_4-p_5), \tag{4.44}$$

in the soft limit can be written as

$$d\Gamma_3^{Soft} = d\Gamma_2\frac{d^{n-1}p_5}{(2\pi)^{n-1}}\frac{1}{2E_5}, \tag{4.45}$$

where

$$d\Gamma_2 = \prod_{i=3}^{4}\frac{d^{n-1}p_i}{(2\pi)^{n-1}}\frac{1}{2E_i}(2\pi)^n\delta^n(p_1+p_2-p_3-p_4), \tag{4.46}$$

is the two body phase space. Parameterizing gluon's momenta in $p_1+p_2$ rest frame as

$$p_5 = E_5\left(1,0,\cdots,0,\sin\theta_1\sin\theta_2,\sin\theta_1\cos\theta_2,\cos\theta_1\right), \tag{4.47}$$

we can write

$$d\Gamma_3^{Soft} = d\Gamma_2\left(\frac{4\pi}{p_{12}}\right)^{-\frac{\epsilon}{2}}\frac{\Gamma\left(1+\frac{\epsilon}{2}\right)}{\Gamma(1+\epsilon)}\frac{1}{2(2\pi)^2}d\mathcal{S}, \tag{4.48}$$

where

$$d\mathcal{S} = \frac{1}{\pi}\left(\frac{4}{p_{12}}\right)^{\frac{\epsilon}{2}} \int_0^{\delta_s\sqrt{p_{12}}/2} dE_5 E_5^{1+\epsilon}\ \sin^{1+\epsilon}\theta_1 d\theta_1 \sin^{\epsilon}\theta_2 d\theta_2. \tag{4.49}$$

Let us now carry out the $d\mathcal{S}$ integrals over eikonal factor

$$\frac{2p_1\cdot p_2}{p_1\cdot p_5 p_2\cdot p_5} \tag{4.50}$$

appearing in 4.42 and 4.43. Substituting

$$\begin{aligned} 2p_1\cdot p_2 &= p_{12}, \\ p_1\cdot p_5 &= \frac{\sqrt{p_{12}}}{2}E_5(1-\cos\theta_1), \\ p_2\cdot p_5 &= \frac{\sqrt{p_{12}}}{2}E_5(1+\cos\theta_1), \end{aligned} \tag{4.51}$$

it factors into an energy integral and an angular integral:

$$\begin{aligned} J &= \frac{1}{\pi}\left(\frac{4}{p_{12}}\right)^{\frac{\epsilon}{2}} \int_0^{\delta_s\sqrt{p_{12}}/2} dE_5 E_5^{-1+\epsilon} \\ &\times \int_0^{\pi} \sin^{1+\epsilon}\theta_1 d\theta_1 \int_0^{\pi} \sin^{\epsilon}\theta_2 d\theta_2 \frac{4}{(1+\cos\theta_1)(1-\cos\theta_2)}. \end{aligned} \tag{4.52}$$

The energy integral can be done trivially and gives

$$\frac{1}{\epsilon}\left(\delta_s\frac{\sqrt{p_{12}}}{2}\right)^{\epsilon}. \tag{4.53}$$

To carry out angular integral we use the result [79, 80, 81]

$$\int_0^{\pi} d\theta_1 \sin^{n-3}\theta_1 \int_0^{\pi} d\theta_2 \sin^{n-4}\theta_2 \frac{(a+b\cos\theta_1)^{-1}}{A+B\cos\theta_1+C\sin\theta_1\cos\theta_2}$$

$$= \frac{2\pi}{aA(n-4)}\left(\frac{A+B}{2A}\right)^{n/2-3}\left[1+\frac{1}{4}(n-4)^2 Li_2\left(\frac{A-B}{2A}\right)\right],$$

if $A^2 = B^2 + C^2$, $b = -a$, $Li_2(0) = 0$. The dilogarithm function $Li_2$ is very briefly discussed in the appendix. Using this the angular integral gives

$$\int_0^{\pi} \sin^{1+\epsilon}\theta_1 d\theta_1 \int_0^{\pi} \sin^{\epsilon}\theta_2 d\theta_2 \frac{4}{(1+\cos\theta_1)(1-\cos\theta_2)} = \frac{8\pi}{\epsilon}. \tag{4.54}$$

Note that this pole comes when the gluon becomes collinear to the quark or antiquark line. With this we have

$$J = \frac{8}{\epsilon^2} + \frac{8 \ln \delta_s}{\epsilon} + 4 \ln^2 \delta_s. \tag{4.55}$$

This gives finally

$$\begin{aligned} d\Gamma_3 \overline{|M_1 + M_2|^2}_{q\overline{q}} &\overset{soft}{\simeq} a_s C_F f(\epsilon, \mu_R^2, p_{12})\ d\Gamma_2 \overline{|M^{(0)}|^2}_{q\overline{q}} \\ &\times \left( \frac{16}{\epsilon^2} + \frac{16 \ln \delta_s}{\epsilon} + 8 \ln^2 \delta_s \right), \end{aligned} \tag{4.56}$$

and

$$\begin{aligned} d\Gamma_3 \overline{|M_1 + M_2|^2}_{gg} &\overset{soft}{\simeq} a_s C_A f(\epsilon, \mu_R^2, p_{12})\ d\Gamma_2 \overline{|M^{(0)}|^2}_{gg} \\ &\times \left( \frac{16}{\epsilon^2} + \frac{16 \ln \delta_s}{\epsilon} + 8 \ln^2 \delta_s \right), \end{aligned} \tag{4.57}$$

where

$$f(\epsilon, \mu_R^2, p_{12}) = \frac{\Gamma\left(1 + \frac{\epsilon}{2}\right)}{\Gamma(1+\epsilon)} \left( \frac{4\pi \mu_R^2}{p_{12}} \right)^{-\epsilon/2}. \tag{4.58}$$

We can now write the final expression for soft part of cross-section

$$\begin{aligned} d\sigma^{soft} \simeq\ & a_s dx_1 dx_2 f(\epsilon, \mu_R^2, p_{12}) \left( \frac{16}{\epsilon^2} + \frac{16 \ln \delta_s}{\epsilon} + 8 \ln^2 \delta_s \right) \\ & \times \Bigg[ \Bigg( C_F \sum_i d\sigma^{(0)}_{q_i \overline{q}_i}(x_1, x_2, \epsilon) f_{q_i}(x_1) f_{\overline{q}_i}(x_2) + x_1 \leftrightarrow x_2 \Bigg) \\ & + C_A\ d\sigma^{(0)}_{gg}(x_1, x_2, \epsilon) f_g(x_1) f_g(x_2) \Bigg]. \end{aligned} \tag{4.59}$$

The pole of order 2 comes from gluons which are both soft and collinear. Note that the coefficient of this double pole has the same coefficient but opposite sign to what was obtained in the virtual case. Thus we see that the order 2 pole cancels between real emission and virtual contributions. The simple poles in $\epsilon$ still remain uncanceled. Let us next take up the collinear singularities.

## Collinear

First we will give details for a $q\overline{q}$ initiated process with emission of a gluon in the final state. The other processes will follow the similar steps. Let us consider the leading order

$q\overline{q}$ initiated process. In this we properly include all the contributions coming from SM, gravity mediated processes and their interference with SM. Let a fraction $x_1$ of hadron $H_1$ momentum be carried by the quark carrying momentum $p_1$, and a fraction $x_2$ of hadron $H_2$ be carried by the anti-quark carrying momentum $p_2$. Next consider a next-to-leading order process, with a quark and an anti-quark in the initial state which has as its hard scattering part the above leading order process. For clarity we will use $\overline{p}_1$ instead of $p_1$ for the momentum of the incoming quark. Let $y$ be the fraction of hadron momentum carried by $\overline{p}_1$. Also let $z$ denote the fraction of $\overline{p}_1$ that enters into the hard scattering with $1-z$ taken away by the final state gluon. With this we can write the momenta in the collinear limit as

$$\begin{aligned}
\overline{p}_1 &= (P, 0, \cdots, 0, P) \\
\overline{p}'_1 &= \left(zP + \frac{{p_t}^2}{2zP}, \vec{p}_t, zP\right) \\
p_5 &= \left((1-z)P + \frac{{p_t}^2}{2(1-z)P}, -\vec{p}_t, (1-z)P\right).
\end{aligned} \tag{4.60}$$

In this limit the matrix elements can be simplified to obtain

$$\begin{aligned}
\overline{|M|^2}(\overline{p}_1 + p_2 \rightarrow p_3 + p_4 + p_5) &\overset{coll}{\simeq} \overline{|M^{(0)}|^2}(z\overline{p}_1, p_2 \rightarrow p_3 + p_4) \\
&\quad \times P_{qq}(z, \epsilon) g_s^2 \mu_R^{-\epsilon} \frac{-1}{2z\overline{p}_{15}}.
\end{aligned} \tag{4.61}$$

The 3-body phase space can again be simplified in the same limit. To do the integral over $d^{n-1}p_5$ we note that

$$\overline{p}_{15} = \frac{-p_t^2}{1-z}, \tag{4.62}$$

using this we can readily write

$$d^{n-1}p_5 = P dz \left[-(1-z) d\overline{p}_{15}\right]^{\frac{n-2}{2}} d^{n-1}p_5 = P dz \left[-(1-z) d\overline{p}_{15}\right]^{\frac{n-2}{2}} \frac{\pi^{1+\epsilon/2}}{\Gamma(1+\frac{\epsilon}{2})}. \tag{4.63}$$

Finally the integral over the final state gluon momentum in the phase space integral can be written as

$$\frac{d^{n-1}p_5}{2E_5(2\pi)^{n-1}} = \frac{(4\pi)^{-\epsilon/2}}{16\pi^2\Gamma(1+\frac{\epsilon}{2})} dz d\overline{p}_{15} \left[-(1-z) d\overline{p}_{15}\right]^{\frac{\epsilon}{2}}. \tag{4.64}$$

Collinear singularities get revealed when integration over $\overline{p_{15}}$ is carried out in the collinear region

$$0 < -\overline{p}_{15} < \delta_c \overline{p}_{12}, \tag{4.65}$$

giving

$$\int_0^{\delta_c \overline{p}_{12}} -d\overline{p}_{15}(-\overline{p}_{15})^{-1+\frac{\epsilon}{2}} = \frac{2}{\epsilon}(\delta_c \overline{p}_{12})^{\frac{\epsilon}{2}}. \tag{4.66}$$

Thus we can write the hard collinear part of cross-section as

$$\begin{aligned} d\sigma^{HC} &= f_{q_i/H_1}(y)dy f_{\overline{q}_i/H_2}(x_2)dx_2 \; d\hat{\sigma}^{(0)}_{q_i\overline{q}_i}(z\overline{p}_{12}, p_{23}, p_{24}) \\ &\times a_s(\mu_R^2)\left(\frac{4\pi\mu_R^2}{\overline{p}_{12}}\right)^{-\epsilon/2} \frac{\Gamma\left(1+\frac{\epsilon}{2}\right)}{\Gamma(1+\epsilon)} \\ &\times \left(\frac{1}{\epsilon}\right)\delta_c^{\epsilon/2} P_{qq}(z,\epsilon)dz(1-z)^{\epsilon/2}\delta(yz-x_1)dx_1. \end{aligned} \tag{4.67}$$

Note that in writing the above expression we have appropriately absorbed a factor of $1/z$ in the flux factor of $d\hat{\sigma}^{(0)}_{q_i\overline{q}_i}$. In order to be able to factorize collinear singularities we require to have $d\hat{\sigma}^{(0)}_{q_i\overline{q}_i}$ in the above expression same as that appears at the leading order. This is done by the delta function which ensures that $x_1$ enters into the hard scattering. Remembering that $\overline{p}_1 = yp_{H_1}$ and $p_1 = x_1 p_{H_1}$ we can write $\overline{p}_1 = y/x_1 p_1$. Thus $z\overline{p}_{12} = zy/x_1 p_1 = p_1$ Making this substitution and carrying out integration over $y$ we obtain

$$\begin{aligned} d\sigma^{HC} &= f_{q/H_1}(x_1/z)dx_1 f_{\overline{q}/H_2}(x_2)dx_2 \; d\hat{\sigma}^{(0)}_{q_i\overline{q}_i}(p_{12}, p_{23}, p_{24}) \\ &\times a_s(\mu_R^2)\left(\frac{4\pi\mu_R^2}{p_{12}}\right)^{-\epsilon/2} \frac{\Gamma\left(1+\frac{\epsilon}{2}\right)}{\Gamma(1+\epsilon)} \\ &\times \left(\frac{1}{\epsilon}\right)\delta_c^{\epsilon/2} P_{qq}(z,\epsilon)\frac{dz}{z}\left(\frac{1-z}{z}\right)^{\epsilon/2}. \end{aligned} \tag{4.68}$$

The invariants that appear in the argument of the leading order cross-section in above expression pertain to leading order kinematics. We can now rename $\overline{p}_1$ as $p_1$ without causing any confusion. The hard condition sets the limits on $z$ integration. To determine the limits let us first write the energy of the gluon in $p_1 + p_2$ rest frame. Squaring both sides of energy momentum conservation $p_1 + p_2 - p_5 = p_3 + p_4$ relation we obtain

$$(p_1 + p_2)^2 - 2p_5 \cdot (p_1 + p_2) = (p_3 + p_4)^2. \tag{4.69}$$

In the $p_1 + p_2$ rest frame $p_1 + p_2 = \sqrt{p_{12}}(1, 0, 0, 0)$. Using this the gluon's energy evaluates to

$$E_5 = \frac{p_{12} - p_{34}}{2\sqrt{p_{12}}}. \tag{4.70}$$

In the collinear limit we have $(zp_1 + p_2)^2 = (p_3 + p_4)^2$ which gives $p_{34} = zp_{12}$. The hard condition $E_5 > \delta_s\sqrt{p_{12}}/2$ gives the condition on $z$:

$$0 < z < 1 - \delta_s, \quad \text{hard condition.} \tag{4.71}$$

Finally we can write the contribution to Hard Collinear part of cross-section coming from $P_{qq}$ splitting, now allowing either of the quark and anti-quark to emit a gluon.

$$\begin{aligned} d\sigma^{HC} &= \frac{a_s(\mu_R^2)}{\epsilon} dx_1 dx_2 f(\epsilon, \mu_R^2, s) \\ &\times \Bigg[ \sum_i d\hat{\sigma}^{(0)}_{q_i\overline{q}_i}(x_1, x_2, \epsilon) \Bigg\{ \int_{x_2}^{1-\delta_s} \frac{dz}{z} \mathcal{H}(z, \epsilon, \delta_c) P_{qq}(z, \epsilon) f_{q_i}(x_1) f_{\overline{q}_i}(x_2/z) \\ &+ \sum_i \int_{x_1}^{1-\delta_s} \frac{dz}{z} \mathcal{H}(z, \epsilon, \delta_c) P_{qq}(z, \epsilon) f_{q_i}(x_1/z) f_{\overline{q}_i}(x_2) + x_1 \leftrightarrow x_2 \Bigg\}_{q\overline{q}} \Bigg] \end{aligned} \tag{4.72}$$

where

$$\mathcal{H}(z, \epsilon, \delta_c) = \left( \delta_c \frac{1-z}{z} \right)^{\epsilon/2}, \tag{4.73}$$

and $P_{qq}$ is the splitting function in $4 + \epsilon$ dimensions. When quark $q_i$ emits a gluon the combination $f_{q_i}(x_1/z) f_{\overline{q}_i}(x_2)$ appears and when anti-quark $\overline{q}_i$ emits a gluon the combination $f_{\overline{q}_i}(x_1/z) f_{q_i}(x_2)$ enters. $x_1 \leftrightarrow x_2$ is included because the two partons can have their momenta interchanged. Similarly we can find the contributions coming from the $gg$ initiated processes. Here $P_{gg}$ splitting function is involved. The integration limits on $z$ remain the same. In addition to these we also have to include the $qg$ initiated subprocesses. Here a gluon can split into a quark and and anti-quark with one of these entering into the hard scattering. This involves $P_{qg}$ splitting function. Alternatively the initial state fermion can split into gluon and a fermion with the gluon entering into the hard scattering, this involves $P_{gq}$ splitting function. In both of these cases the particle which is emitted in the final state is a fermion, which does not give soft singularities. The upper limit on the $z$ integral is 1 in these cases. Adding all the pieces together we get

$$\begin{aligned} d\sigma^{HC} &= \frac{a_s(\mu_R^2)}{\epsilon} dx_1 dx_2 f(\epsilon, \mu_R^2, p_{12}) \\ &\times \Bigg[ \sum_i d\hat{\sigma}^{(0)}_{q_i\overline{q}_i}(x_1, x_2, \epsilon) \Bigg\{ \int_{x_2}^{1-\delta_s} \frac{dz}{z} \mathcal{H}(z, \epsilon, \delta_c) P_{qq}(z, \epsilon) f_{q_i}(x_1) f_{\overline{q}_i}(x_2/z) \\ &+ \int_{x_1}^{1-\delta_s} \frac{dz}{z} \mathcal{H}(z, \epsilon, \delta_c) P_{qq}(z, \epsilon) f_{q_i}(x_1/z) f_{\overline{q}_i}(x_2) + x_1 \leftrightarrow x_2 \Bigg\}_{q\overline{q}} \end{aligned}$$

$$+\sum_i d\hat{\sigma}^{(0)}_{q_i\overline{q}_i}(x_1,x_2,\epsilon)\Big\{\int_{x_2}^{1}\frac{dz}{z}\mathcal{H}(z,\epsilon,\delta_c)P_{qg}(z,\epsilon)f_{q_i}(x_1)f_g(x_2/z)$$

$$+\int_{x_2}^{1}\frac{dz}{z}\mathcal{H}(z,\epsilon,\delta_c)P_{qg}(z,\epsilon)f_{\overline{q}_i}(x_1)f_g(x_2/z)+x_1\leftrightarrow x_2\Big\}_{qg}$$

$$+d\hat{\sigma}^{(0)}_{gg}(x_1,x_2,\epsilon)\Big\{\int_{x_2}^{1-\delta_s}\frac{dz}{z}\mathcal{H}(z,\epsilon,\delta_c)P_{gg}(z,\epsilon)f_g(x_1)f_g(x_2/z)+x_1\leftrightarrow x_2\Big\}_{gg}$$

$$+d\hat{\sigma}^{(0)}_{gg}(x_1,x_2,\epsilon)\Big\{\int_{x_2}^{1-\delta_s}\frac{dz}{z}\mathcal{H}(z,\epsilon,\delta_c)P_{gq}(z,\epsilon)\sum_i f_g(x_1)f_{q_i}(x_2/z)$$

$$+\int_{x_2}^{1-\delta_s}\frac{dz}{z}\mathcal{H}(z,\epsilon,\delta_c)P_{gq}(z,\epsilon)\sum_i f_g(x_1)f_{\overline{q}_i}(x_2/z)+x_1\leftrightarrow x_2\Big\}_{qg}\Bigg]. \quad (4.74)$$

In the above expression we see that the collinear poles are proportional to the leading order cross-sections. Let us introduce the convolution symbol $\otimes$ commonly used. It is defined as

$$\begin{aligned}(f\otimes g)(x) &= \int_x^1\frac{dz}{z}f(z)g(x/z)\\ &= \int_0^1\int_0^1 dz_1dz_2\ f(z_1)g(z_2)\ \delta(z_1z_2-x).\end{aligned} \quad (4.75)$$

Let us also introduce a symbol $\overline{\otimes}$ if the upper limit of integration is not 1.

$$(f\overline{\otimes}g)(x) = \int_x^{1-\delta_s}\frac{dz}{z}f(z)g(x/z). \quad (4.76)$$

With these we can write the hard collinear piece as

$$\begin{aligned}d\sigma^{HC} &= \frac{a_s(\mu_R^2)}{\epsilon}dx_1dx_2f(\epsilon,\mu_R^2,p_{12})\\ &\times\Big[\sum_i d\hat{\sigma}^{(0)}_{q_i\overline{q}_i}(x_1,x_2,\epsilon)\Big\{(\mathcal{H}P_{qq}\overline{\otimes}f_{\overline{q}_i})(x_2)f_{q_i}(x_1)\\ &+(\mathcal{H}P_{qq}\overline{\otimes}f_{q_i})(x_1)f_{\overline{q}_i}(x_2)+x_1\leftrightarrow x_2\Big\}_{q\overline{q}}\\ &+\sum_i d\hat{\sigma}^{(0)}_{q_i\overline{q}_i}(x_1,x_2,\epsilon)\Big\{(\mathcal{H}P_{qg}\otimes f_g)(x_2)(f_{q_i}(x_1)+f_{\overline{q}_i})+x_1\leftrightarrow x_2\Big\}_{qg}\end{aligned}$$

$$+d\hat{\sigma}^{(0)}_{gg}(x_1,x_2,\epsilon)\Big\{(\mathcal{H}P_{gg}\overline{\otimes}f_g)(x_2)f_g(x_1)+x_1\leftrightarrow x_2\Big\}_{gg}$$

$$+d\hat{\sigma}^{(0)}_{gg}(x_1,x_2,\epsilon)\Big\{\sum_i(\mathcal{H}P_{gq}\otimes f_{q_i})(x_2)f_g(x_1)$$

$$+\sum_i(\mathcal{H}P_{gq}\otimes f_{\overline{q}_i})(x_2)f_g(x_1)+x_1\leftrightarrow x_2\Big\}_{qg}\Bigg]. \tag{4.77}$$

Thus we can remove these divergences by redefining the bare parton distributions functions which appear in the above expression. We will use $\overline{MS}$ scheme to subtract the singularities. As the renormalization is done at an arbitrary scale $\mu_R$, the mass factorization is carried out at an arbitrary scale $\mu_F$ called the factorization scale. In $\overline{MS}$ the distribution functions are defined as

$$f_q(x)=f_q(x,\mu_F)-\frac{a_s(\mu_R^2)}{\epsilon}\frac{\Gamma\left(1+\frac{\epsilon}{2}\right)}{\Gamma(1+\epsilon)}\left(\frac{\mu_F^2}{4\pi\mu_R^2}\right)^{\frac{\epsilon}{2}}\Big[(P_{qq}\otimes f_q(x)+(P_{qg}\otimes f_g)(x)\Big],$$

$$f_g(x)=f_g(x,\mu_F)-\frac{a_s(\mu_R^2)}{\epsilon}\frac{\Gamma\left(1+\frac{\epsilon}{2}\right)}{\Gamma(1+\epsilon)}\left(\frac{\mu_F^2}{4\pi\mu_R^2}\right)^{\frac{\epsilon}{2}}\Big[(P_{gg}\otimes f_g)(x)+(P_{gq}\otimes(f_q+f_{\overline{q}}))(x)\Big]. \tag{4.78}$$

This prescription subtracts a finite piece $\gamma_E-\ln 4\pi$ in addition to the pole. The counter terms to cancel collinear singularities are obtained by substituting the above parton redefinitions in the leading order cross-section

$$\begin{aligned} d\sigma^{(0)} &= dx_1dx_2\Big(\sum_i d\hat{\sigma}^{(0)}_{q_i\overline{q}_i}(x_1,x_2,\epsilon)\Big[f_{q_i}(x_1)f_{\overline{q}_i}(x_2)+f_{\overline{q}_i}(x_1)f_{q_i}(x_2)\Big] \\ &\quad +d\hat{\sigma}^{(0)}_{gg}(x_1,x_2,\epsilon)f_g(x_1)f_g(x_2)\Big). \end{aligned} \tag{4.79}$$

There is a cancellation of singularities, however the cancellation is not complete due to the difference in the upper limits of integration in $\otimes$ and $\overline{\otimes}$. Consider the term

$$-\frac{1}{\epsilon}\left(\frac{\mu_F^2}{p_{12}}\right)^{\epsilon/2}\left[(P_{qa}\otimes f_a)(x)-\left(\frac{\mu_R^2}{p_{12}}\right)^{-\epsilon/2}(\mathcal{H}P_{qa}\otimes f_a)(x)\right], \tag{4.80}$$

where $a$ labels partons and summation over repeated $a$ is implied. We can write the first term as

$$(P_{qa}\otimes f_a)(x)=(P_{qa}\;\overline{\otimes}\;f_a)(x)+\int_{1-\delta_{aq}\delta_s}^1\frac{dz}{z}P_{qa}(z)f_a(x/z). \tag{4.81}$$

Expanding the second term in (4.80) in powers of $\epsilon$ and using $P_{ij}(z,\epsilon) = P_{ij}(z) - \epsilon/2P'_{ij}(z)$ we obtain to order $\epsilon$.

$$-\left\{\frac{1}{\epsilon} - \frac{1}{2}\ln\left(\frac{p_{12}}{\mu_F^2}\right)\right\}\int_{1-\delta_{aq}\delta_s}^{1}\frac{dz}{z}P_{qa}(z)f_a(x/z) - \frac{1}{2}P'_{qa}$$

$$+\frac{1}{2}\int_x^{1-\delta_{aq}\delta_s}\frac{dz}{z}P_{qa}(z)\ln\left(\delta_c\frac{1-z}{z}\frac{p_{12}}{\mu_F^2}\right)f_a(x/z) \qquad (4.82)$$

The integral in the first term can be evaluated easily using the definition of plus prescription. Since for the off diagonal splitting functions the lower limits of the integrals are also 1, the integrals vanish for these splittings. The diagonal ones are

$$\begin{aligned}
A_{q\to q+g} \equiv \int_{1-\delta_s}^{1}\frac{dz}{z}P_{qq}(z) &= 4C_F\left(2\ln\delta_s + \frac{3}{2}\right), \\
A_{g\to g+g} \equiv \int_{1-\delta_s}^{1}\frac{dz}{z}P_{gg}(z) &= \left(\frac{22}{3}C_A - \frac{8}{3}n_f T_F + 8C_A\ln\delta_s\right), \\
A_{q\to g+q} &= 0, \\
A_{g\to q+\overline{q}} &= 0, \qquad (4.83)
\end{aligned}$$

where the terms of order $\delta_s$ have been dropped.

$$\begin{aligned}
d\sigma^{HC+CT} &= a_s(\mu_R^2)dx_1dx_2f(\epsilon,\mu_R^2,s) \\
&\times\Bigg[\sum_i d\hat{\sigma}^{(0)}_{q_i\overline{q}_i}(x_1,x_2,\epsilon)\Bigg\{\frac{1}{2}f_{\overline{q}_i}(x_1,\mu_F)\tilde{f}_{q_i}(x_2,\mu_F) + \frac{1}{2}\tilde{f}_{\overline{q}_i}(x_1,\mu_F)f_{q_i}(x_2) \\
&+2\left(-\frac{1}{\epsilon} + \frac{1}{2}\ln\frac{p_{12}}{\mu_F^2}\right)A_{q\to q+g}\ f_{\overline{q}_i}(x_1,\mu_F)f_{q_i}(x_2,\mu_F) + x_1\leftrightarrow x_2\Bigg\} \\
&+d\hat{\sigma}^{(0)}_{gg}(x_1,x_2,\epsilon)\Bigg\{2\ \frac{1}{2}\tilde{f}_g(x_1,\mu_F)f_g(x_2,\mu_F) \\
&+2\left(-\frac{1}{\epsilon} + \frac{1}{2}\ln\frac{p_{12}}{\mu_F^2}\right)A_{g\to g+g}\ f_g(x_1,\mu_F)f_g(x_2,\mu_F)\Bigg\}\Bigg]. \qquad (4.84)
\end{aligned}$$

Factors of 2 appear because both the incoming partons can emit gluons. The function $\tilde{f}_{q,g}$ are defined by

$$\tilde{f}_q(x,\mu_F) = \int_x^{1-\delta_s}\frac{dz}{z}f_q\left(\frac{x}{z},\mu_F\right)\tilde{P}_{qq}(z) + \int_x^1\frac{dz}{z}f_g\left(\frac{x}{z},\mu_F\right)\tilde{P}_{qg}(z),$$

$$\tilde{f}_g(x,\mu_F) \;=\; \int_x^{1-\delta_s} \frac{dz}{z} f_q\left(\frac{x}{z},\mu_F\right)\tilde{P}_{gq}(z) + \int_x^1 \frac{dz}{z} f_g\left(\frac{x}{z},\mu_F\right)\tilde{P}_{gg}(z), \tag{4.85}$$

with

$$\tilde{P}_{ij}(z) = P_{ij}(z)\ln\left(\delta_c \frac{1-z}{z}\frac{p_{12}}{\mu_F^2}\right) + 2P'_{ij}(z). \tag{4.86}$$

Let us now add all the order $a_s$ pieces together; the virtual cross-section $d\sigma^{virt}$ in Eq.( 4.38), the soft piece $d\sigma^{soft}$ in Eq. (4.59) and the mass factorized hard collinear contribution $d\sigma^{HC+CT}$ as given in Eq. (4.84). We see that all the poles in $\epsilon$ cancel in the sum

$$d\sigma^{2-body} = d\sigma^{virt} + d\sigma^{soft} + d\sigma^{HC+CT}. \tag{4.87}$$

This finite result is a 2-body contribution and depends on the factorization scale $\mu_F$. It also depends on the slicing parameters $\delta_s$ and $\delta_c$. By itself it is not a physical quantity. To this we should add the finite hard noncollinear 3-body contribution $d\sigma^{3-body}$

$$d\sigma = d\sigma^{2-body} + d\sigma^{3-body}. \tag{4.88}$$

The sum of 2-body and 3-body contribution is physical and it should be independent of the slicing parameters, at least, over some range of these parameters.

## 4.4 Phase Space

Next we need to determine the 2-body and 3-body phase space over which we will integrate the matrix elements. Further we need to find the transformation to boost from the parton frame to center of mass frame of hadrons that is the lab frame. It is important as many kinematical constraints will be imposed on the photons which pertain to laboratory frame.

Cross-section for production of $N$ particles with momenta $k_1,\ k_2,\ \ldots\ ,k_N$ in final state when two particles with momenta $k_a, k_b$ with masses $m_a$ and $m_b$ respectively scatter is

$$d\sigma = \frac{1}{\Phi}\overline{|\mathcal{M}|^2}(2 \to N)\ d\Gamma_N, \tag{4.89}$$

where the flux factor is given by

$$\Phi = 4\sqrt{(k_a \cdot k_b)^2 - m_a^2 m_b^2}. \tag{4.90}$$

The $N$ body Lorentz invariant phase space $\Gamma_N$ in n dimensions has the following expression.

$$\prod_i \left(\frac{d^{n-1}k_i}{(2\pi)^{n-1}}\frac{1}{2E_i}\right)(2\pi)^n \delta^n(k_a + k_b - \Sigma k_i). \tag{4.91}$$

$\overline{|\mathcal{M}|^2}(2 \to N)$ represents the matrix element square, averaged over initial and summed over final spin, colour and polarizations.

**2 →2 phase space.** Let us consider the process $p_1 + p_2 \to p_3 + p_4$ and evaluate $2 \to 2$ phase space in $n$ dimensions. In $p_1 + p_2$ rest frame

$$\delta^n(p_1 + p_2 - p_3 + p_4) = \delta^{n-1}(\mathbf{p_3} + \mathbf{p_4})\delta(E_{cm} - E_1 - E_2) \tag{4.92}$$

Integrating over $\mathbf{p_4}$ using the $\delta$ function we can write the 2-body phase space as

$$d\Gamma_2 = \frac{d^{n-1}p_3}{(2\pi)^{n-1}}\frac{1}{2\mathcal{E}_1}\frac{1}{2\mathcal{E}_2}2\pi\delta(E_{cm} - \mathcal{E}_1 - \mathcal{E}_2), \tag{4.93}$$

where

$$\mathcal{E}_1 = \sqrt{p_3^2 + m_3^2}, \qquad \mathcal{E}_2 = \sqrt{p_3^2 + m_4^2}.$$

Here we have not put the final state masses to be zero. We will eventually make this identification. If we denote the angle between $\mathbf{p_1}$ and $\mathbf{p_3}$ by $\theta$ and define $y = \cos\theta$, then we can write

$$d^{n-1}p_3 = p_3^{n-2}dp_3 d\Omega_{n-2}, \tag{4.94}$$

where $d\Omega_{n-2}$ denotes volume of a $n-2$ dimensional sphere and it evaluates to

$$d\Omega_{n-2} = \frac{2\pi^{(n-2)/2}}{\Gamma(n/2-1)}(1-y^2)^{n/2-2}dy. \tag{4.95}$$

Substituting the above two equations we can write the 2-body phase space as

$$d\Gamma_2 = \frac{p_3^{n-2}dp_3}{(2\pi)^{n-1}}\frac{1}{2\mathcal{E}_1}\frac{1}{2\mathcal{E}_2}2\pi\delta(E_{cm}-\mathcal{E}_1-\mathcal{E}_2)d\Omega_{n-2} \tag{4.96}$$

In Eq. (4.96) substitute $t = p_3^2$ and define $\alpha = \sqrt{t+m_3^2} + \sqrt{t+m_4^2}$, this gives

$$d\Gamma_2 = \frac{1}{4}\frac{d\alpha}{\alpha}\left(\frac{[\alpha^2-(m_3-m_4)^2]^{1/2}[\alpha^2-(m_3+m_4)^2]^{1/2}}{2\alpha}\right)^{n-3}\frac{2\pi\delta(E_{cm}-\alpha)}{(2\pi)^{n-1}}d\Omega_{n-2}$$

Integrating over $\alpha$ and putting $E_{cm} = \sqrt{s}$ we obtain

$$d\Omega_{n-2}\frac{2\pi}{4\sqrt{s}}{\Pi_o}^{n-3}, \tag{4.97}$$

where

$$\Pi_o = \frac{[s-(m_3-m_4)^2]^{1/2}[s-(m_3+m_4)^2]^{1/2}}{2\sqrt{s}}. \tag{4.98}$$

Defining

$$\Pi_i = \frac{[s-(m_1-m_2)^2]^{1/2}[s-(m_1+m_2)^2]^{1/2}}{2\sqrt{s}}, \tag{4.99}$$

we can write $\Phi = 4\sqrt{s}\Pi_i$ and the cross-section can be expressed as

$$d\sigma = \frac{1}{4\sqrt{s}\Pi_i}\frac{2\pi}{4\sqrt{s}}\overline{\sum}|\mathcal{M}|^2\Pi_o^{n-3}d\Omega_{n-2}, \tag{4.100}$$

or explicitly

$$\begin{aligned} d\sigma &= \frac{1}{32\pi s}\frac{1}{2^{n-4}\pi^{n/2-2}\Gamma(n/2-1)} \\ &\quad\times\frac{\Pi_o^{n-3}}{\Pi_i}\overline{|\mathcal{M}|^2}(1-y^2)^{n/2-2}dy. \end{aligned}$$

If all the masses are equal $\Pi_0 = \Pi_i$. As we have taken care of all the singularities using phase space slicing method, the phase space integrals are required only in $n = 4$ dimensions. We can finally, write $d\sigma$ for equal masses in initial and final state in 4 dimensions, defining $v = cos^2(\theta/2)$, as

$$d\sigma = \frac{1}{16\pi s}\overline{|\mathcal{M}|^2}dv. \tag{4.101}$$

In the $CM$ frame of colliding hadrons $H_1$ and $H_2$ carrying a centre of mass energy $(p_{H_1} + p_{H_2})^2 = S$ the incoming parton momenta are

$$p_{1cmH} = \frac{\sqrt{S}}{2}\Big(x_a, 0, 0, x_a\Big), \tag{4.102}$$

$$p_{2cmH} = \frac{\sqrt{S}}{2}\Big(x_b, 0, 0, -x_b\Big). \tag{4.103}$$

In the CM frame of partons $p_1^3 + p_2^3 = 0$, using this we can determine the transformation matrix to boost to $CM$ frame of partons.

$$\begin{pmatrix} \cosh\chi & \sinh\chi \\ \sinh\chi & \cosh\chi \end{pmatrix}, \tag{4.104}$$

which transforms the 0 and 3 components of momenta. The entries of the matrix are given by

$$\cosh\chi = \frac{x_b + x_a}{2\sqrt{x_a x_b}}, \quad \sinh\chi = \frac{x_b - x_a}{2\sqrt{x_a x_b}}. \tag{4.105}$$

Let us parameterize the momenta in $p_1 + p_2$ rest frame as

$$\begin{aligned} p_3 &= \left(p_3^0, 0, |\mathbf{p_3}|\sin\theta, |\mathbf{p_3}|\cos\theta\right), \\ p_4 &= \left(p_3^0, 0, -|\mathbf{p_3}|\sin\theta, -|\mathbf{p_3}|\cos\theta\right), \end{aligned} \tag{4.106}$$

and apply the inverse transformation obtained by replacing $\chi \to -\chi$

$$\begin{pmatrix} \cosh\chi & -\sinh\chi \\ -\sinh\chi & \cosh\chi \end{pmatrix}, \tag{4.107}$$

to obtain momenta in Laboratory frame

$$p_{3cmH} = \frac{\sqrt{S}}{2}\Big([x_a v + x_b(1-v)],\ 2\sqrt{x_a x_b v(1-v)},\ 0,\ [x_a v - x_b(1-v)]\Big), \tag{4.108}$$

where $v = cos^2(\theta/2)$.

**2 →3 phase space.** In the CM frame of the two final state photons we can parameterize the momenta as follows. We can take $p_1$ to define the $z$ axis, and using $p_1$ and $p_2$ define a plane. The momentum $p_5$ is determined by momentum conservation.

$$\begin{aligned} p_1 &= E_1\Big(1\ , 0,\ 0, 1\Big), \\ p_2 &= E_2\Big(1,\ 0,\ \sin\psi,\ \cos\psi\Big), \end{aligned}$$

$$\begin{aligned} p_3 &= \frac{\sqrt{s_2}}{2}(1, \sin\theta_2 \sin\theta_1, \cos\theta_2 \sin\theta_1, \cos\theta_1), \\ p_4 &= \frac{\sqrt{s_2}}{2}(1, -\sin\theta_2 \sin\theta_1, -\cos\theta_2 \sin\theta_1, -\cos\theta_1), \end{aligned} \tag{4.109}$$

where $\sin\psi > 0$. The three body processes are characterized by five independent scalar quantities:

$$\begin{aligned} p_{12} &= (p_1 + p_2)^2, \\ p_{15} &= (p_1 - p_5)^2, \\ p_{25} &= (p_2 - p_5)^2, \\ p_{13} &= (p_1 - p_3)^2, \\ p_{24} &= (p_2 - p_4)^2. \end{aligned} \tag{4.110}$$

Of course any other set of five independent scalars can be chosen. For convenience let us introduce the variables $x$ and $y$, where $x = p_{34}/p_{12}$ and $y$ is the cosine of the angle between $p_1$ and $p_5$. We have

$$0 \le x \le 1, \quad -1 \le y \le 1, \tag{4.111}$$

and

$$p_{15} = -\frac{p_{12}}{2}(1-x)(1-y), \quad p_{25} = -\frac{p_{12}}{2}(1-x)(1+y). \tag{4.112}$$

The phase space is given in 4-dimensions by

$$d\Gamma_3 = \frac{1}{(4\pi)^2}\,\frac{1}{16\pi} d\cos\theta_1 dx \frac{x p_{12}}{2\pi}(1-x) dy d\theta_2. \tag{4.113}$$

We want to express the momenta in the Lab-frame. The transformation matrix can be obtained by first boosting to the $p_1 + p_2$ rest frame and rotating to align $p_1$ and $p_2$ parallel to the $z-$axis. Finally we will boost to the laboratory frame. First let us ensure $(p_1 + p_2)^{(2)} = 0$.

$$\begin{pmatrix} \cosh\chi & \sinh\chi \\ \sinh\chi & \cosh\chi \end{pmatrix} \begin{pmatrix} E_1 \\ E_2 \sin\psi \end{pmatrix} = \begin{pmatrix} A \\ 0 \end{pmatrix}. \tag{4.114}$$

We make another boost along the $z-$ axis to make the $z$ components back to back.

$$\begin{pmatrix} \cosh\bar{\chi} & \sinh\bar{\chi} \\ \sinh\bar{\chi} & \cosh\bar{\chi} \end{pmatrix} \begin{pmatrix} A \\ E_1 + E_2\cos\psi \end{pmatrix} = \begin{pmatrix} B \\ 0 \end{pmatrix}. \tag{4.115}$$

The energy components $A$ and $B$ are positive. Solving the above equations we obtain

$$\begin{aligned}
\cosh\chi &= \frac{E_1+E_2}{\sqrt{(E_1+E_2)^2-E_2^2\sin^2\psi}}, \quad \sinh\chi = \frac{-E_2\sin\psi}{\sqrt{(E_1+E_2)^2-E_2^2\sin^2\psi}}, \\
\cosh\bar{\chi} &= \frac{A}{\sqrt{A^2-(E_1+E_2\cos\psi)^2}}, \quad \sin\bar{\chi} = \frac{-(E_1+E_2\cos\psi)}{\sqrt{A^2-(E_1+E_2\cos\psi)^2}}. \qquad (4.116)
\end{aligned}$$

Making the above transformations successively we can determine $p_1$, and the angle $\alpha$ which it makes with the $z$-axis after the transformations.

$$p_1 = (E_1\cosh\bar{\chi}\cosh\chi + E_1\sinh\bar{\chi}, 0, E_1\sinh\chi, E_1\sinh\bar{\chi}\cosh\chi + E_1\cosh\bar{\chi}) \qquad (4.117)$$

$$\cos\alpha = \frac{1}{H}(E_1\sinh\bar{\chi}\cosh\chi + E_1\cosh\bar{\chi}), \quad \sin\alpha = -\frac{E_1\sinh\chi}{H}, \qquad (4.118)$$

where

$$H = \left(E_1^2\sinh^2\chi + (E_1\sinh\bar{\chi}\cosh\chi + E_1\cosh\bar{\chi})^2\right)^{1/2}. \qquad (4.119)$$

Note that we have put a minus sign in the above expression because $\sinh\chi$ is negative. After rotating by an angle $\alpha$ we get $p_1$ in $p+p_2$ rest frame aligned along the positive $z$ direction.

$$p_1 = \left[\frac{E_1E_2}{2}(1-\cos\psi)\right]^{1/2}(1,\ 0,\ 0,\ 1). \qquad (4.120)$$

As a check we can find $p_2$ and it comes out to be as expected

$$p_1 = \left[\frac{E_1E_2}{2}(1-\cos\psi)\right]^{1/2}(1,\ 0,\ 0,\ -1). \qquad (4.121)$$

Finally we boost to the laboratory frame making the transformation (4.107) and obtain the momenta as given in Eq. 4.102 and Eq. 4.103.

### 4.4.1 Conversion factor

Till now all the calculations have been carried out in natural units. But we need to convert to SI units for making numerical predictions. In the following we will briefly summarize the system of natural units and the conversion from it to SI units.

We know that there are three fundamental constants of nature, the velocity of light in vacuum $c$ (Special Relativity), the Planck's constant $\hbar$ (Quantum Mechanics) and the Newtons's constant $G$ (Gravity). Also there are three dimensions $M, L$ and T. The dimensions of fundamental constants are as follows

$$[\hbar] = \frac{ML^2}{T}, \quad [c] = \frac{L}{T}, \quad [G] = \frac{L^3}{MT^{-2}} \qquad (4.122)$$

Let us take a system of units, called natural units, such that the velocity of light is a dimensionless number and equals unity, that is $c = 1$. This puts time and length dimensions of equal footing: $L = T$. Next we can choose to make one of $\hbar$ and G to be equal to unity. For our purpose obvious choice is $\hbar = 1$. We see that it makes the length to have dimensions of inverse mass, $L = M^{-1}$. Now there is no freedom left and the dimension of $G$ is completely determined by the above relations. Depending on the context, one may instead choose $c = G = 1$, and this would fix the dimensions of $\hbar$. Let us now determine the factor with which to multiply the cross-section to convert to SI units from natural units. Remembering that cross-section has dimensions of area which is $L^{-2}$ and noting

$$\sigma = k\frac{1}{(\text{Energy})^2}, \tag{4.123}$$

where $k$ is a dimensionless number, we can determine the conversion factor.

$$L^2 = [\hbar]^{n_1}[c]^{n_2}\left(\frac{ML^2}{T^2}\right)^{-2}, \tag{4.124}$$

where we have used the fact that energy has dimensions

$$E = \frac{ML^2}{T^2}. \tag{4.125}$$

Solving for $n_1$ and $n_2$ we obtain $n_1 = n_2 = 2$. So we have to multiply by a factor of $(\hbar c)^2$. It is customary to use *barn* as unit for cross-section which is defined by the relation

$$1b = 10^{-24}cm^2. \tag{4.126}$$

This gives

$$(\hbar c)^2 = 0.3894 \times 10^9 \ (GeV)^2 pb, \tag{4.127}$$

where $pb = 10^{-12}b$ is pico barn.

# Chapter 5

# Results and Conclusions

In the preceeding chapters we have presented the details of the next-to-leading order calculation for the production of two direct isolated photons at the hadron colliders. This calculation was based on the semi-analytical two cutoff phase space slicing method. We presented all the order $\alpha_s$ pieces: $d\sigma^{soft}$, $d\sigma^{HC+CT}, d\sigma^{virt}$. The full matrix elements squares for real emission processes which go into evaluation of the 3-body hard non-collinear contribution were not presented as the expressions are large. We also discussed the smooth cone isolation prescription which we will use to remove the fragmentation photons. In this chapter we will present the results obtained form our Monte Carlo code based on the method of two cutoff phase space slicing. Various kinematical distributions will be presented here both to leading order and next-to-leading order in strong coupling constant in the ADD and unparticle models. We will show that inclusion of higher order QCD radiative corrections reduces the sensitivity to the factorization scale and enhances the cross sections significantly.

Let us define the kinematical variables below. The incoming hadron momenta will be labeled by $P_1$ and $P_2$ and the square of the sum of momenta of two final state photons by $Q^2$.

1. Invariant Mass $Q$ of photon pair

$$Q^2 = (p_3 + p_4)^2 \tag{5.1}$$

2. Rapidity $Y$ of photon pair

$$Y = \frac{1}{2} \ln \left( \frac{P_1 \cdot Q}{P_2 \cdot Q} \right) \tag{5.2}$$

3. Rapidity $y^\gamma$ of a photon

$$y^\gamma = \frac{1}{2} \ln \left( \frac{E + p_z}{E - p_z} \right) \tag{5.3}$$

where $E$ and $p_z$ are its energy and the longitudinal momentum respectively.

4. cos$\theta^*$

$$\cos\theta^* = \frac{P_1.(p_3 - p_4)}{P_1.(p_3 + p_4)} \tag{5.4}$$

5. Transverse momentum $Q_T$

$$Q_T = \sqrt{q_x^2 + q_y^2}. \tag{5.5}$$

At LO, the photon pairs will have zero $Q_T$ as incoming partons have no transverse momentum, and hence $Q_T$ distribution will be proportional to $\delta(Q_T)$. However, at NLO, the photon pairs will be accompanied by a quark (anti-quark) or a gluon in the final state resulting in a non-zero $Q_T$.

The material in the following pages is presented as follows. First we will present results for photon pair production in the context of scalar unparticles. This will be presented only to leading order in QCD. Here we will present the matrix elements as they were not given in the previous chapter. Next we will present the results in the ADD model and the unparticle model with spin-2 unparticles. These results will be presented at full next-to-leading order in QCD.

## 5.1 $PP \to \gamma\gamma$ with scalar unparticles

The operators that describe the interaction of scalar unparticle fields with those of the SM are given in Eq. (2.34). At leading order two photons are produced by quark anti-quark annihilation in SM and through quark anti-quark annihilation with an intermediate scalar unparticle propagator. At this order $gg$ initiated processes also occur as gluons couple to scalar unparticles. The SM contribution is given in Eq. (4.3). Below we give the contributions coming from unparticle mediated partonic subprocesses :

$$\begin{aligned}
|\overline{M}_{q\bar{q}}|^2 &= \frac{1}{8N_c}\,\lambda_s^4\,\chi_u^2\left(\frac{s}{\Lambda_u^2}\right)^{2d_u-1}, \\
|\overline{M}_{gg}|^2 &= \frac{1}{8(N_c^2-1)}\frac{1}{4}\,\lambda_s^4\,\chi_u^2\left(\frac{s}{\Lambda_u^2}\right)^{2d_u}.
\end{aligned} \tag{5.6}$$

where $\chi_u = A_{d_u}/(2\sin(d_u\pi))$ and $N_c$ is the number of colors. $A_{d_u}$ is defined in (2.29). The variables $s, t$ and $u$ are the Mandelstam invariants which are given in Eq. (4.8). In the above matrix elements we have already done spin and colour averages and included the a factor of 1/2 for identical photons. Note that the interference with SM matrix elements vanishes. This happens because there is no $gg$ initiated process at LO in SM and because

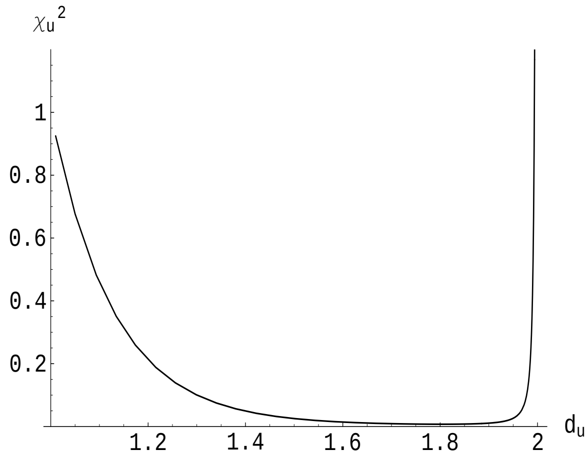


Figure 5.1: The function $\chi_u^2$ showing its variation with the scaling dimension $d_u$ of the unparticle operator.

the interference of $q\overline{q}$ initiated process is zero due to trace over an odd number of Dirac gamma matrices.

Before, we present the effects of unparticles on various distributions of di-photon system at the LHC, we discuss the coefficient $\chi_u^2$ that appears in the above equations. Unitarity imposes constraint [82] on the scaling dimension of these operators, which for scalar unparticle is $d_u > 1$. In Fig. (5.1), we have plotted it against the scaling dimension $d_u$ of the unparticle operator. $\chi_u$ is negative when $1 < d_u < 2$ and singular as $d_u \to 2$. As $d_u \to 1$, $\chi_u$ approaches a limiting value and as we go below $d_u = 1.01$, the variation is found to be mild. In the plateau region, where $1.3 < d_u < 1.9$, the function is almost constant and relatively small. For our numerical analysis we have taken $\lambda_s$ in the range $0.4 \leq \lambda_s < 1$, so that the unparticle effects are treated as perturbation. The other parameter that appears in this model is $\Lambda_u$ which we choose to be 1 TeV.

We will carry out analysis for the LHC with $\sqrt{S} = 14$ TeV. We have imposed the cuts: rapidity $|y^\gamma| < 2.5$, and transverse momentum of the photons $p_T^\gamma > 40$ GeV [83] for all the distributions that we have reported here in order to make our predictions for an environment which is as close as possible to that of the experiment. Moreover, for the invariant mass distribution, in order to suppress the SM background and also to enhance the signal we have imposed an angular cut on the photons $|\cos\ \theta_\gamma| < 0.8$, where $\theta_\gamma$ is the angle of the photons in the lab frame. Similarly, for the angular and rapidity distributions, to suppress the background, we have considered only those events that satisfy the constraint $Q > 600$ GeV. For all our plots, we have used MRST 2001 leading order (LO) parton density sets [84].

In Fig. 5.2 (left panel) we have plotted $d\sigma/dQ$ distribution for $Q$ between $100 < Q < 900$ GeV. Here we have chosen $d_u = 1.01$ and $\Lambda_u = 1$ TeV. With this choice of parameters, we find that the unparticle effects can be seen only in the large $Q$ region. In addition, we have presented different contributions coming from various sub-processes to the cross section. The quark anti-quark initiated process dominates over the gluon initiated process due to higher power of scale in the later case.

In Fig. 5.2 (right panel) we show the variation of the invariant mass distribution with respect to the scaling dimension $d_u$ for $\Lambda_u = 1$ TeV. As expected, we find that the unparticle effects show up significantly when the value of $d_u$ decreases. When $d_u$ is around 1.9, the unparticle effects are completely washed away.

We have also studied the effects of $\lambda_s$ variations on the distributions. They are shown in Fig. 5.3 for $d_u = 1.01$. From the figure, we see that in the region where $d_u$ is below 1.1 and $\lambda_s$ above 0.6 the scalar unparticle contribution is substantial even at low energies.

In Fig. 5.4 and Fig. 5.5 we have plotted the angular and rapidity distributions. These have been obtained for $d_u = 1.01$, $\Lambda_u = 1$ TeV. We show the results for two different choices of the coupling constants. To enhance the signals an integration over $Q$ in the range $600 < Q < 0.9\Lambda_u$ has been carried out. We see from Fig. 5.4 that the signal differs appreciably from SM prediction for both the choices $\lambda_s = 0.4, 0.6$ of the coupling constant. In the rapidity distributions shown in Fig. 5.5 we see that the signal is different significantly from the SM predictions in the central region of rapidities $Y$ and $y^\gamma$.

## 5.2 $PP \to \gamma\gamma$ in ADD and unparticle model

In this section we will present the next-to-leading order results for both the unparticle model and ADD model. Here only spin-2 unparticles will be considered. Let us make some general remarks first.

**General remarks.** The kinematical distributions will be presented for the LHC with a centre of mass energy 14 TeV. In our analysis we will use CTEQ6L and CTEQ6M [85] parton density sets for leading order and next-to-leading order kinematical distributions with the corresponding value of strong coupling constant $\alpha_s(M_Z) = 0.118$. The fine structure constant will be taken as $\alpha_{em}(M_W) = 1/128$. Unless mentioned otherwise we identify the renormalization and factorization scales to the invariant mass of the photon pair, ie., $\mu_R = \mu_F = Q$. As already mentioned in previous chapters we will treat all the quarks to be massless.

We have seen in chapter 4 that the phase space slicing parameters $\delta_s$ and $\delta_c$ are introduced at the intermediate stages of calculation and the final results should be independent of these parameters. To check this we will present the variation of the sum of 2-body and 3-body contributions with the variation of the slicing parameters. The region in which the sum is stable under variations will be chosen for further study.

We have imposed the kinematical cuts on the photons as used by the ATLAS detector [86]:

1. $p_T^\gamma > 40$ (25) GeV for harder (softer) photon,

2. $|\eta_\gamma| < 2.5$ for each photon.

The photons are restricted to have a separation of at least $R_{\gamma\gamma} = 0.4$ in the pseudo-rapidity azimuthal angle, $\eta - \phi$, plane. In addition to these constraints, we impose smooth cone isolation criterion on photons given in (4.1). $R_0 = 0.4$ is taken for the cone radius. Unless otherwise specified we use $n = 2$ and $E_T^{iso} = 15$ GeV which appear in $\mathcal{H}(R)$.

As SM NLO results exist in literature [17, 25, 21] , to check our code we have compared our results with [25] using their isolation criterion

$$[\mathcal{H}(R) = p_T(\gamma)\epsilon\left([1-\cos(R)]/[1-\cos(R_0)]\right)^n] \tag{5.7}$$

and their choice of $\mu_F$, $\mu_R$ and parton distribution sets. We have found good agreement with [25].

### 5.2.1 Large extra dimension model

A leading order study for effects of the ADD model KK gravitons on production of two direct photons was carried out in [37]. Here it was also shown that unitarity restricts the largest invariant mass of the two photons to be less than the cutoff scale $M_S$. Following [37] we will restrict to $Q < 0.9M_S$ in our study. As a check we reproduced the leading order results presented in this paper and found good agreement. Results that are more precise and less sensitive to the $\mu_F$ will be presented in this section.

Before proceeding further we present the stability of the sum of 2-body and 3-body contributions against the variation of the slicing parameters $\delta_s$ and $\delta_c$. In Fig. 5.6 and Fig. 5.7 the individual 2-body and 3-body order $\alpha_s$ contributions and their sum are presented in invariant mass distribution in the SM and SM+ADD respectively as a function of $\delta_s$ with $\delta_c$ fixed at $10^{-5}$. From these figures it is clear that the sum is fairly stable against the variation of slicing parameters; this serves as a check on the numerical implementation of the phase space slicing in our numerical code. For all further analysis, we choose $\delta_s = 10^{-3}$ and $\delta_c = 10^{-5}$.

First, we present our results for the invariant mass distribution. In Fig. 5.8 (left panel), we present LO and NLO contributions to the signal (SM+ADD) and the SM background against $Q$ between 300 GeV and 1 TeV. We choose the fundamental scale $M_S = 2$ TeV and the number of extra dimensions $d = 3$. We do not treat the gluon-gluon fusion process through quark loop as LO as its contribution is significant only at small $Q$ and there is no reason to consider it as a LO piece at high Q values.

For the above choice of parameters the signal starts deviating from the SM background around $Q = 500$ GeV. The value of $Q$ at which the deviation occurs depends very much on the choice of the parameters, namely the scale $M_S$, $d$ and the cut-off scale $\Lambda$ for the summation of the KK modes. In Fig. 5.8 (right panel) we show how the invariant mass distribution depends on the choice of the fundamental scale $M_S$ when $d = 3$. As expected smaller the $M_S$, the larger the deviation one observes. The dependence on the number of extra dimensions $d$ is presented in Fig. 5.9 (left panel) for $d = 3 - 6$ keeping $M_S = 2$ TeV fixed. We find that the ADD contribution decreases with increase in $d$. In Fig. 5.9 (right panel) we present the cut-off scale $\Lambda$ dependence for $\Lambda = 0.6 M_S$ to $M_S$. For lower values of cut-off scale, the number of KK modes available are less and the signal will decrease with decrease in $\Lambda$ as shown in the figure. In the following, we choose $M_S = 2$ TeV, $d = 3$ and $\Lambda = M_S$. For the rest of the kinematic distributions that we have considered, to reduce the SM background and to enhance the signal, we integrate over $Q$ in the range $600 < Q < 1100$ GeV.

In the left panel of Fig. 5.10, we show the production cross section as a function of Y between $-2.0$ and $2.0$ after integrating over $Q$ in the region $600 < Q < 1100$ GeV where the ADD model shows significant contribution over the SM background. From the left panel of this figure, we observe that the signal exceeds the background by more than an order of magnitude at the central rapidity region $Y = 0$.

The transverse momentum of the photon pair is defined by $Q_T = \sqrt{q_x^2 + q_y^2}$. At LO, the photon pairs will have zero $Q_T$ as incoming partons have no transverse momentum, and hence $Q_T$ distribution will be proportional to $\delta(Q_T)$. However, at NLO, the photon pairs will be accompanied by a quark (anti-quark) or a gluon in the final state resulting in a non-zero $Q_T$. The numerical results for the $Q_T$ distribution is presented in the right panel of Fig. 5.10.

In Fig. 5.11, the left panel shows the rapidity distribution of the photons as a function of $y^\gamma$ in the region $-2.0 < y^\gamma < 2.0$. The SM cross sections both at LO and NLO level do not show significant dependence on $y^\gamma$ unlike contribution from the ADD model. We also find that the QCD corrections are large for the signal as compared to the SM background.

Next we present $cos(\theta^*)$ distribution. Since gravitons are spin-2 particles, the angular dependence of the cross section in ADD model will be different from SM. It is shown in the right panel of Fig. 5.11.

**Scale variations.** In this section, we discuss the impact of NLO QCD corrections to various distributions. The uncertainty in LO computation of observables in the hadron colliders originates from two important sources, namely, the missing higher order radiative corrections and the choice of factorization and renormalization scales. The former enters through parton density sets and the latter through the renormalized parameters such as running coupling constant $\alpha_s$ of the theory. The radiative corrections coming from QCD in our case enhance both SM as well as ADD distributions. Hence, the $K$-factor ($K = \sigma^{NLO}/\sigma^{LO}$), that quantifies these effects is always positive for the cases we studied in this paper. It is clear from the plots that the $K$-factor is different for different distributions and also within a given distribution, it varies with the kinematical variable, say $Q$ or $Y$ etc. More importantly, the numerical value of $K$ depends very much on the kinematical cuts imposed on each distribution. We find that the $K$ factors of the distributions reported in the paper are not large and hence our NLO results are stable under perturbation and reliable for further study. Observables are expected to be independent of renormalization and factorization scales, thanks to renormalization group invariance. However, any truncated perturbative expansion does depend on the choice of these scales. This is expected to improve if higher order corrections are included in the perturbative expansion. Indeed, our NLO results of these distributions show significant improvement on the factorization scale uncertainty entering through parton density sets at LO level. In order that the perturbative expansion does not break down these scales should be chosen close to the scale in the problem such as $Q$ or $Q_T$. In the Fig. 5.12 we show the effect of variation of $\mu_F$ between $Q/2$ and $3Q/2$. We studied this variation for $Y$ and $\cos\theta^*$ distributions in the ADD model.

### 5.2.2 Tensor unparticles

The matrix element squares with spin-2 unparticle propagator can be obtained by making the following replacement to $\kappa^2\mathcal{D}(s)$ in chapter 4.

$$\kappa^2\mathcal{D}(s) \to -4\frac{\lambda_t^2}{\Lambda_u^{2d_u}}\frac{C_T d_u(d_u-1)}{4^{d_u-1}}\frac{\Gamma(2-d_u)}{\Gamma(d_u+2)}e^{-i\pi d_u}s^{d_u-2} \tag{5.8}$$

The scale $\Lambda_u$ at which scale invariance sets in the BZ sector is chosen to be 1 TeV. Scale invariance restricts the scaling dimension of tensor operators to $d_u \geq 3$, in our calculation we have chosen $d_u = 3.01$. The coupling $\lambda_t$ is taken to be of order one.

To show that the results are independent of the choice of the slicing parameters $\delta_s$ and $\delta_c$, we have plotted 2-body and 3-body pieces of $d\sigma/dQ$ as functions of $\delta_s$ with $\delta_c$ kept fixed at a very small value $10^{-5}$ in Fig. 5.13. We see that the sum is fairly stable under the variation. For rest of our numerical study, we have chosen $\delta_s = 10^{-3}$ and $\delta_c = 10^{-5}$.

We present various subprocess contributions to NLO in QCD in the invariant mass distribution for the range $400 < Q < 900$ GeV in Fig. 5.14. In the SM both $q\bar{q}$ and $qg$ subprocess contributions are positive with $q\bar{q}$ contribution being dominant over that of $qg$ for the range of $Q$ considered. In the unparticle sector the $q\bar{q}$ and $gg$ subprocess contributions via the pure unparticle exchange (direct) are positive while the $qg$ contribution is negative. At the interference level the $gg$ interference with the SM box has a positive contribution and is almost constant for the range of $Q$ considered. However, the interference of both $q\bar{q}$ and $qg$ subprocesses with the SM have negative contributions and are larger in magnitude compared to the direct ones. The direct unparticle exchange contributions can become significant in the large $Q$ region because the cross sections go as powers of $Q/\Lambda_{\mathcal{U}}$, thus leading to the visibility of the unparticles only in that region of $Q$. It is worth noting that only the $gg$ initiated subprocess has the dominant contribution over the rest in this region.

In Fig. 5.15 we present our results for $d\sigma/dQ$ (left panel) for $Q$ between 400 and 900 GeV and $d\sigma/dY$ (right panel) for $|Y| < 2.0$, where $Y$ is the rapidity of the diphoton system. The short dashed (LO) and the long dashed lines (NLO) correspond to SM distributions. The dotted (LO) and the solid (NLO) lines correspond to the signal (SM+UP) of the unparticle physics. As expected we find that the unparticle contribution to the invariant mass distribution grows with $Q$ and it dominates over the SM contributions above $Q = 600$ GeV. The precise value where this happens will depend very much on the choice of $\Lambda_{\mathcal{U}}$ and other unparticle parameters. Since unparticle effects can be seen in the larger values of $Q$, rapidity distributions are computed by integrating $Q$ between 600 and 900 GeV. Near the central value of $Y$, we find large enhancement of the cross section from the SM results if we include unparticle contributions.

At next-to-leading order the total transverse energy of the hadrons is due to a single parton around the photons and does not correspond to the actual hadronic energy in an experiment. Hence the $E_T^{iso}$ at the parton level is a crude estimate of that of the jets at the detector level. To show the dependence on $E_T^{iso}$ we present the invariant mass distribution for $E_T^{iso} = 15$ GeV and $E_T^{iso} = 30$ GeV, for $n = 2$. To study the dependence of our predictions on the choice of $\mathcal{H}(R)$ we have varied it by changing $n$ from 1 to 2 and keeping $E_T^{iso}$ fixed at a value of 15 GeV. These variations are shown in Fig. 5.16 and show a very small dependence for $R_0 = 0.4$.

Until now our analysis was restricted to the case where $3 < d_u < 4$, which was essential for a tensor unparticle as a consequence of scale invariance. There are no known examples of unitary quantum field theory that are scale invariant but not conformal invariant. For conformal invariance, unitarity demands that $d_u > 4$ for the tensor unparticles. In Fig. 5.17 (left panel) the unparticle sector as a result of scale invariance and not conformal ($d_u = 3.01$) is contrasted to the case where the unparticle sector is conformal ($d_u = 4.001$). This is to both LO and NLO in QCD and for $\Lambda_u = 1$ TeV. In Fig. 5.17 (right panel) we have considered the invariant mass distribution for $d_u > 4$ to LO in QCD. For this plot we have considered $\Lambda_u = 2$ TeV and have probed $Q < 0.9\Lambda_u$. Closer to $d_u = 4$ there could still be sufficient unparticle contribution for the tensor operator. The turn-around with energy behaviour of the unparticle effects is a typical feature of any physics beyond the SM. One observes a similar behaviour in models with large extra-dimensions. The origin of this turn around contribution comes from the terms proportional to $(s/\Lambda_u)^{d_u}$ in the matrix elements involving unparticles.

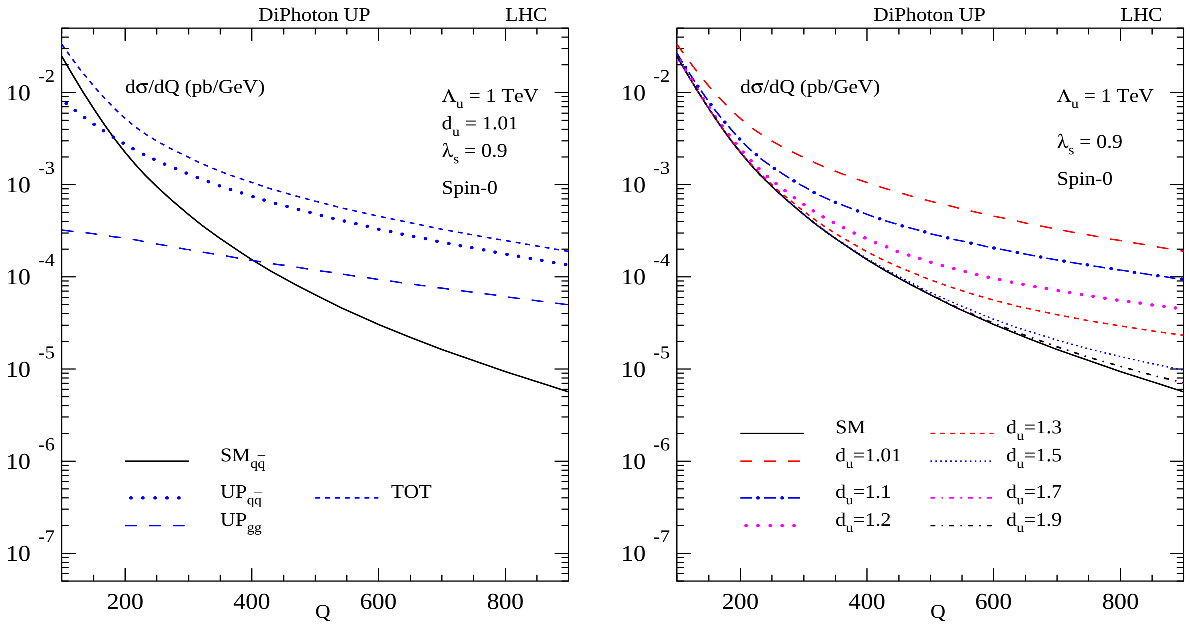


Figure 5.2: Spin-0 unparticles: Invariant mass distribution for the choice $\Lambda_u = 1$ TeV and $\lambda_s = 0.9$. We imposed an angular cut $|\cos\ \theta_\gamma| < 0.8$ on the photons to suppress the SM background. Left panel: The contribution of the various sub processes with $d_u = 1.01$. Right panel: Variation with $d_u$.

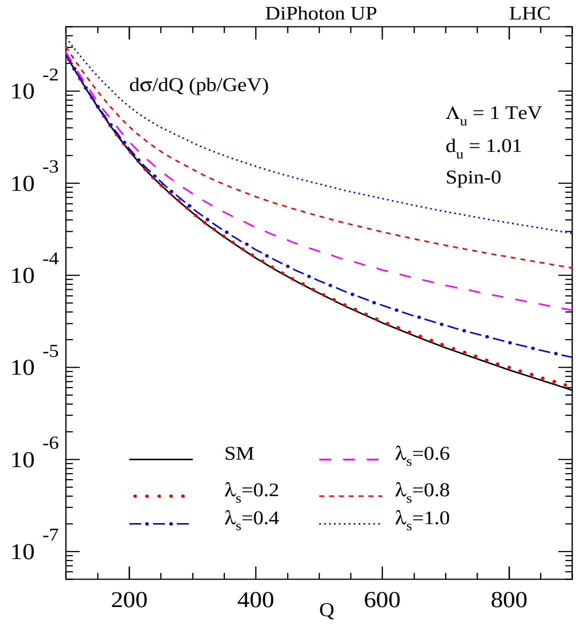


Figure 5.3: Spin-0 unparticles: Invariant mass distribution is plotted for various values of the coupling $\lambda_s$ for spin-0 with $\Lambda_u = 1$ TeV and $d_u = 1.01$, with an angular cut on the photons $|\cos\theta_\gamma| < 0.8$.

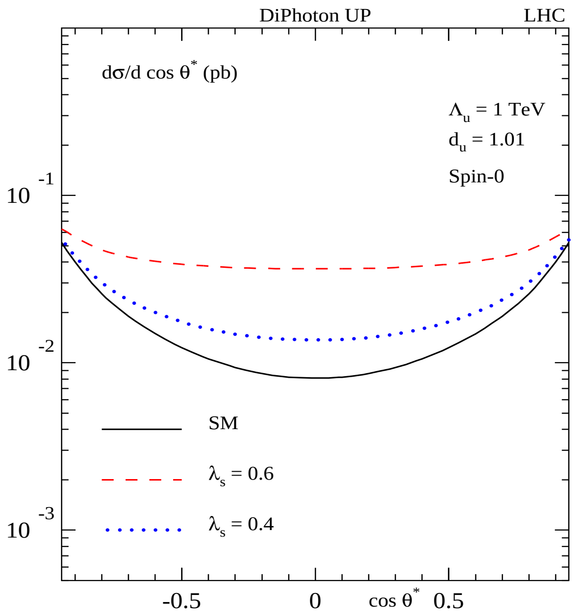


Figure 5.4: Spin-0 unparticles: Angular distributions $d\sigma/d\cos\theta^*$ of the photons for spin-0 with $\Lambda_u = 1$ TeV and $d_u = 1.01$. We have taken couplings $\lambda_s = 0.6, 0.4$ integrating Q in the range 600 GeV $< Q < 0.9\Lambda_u$.

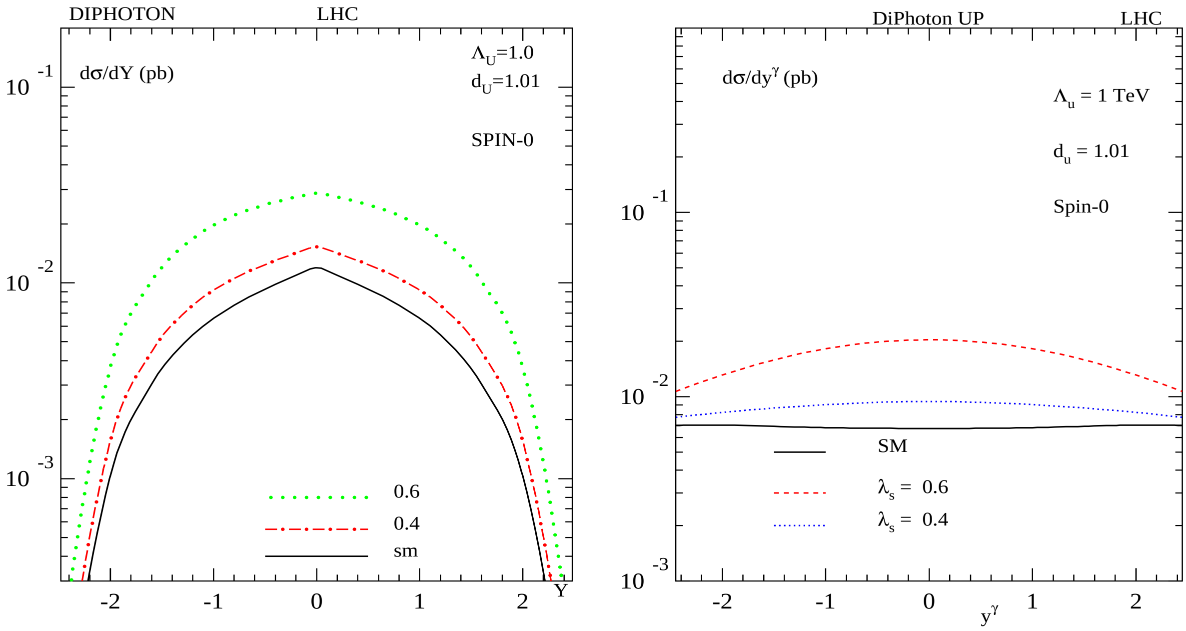


Figure 5.5: Spin-0 unparticles: Left Panel:$d\sigma/dY$ of the di-photon system. Right panel: $d\sigma/dy^\gamma$ of photons. $\Lambda_u = 1$ TeV and $d_u = 1.01$. We have taken the couplings to be $\lambda_s = 0.6, 0.4$ with Q in the region 600 GeV $< Q < 0.9\Lambda_u$.

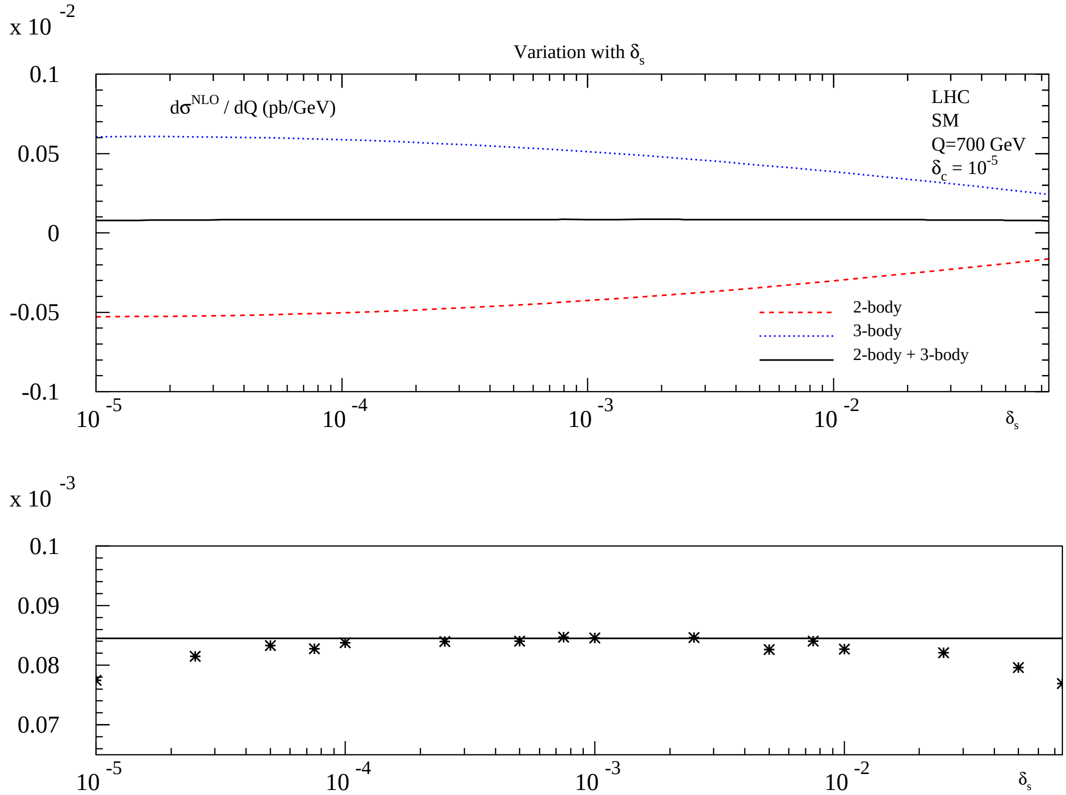


Figure 5.6: ADD: Stability of the order $\alpha_s$ contribution to the SM cross section against the variation of the slicing parameter $\delta_s$ (top), with $\delta_c = 10^{-5}$ fixed, in the invariant mass distribution of the di-photon. Below is shown the variation of the sum of 2-body and 3-body contributions over the range of $\delta_s$ considered and contrasted against the one at $\delta_s = 10^{-3}$.

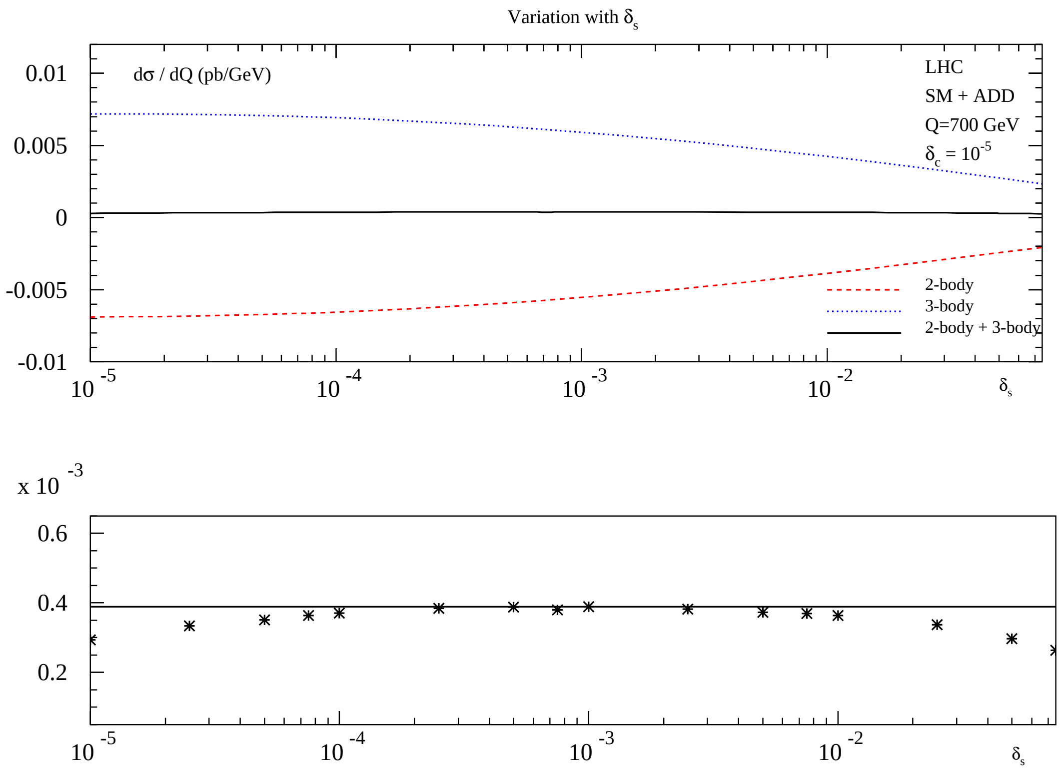


Figure 5.7: ADD: Stability of the order $\alpha_s$ contribution to the SM+ADD cross section against the variation of the slicing parameter $\delta_s$ (top), with $\delta_c = 10^{-5}$ fixed, in the invariant mass distribution of the di-photon with $M_S = 2$ TeV and $d = 3$. Below is shown the variation of the sum of 2-body and 3-body contributions over the range of $\delta_s$ considered and contrasted against the one at $\delta_s = 10^{-3}$.

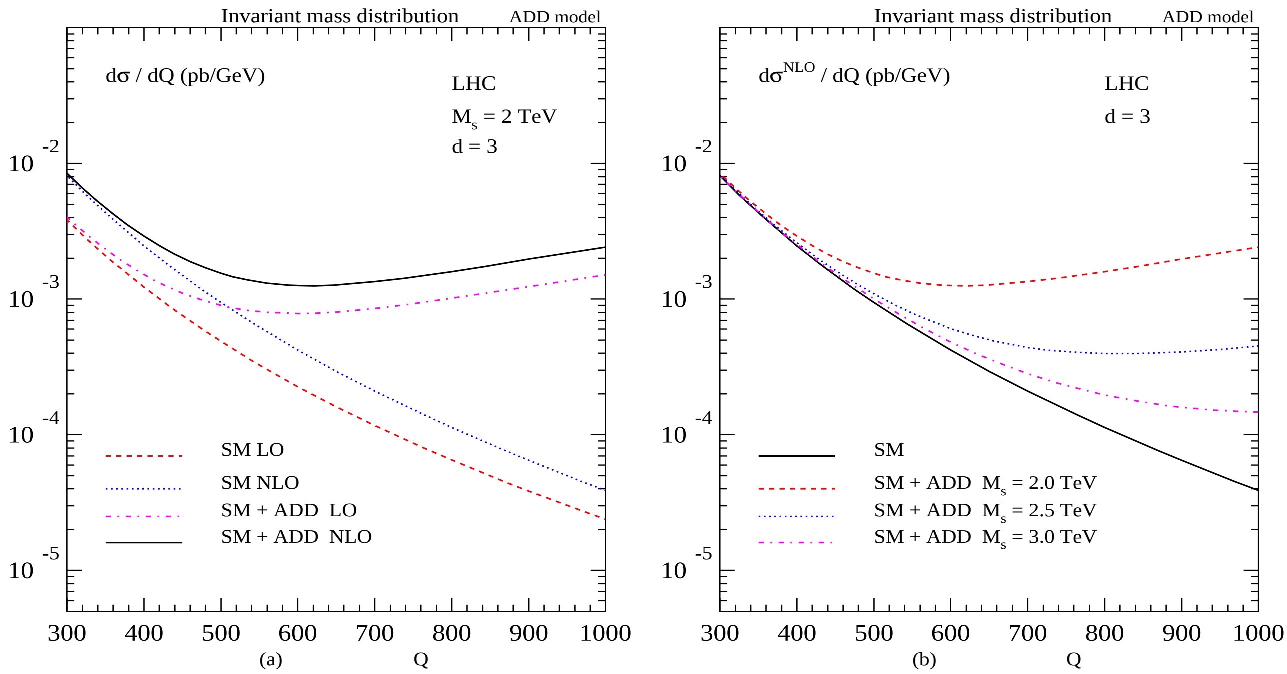


Figure 5.8: ADD: Invariant mass distribution of the di-photon production in the ADD model at the LHC. Both SM and the signal (SM+ADD) are presented at LO and NLO for $M_S = 2$ TeV and $d = 3$ in the left panel. Further the dependence of the cross sections on the scale $M_S$ in right panel has been shown to NLO in QCD.

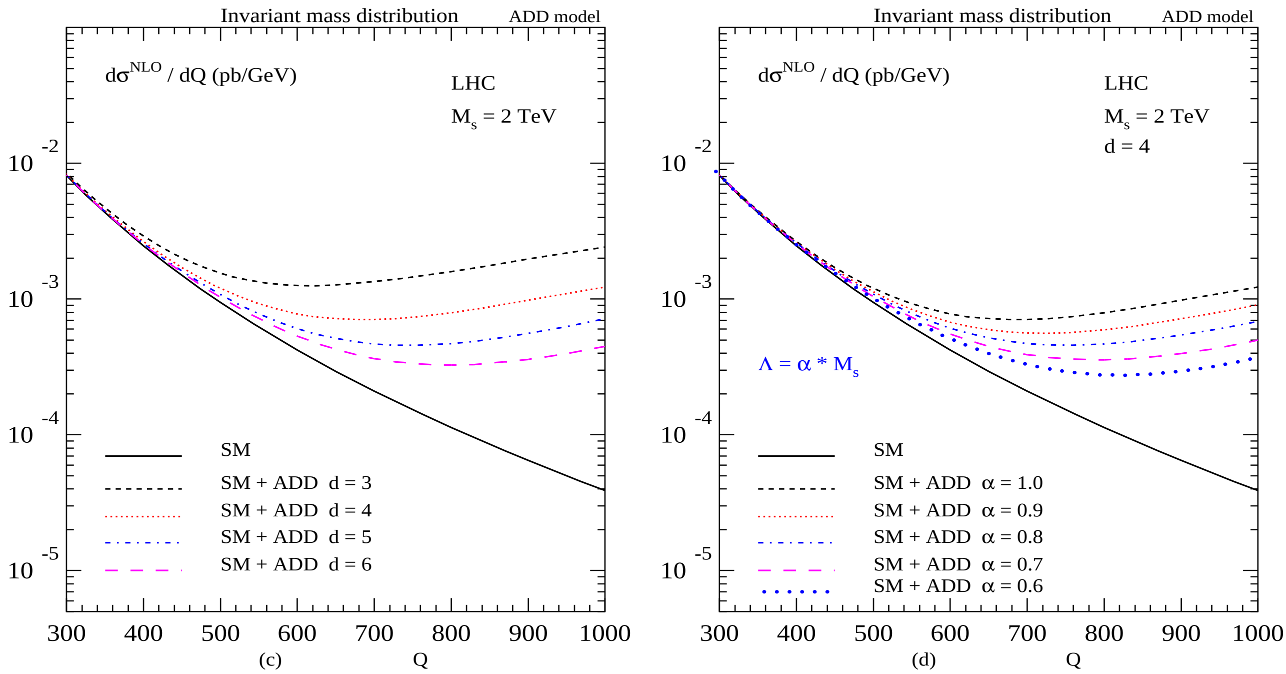


Figure 5.9: ADD: Invariant mass distribution of the di-photon production in the ADD model at the LHC. The dependence of the cross sections on the number $d$ of extra dimensions is presented in the left panel and on the cut-off scale $\Lambda$ for the summation over virtual KK modes in the right panel to NLO in QCD.

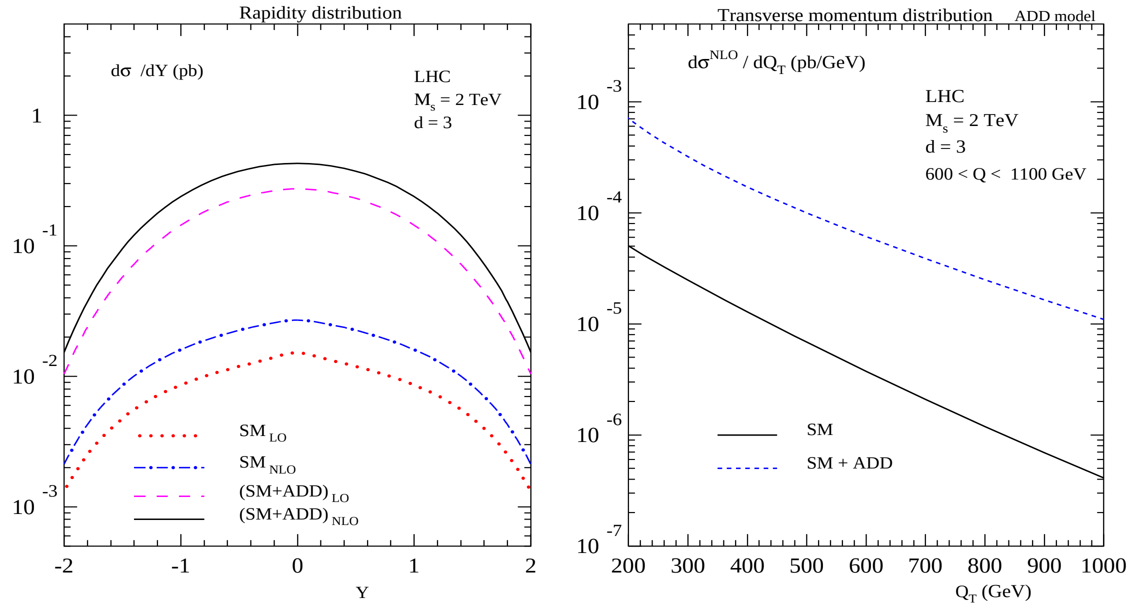


Figure 5.10: ADD: Transverse momentum rapidity $d\sigma/dY$ (left) and $d\sigma/dQ_T$ (right) distributions of the di-photon production are presented in the ADD model with $M_S = 2$ TeV, $d = 3$ and by integrating over $Q$ in the range $600 \ < Q \ < 1100$ GeV.

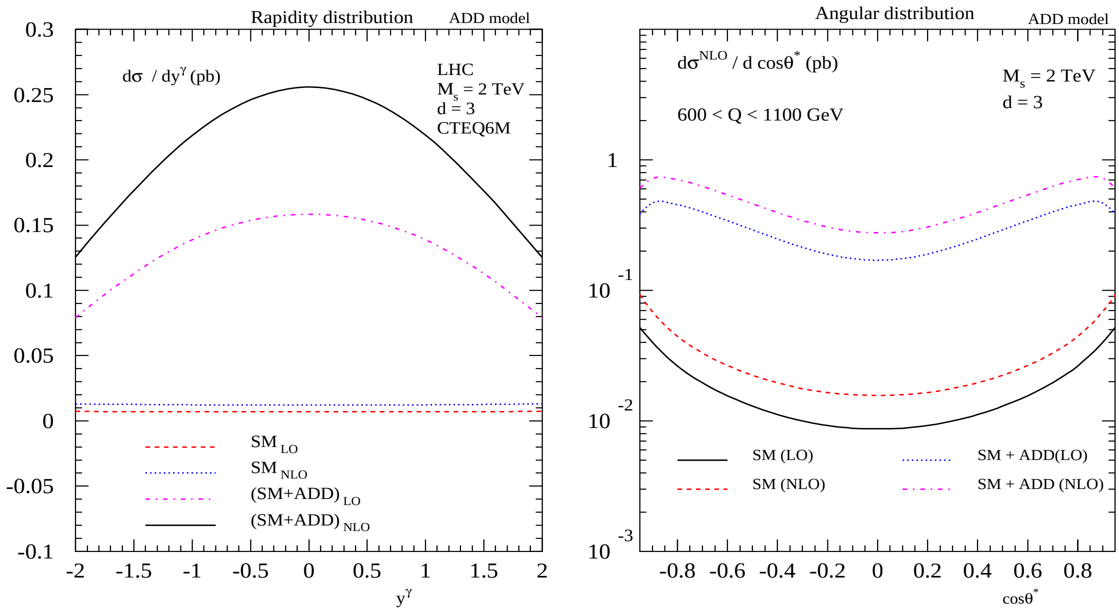


Figure 5.11: ADD: Rapidity $d\sigma/dy^\gamma$ (left) and angular distributions $d\sigma/d\ \cos\theta^*$ (right) of the photons are presented in the ADD model with $M_S = 2$ and $d = 3$. Both of these distributions are obtained by integrating over the invariant mass of the di-photon in the range 600 $< Q$ $<$ 1100 GeV.

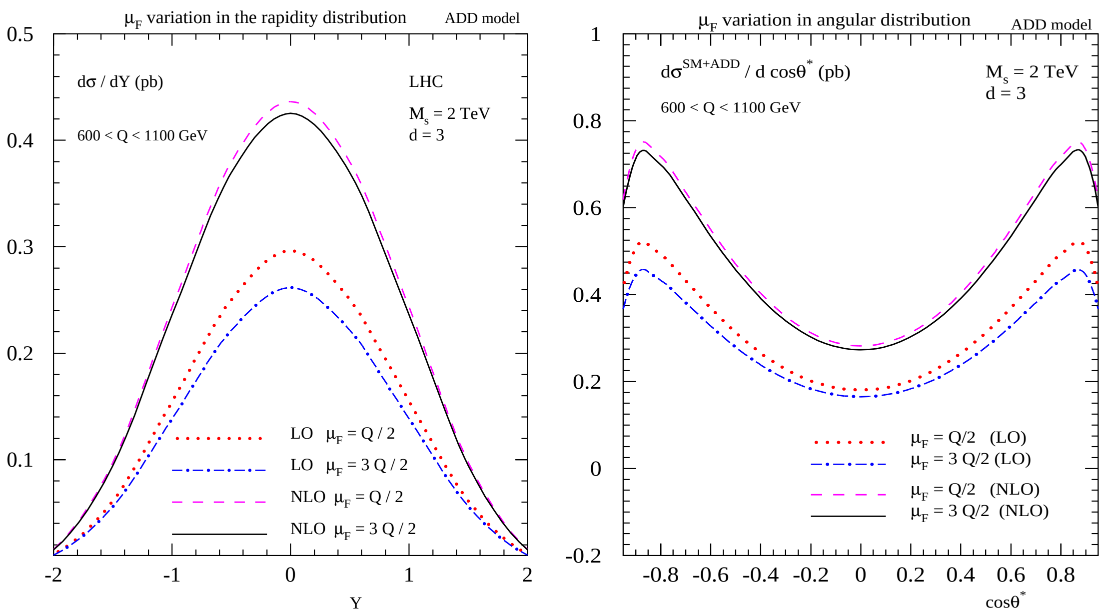


Figure 5.12: ADD: Factorization scale dependency of the LO and NLO cross sections in the ADD model with $M_S = 2$ TeV and $d = 3$ for a scale variation of $Q/2 < \mu_F < 3Q/2$. For both the rapidity (left) and angular (right) distributions of the di-photon production, we have integrated over the invariant mass in the range $600 \ < Q \ < 1100$ GeV.

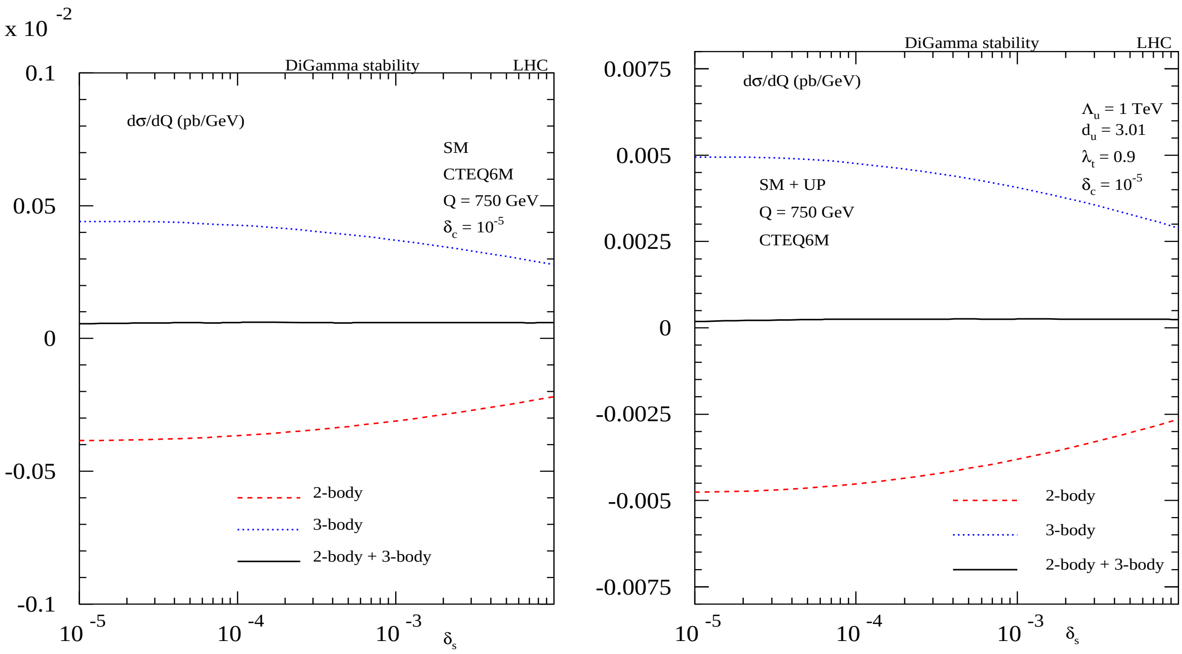


Figure 5.13: Spin-2 unparticles: Plots showing stability of $d\sigma/dQ$ for the SM (left panel) and the SM+ UP (right panel) against $\delta_s$ variation with the choice of $\delta_c = 10^{-5}$.

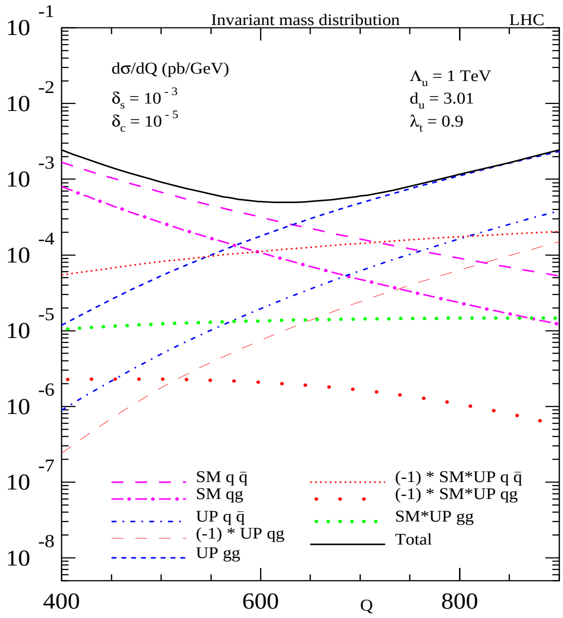


Figure 5.14: Spin-2 unparticles: Subprocess contributions in the SM and unparticle model in the invariant mass distribution at NLO for $400 < Q < 900$ GeV.

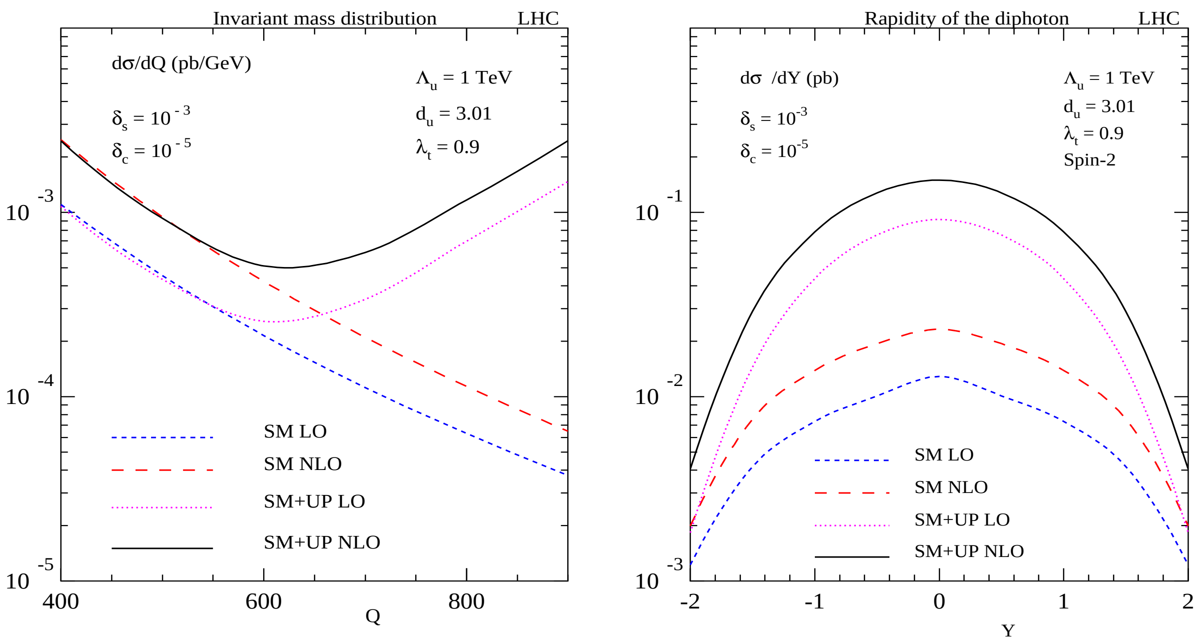


Figure 5.15: Spin-2 unparticles: Plots showing invariant mass (left panel) and rapidity (right panel) distributions of the diphoton system with $d_u = 3.01$, $\Lambda_u = 1$ TeV and $\lambda_t = 0.9$. For rapidity distribution $Q$ is integrated in the range 600 GeV $< Q < 0.9\Lambda_u$.

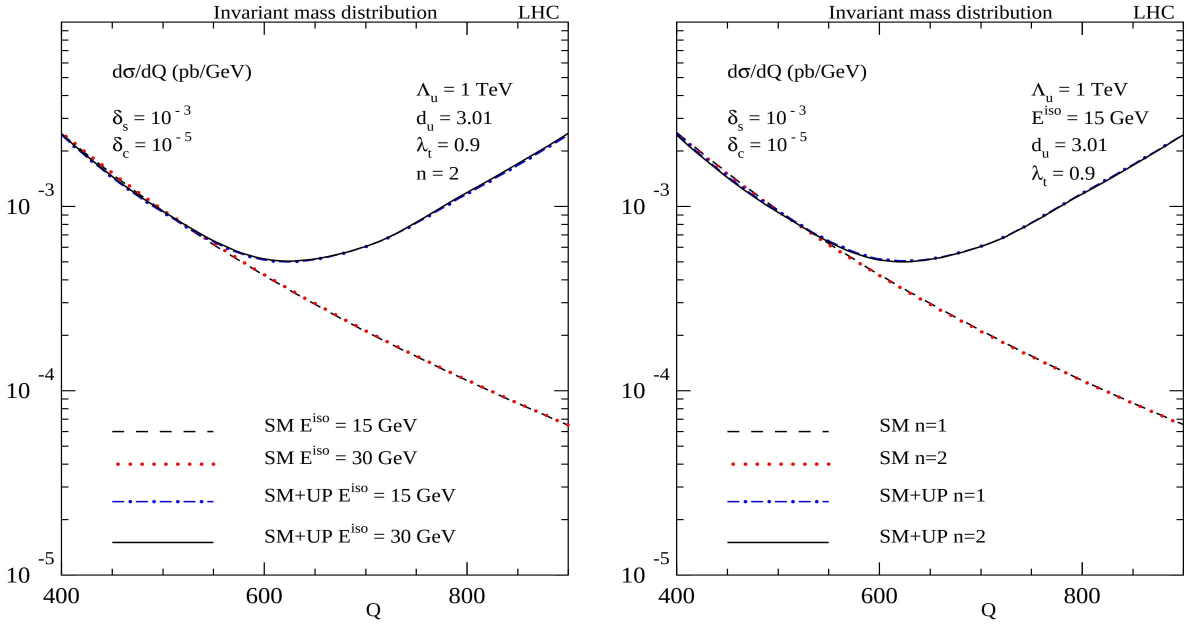


Figure 5.16: Spin-2 unparticles: Dependence on isolation parameters $E_T^{iso}$ (left panel) and $n$ (right panel) is shown in invariant mass distribution for the range $400 < Q < 900$ GeV.

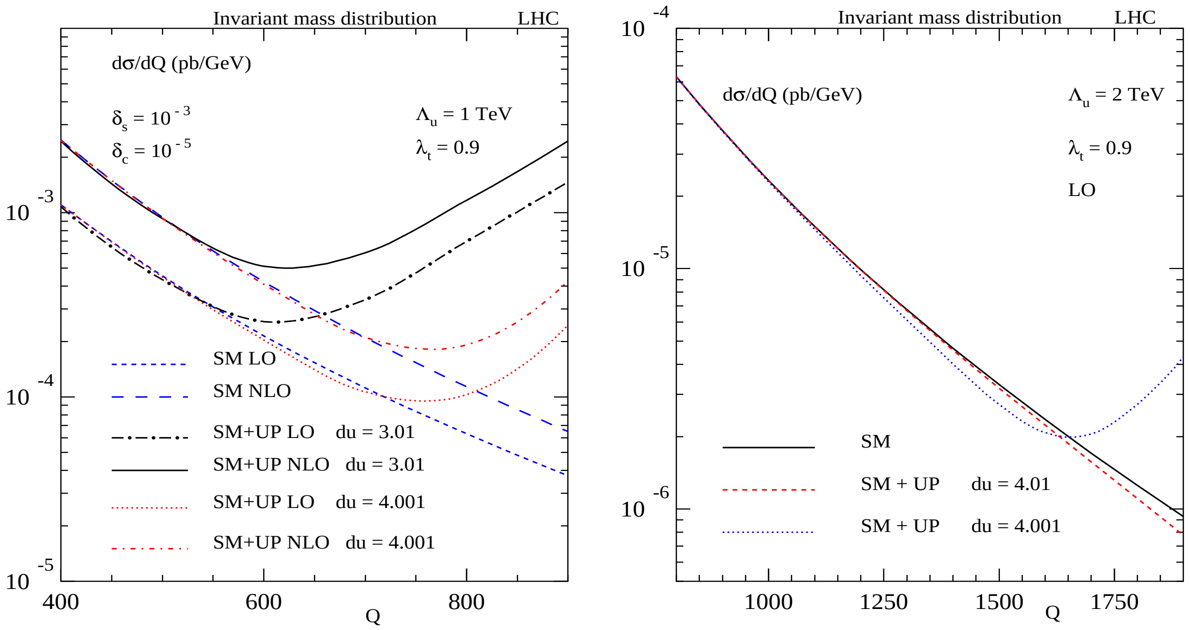


Figure 5.17: Spin-2 unparticles: Invariant mass distribution of the diphoton system (left panel) for $d_u > 4$ (conformal invariance) is contrasted with the $3 < d_u < 4$ (scale invariance). To LO in QCD and for $\Lambda_u = 2$ TeV (right panel), we have plotted the invariant mass distribution of the diphoton system for $d_u > 4$.

# Chapter 6

# Summary and conclusions

In this section we summarize the thesis and conclude. In this thesis we have considered production of isolated direct photon pairs in hadronic collisions at the LHC at $14TeV$. This process is one of the important discovery channels at the LHC. Here we carried out the study at next-to-leading order accuracy in strong coupling in the extra dimension model of ADD and the unparticle model. The necessity of going beyond leading order is two fold. A NLO computation includes higher order piece which is missing in a LO computation and thus makes the predictions more accurate. Secondly it makes the observable less sensitive to the choice of factorization scale $\mu_F$ and the renormalization scale $\mu_R$ (if LO starts at order $\alpha_s$). As we have seen in the previous chapters, LO predictions are very sensitive to the choice of factorization scale. This scale enters at LO through parton distribution functions and is arbitrary to a large extent. The sensitivity to $\mu_F$ is reduced at NLO as the (reduced) hard partonic crosssection, now, also depends on the $\mu_F$ and partially cancels $\mu_F$ dependence of the observable coming from parton distribution functions.

The task involved two components of calculation. Analytical calculation of matrix elements was carried out using FORM. The numerical computations to obtain various kinematical distributions were implemented using FORTRAN 77. The requirement of experimental cuts of the final state particles and necessity of obtaining many kinematical distributions give the Monte Carlo methods an edge over completely analytical methods. Using Monte Carlo methods the programs can be tailored easily to impose various kinematical cuts and obtain many kinematical distributions simultaneously. We developed our Monte Carlo code using integrator VEGAS, based on the two cutoff phase space slicing method. In this method two small dimensionless parameters $\delta_s$ and $\delta_c$ are introduced to divide the phase space into regions which contain soft and collinear singularities. These singularities appear as poles in $\epsilon$ in dimensional regularization and are canceled with virtual contributions or mass factorized. The remaining finite pieces are integrated using Monte Carlo.

Various checks on the code were carried out to ensure that the slicing method has been implemented correctly. The first is to check that the observables do not depend on the arbitrary slicing parameters $\delta_s$ and $\delta_c$ which appear at the intermediate stages of the computation. We found that the sum of 2-body and 3-body (explained in previous chapters) is fairly independent of the slicing parameters over a wide range.

We obtained many kinematical distributions at NLO accuracy both in the ADD model and spin-2 unparticle model such as invariant mass ($Q$), transverse momentum $Q_T$, rapidity of photon pair ($Y$), rapidity of individual photons ($y^\gamma$), and ($\cos\theta^*$) distributions were obtained. In order to isolate the direct photons we used the isolation cuts used by ATLAS and CMS in their Higgs search studies. In additions, to suppress the contributions coming from photons arising from fragmentation of partons, we used the smooth cone isolation criterion advocated by Frixione.

Photon pair production with scalar unparticles was presented to LO accuracy for the choice $\Lambda_u = 1TeV$. the scaling dimesion $d_u$ was chosen to be $d_u = 1.01$ as a default choice for presenting many kinematical distributions, however effects of variation of $d_u$ and the scalar coupling constant $\lambda_s$ were also presented. We observed that the scalar unparticle effects could be observed easily over a wide region of parameter space.

In the ADD model we used $M_S = 2TeV$ and number of extra spatial dimensions $d = 3$ as the default choices and presented various distributions. We observed significant enhancements in the predictions as we move from LO to NLO. This was observed in all the distributions presented here. We also studied the effects of varying $M_S$ and $d$ on the signal. As expected we found decrease in signal with increase in the values of these parameters. For angular, $Q_T$ and rapidity distributions, integrations over a Q range were carried out in general to enhance the signals. Lastly we could show that the sensitivity to the factorization scale $\mu_F$ was significantly reduced and the new results are more precise. This makes these new results more suitable for further study and useful to constrain various parameters of these two models.

For spin-2 unparticles we used the following choices for the parameters: $\Lambda_u = 1TeV$ and $d_u = 3.01$ and the coupling constant to be close to 1. Again significant enhancement over SM predictions were obtained. Also increase in signals in going from LO to NLO was observed. We also varied the isolation parameters which appear in smooth cone isolation criterion to see the effect of the variation. We did not find any significant variations.

We observe here that our Monte Carlo base FORTRAN code which uses the two cutoff phase space slicing method is capable of easily accommodating new processes in various models. Many distributions can be obtained easily from this code for studying SM and new physics scenarios.

# Chapter 7

# Appendix

## 7.1 Feynman rules and diagrams

In Fig. 7.1 we give Feynman rules for spin-0 unparticle, the corresponding vertices for spin-2 KK coupling to SM fields are given in Fig. 7.2. The spin-2 unparticle vertices are same as that of spin-2 KK vertices (as the coupling in both the cases is through the SM energy momentum tensor ) except for small modification of the coupling constant.

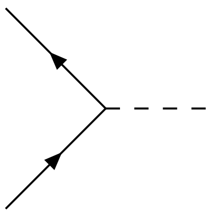

$$i \frac{\lambda_s}{\Lambda_u^{d_u - 1}}$$

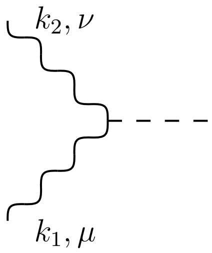


$$-i \frac{\lambda_s}{\Lambda_u^{d_u}} (-p_1 \cdot p_2 \; g^{\mu\nu} + p_1^{\nu} p_2^{\mu})$$

Figure 7.1: Spin-0 unparticle vertices.

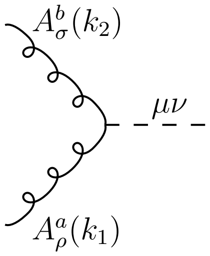


$$-i\kappa/2\delta_{ab}[k_1\cdot k_2 C_{\mu\nu,\rho\sigma}+D_{\mu\nu,\rho\sigma}(k_1,k_2)+\xi^{-1}E_{\mu\nu,\rho\sigma}k_1,k_2]$$

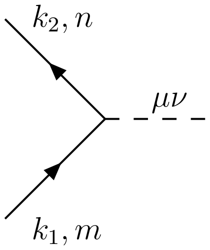


$$-i\kappa/2\delta_{mn}[k_1\cdot k_2 C_{\mu\nu,\rho\sigma}+D_{\mu\nu,\rho\sigma}(k_1,k_2)+\xi^{-1}E_{\mu\nu,\rho\sigma}k_1,k_2]$$

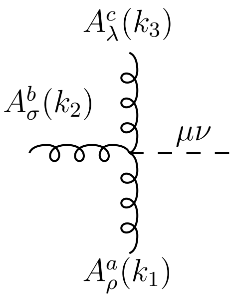


$$g_s\kappa/2f^{abc}[C_{\mu\nu,\rho\sigma}(k_{1\lambda}-k_{2\lambda})+C_{\mu\nu,\rho\lambda}(k_{3\sigma}-k_{1\sigma})$$
$$+C_{\mu\nu,\sigma\lambda}(k_{2\rho}-k_{3\rho}+F_{\mu\nu,\rho\sigma\lambda}(k_1,k_2,k_3))]$$

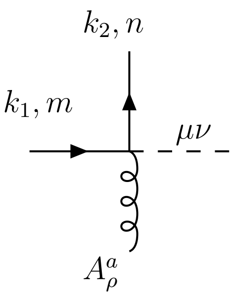


$$ig_s\kappa/4T^a_{nm}(C_{\mu\nu,\rho\sigma}-\eta_{\mu\nu}\eta_{\rho\sigma})\gamma^\sigma$$

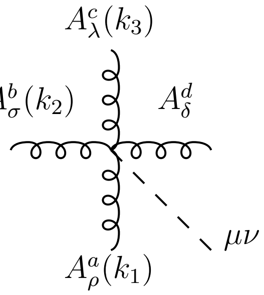


$$-ig_s^2\kappa/2(f^{eac}f^{ebd}G_{\mu\nu,\rho\sigma\lambda\delta} + f^{eab}f^{ecd}G_{\mu\nu,\rho\lambda\sigma\delta}$$
$$+f^{ead}f^{ebc}G_{\mu\nu,\rho\sigma\delta\lambda})$$

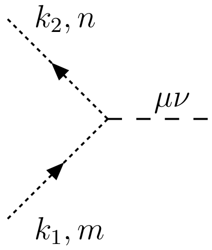


$$-i\kappa/2\delta_{mn}C_{\mu\nu,\rho\sigma}k_1^\rho k_2^\sigma$$

Figure 7.2: Coupling of gravity (spin-2 unparticles) to SM fields. The functions $C_{\mu\nu,\rho\sigma}$, $D_{\mu\nu,\rho\sigma}(k_1, k_2)$, $E_{\mu\nu,\rho\sigma}(k_1, k_2)$, $F_{\mu\nu,\rho\sigma\lambda}(k_1, k_2, k_3)$, $G_{\mu\nu,\rho\sigma\lambda\delta}$ which appear in the Feynman rules are defined in the section 2.1 in the text.

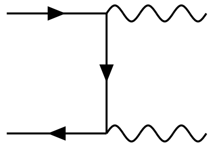

Figure 7.3: Leading order diagram in SM. The diagram with the momenta of final state photons interchanged (which is not shown here) also contributes

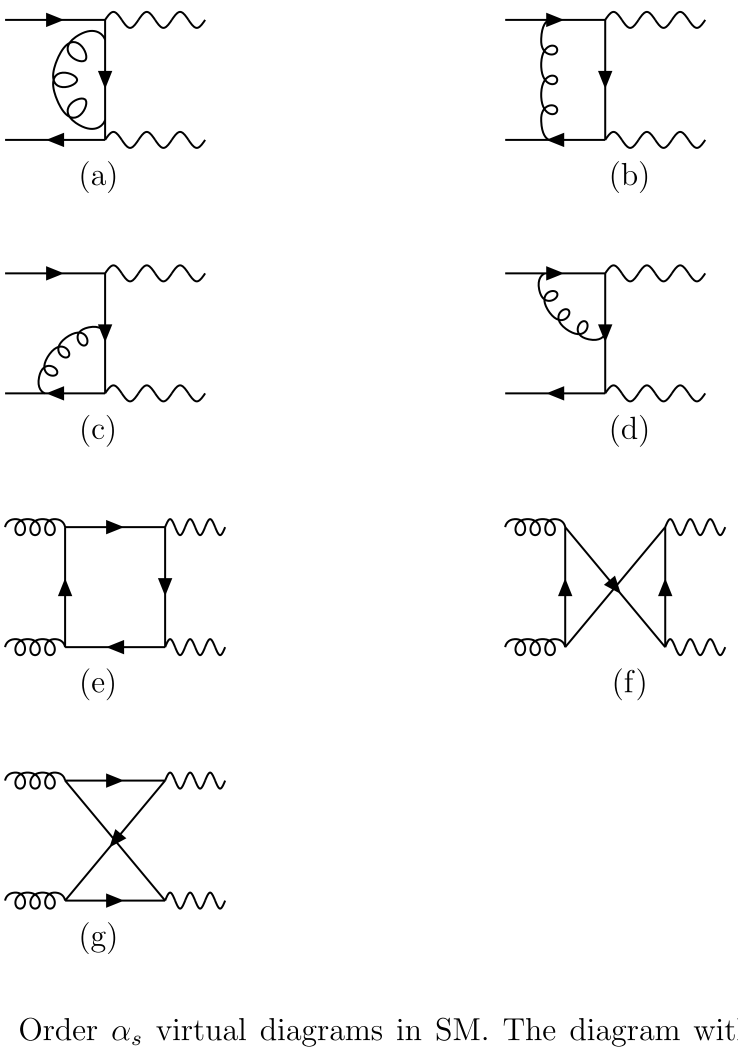


Figure 7.4: Order $\alpha_s$ virtual diagrams in SM. The diagram with the momenta of final state photons interchanged (which is not shown here) also contribute.

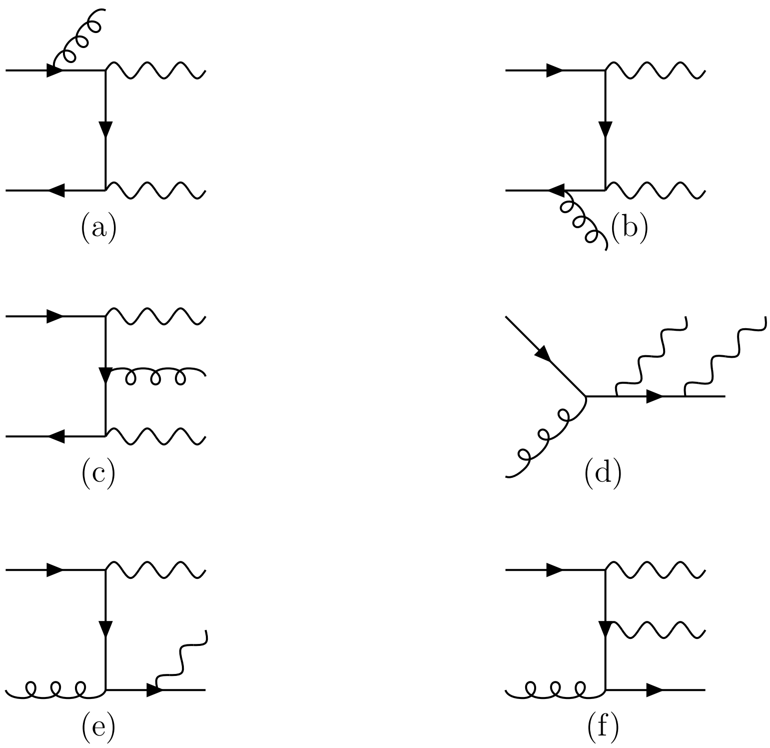


Figure 7.5: Order $\alpha_s$ real emission Feynman diagrams in SM. The diagram with the momenta of final state photons interchanged (which are not shown here) also contribute.


Figure 7.6: LO gravity (spin-2 unparticle) mediated diagrams.

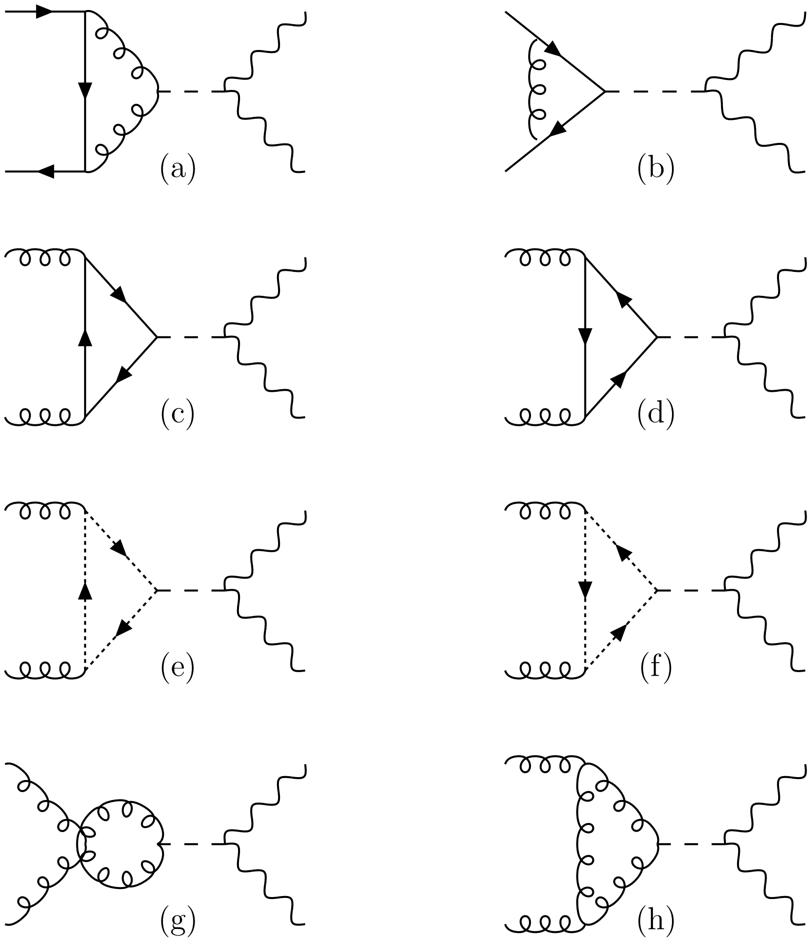


Figure 7.7: Order $\alpha_s$ gravity (spin-2 unparticle) mediated virtual correction Feynman diagrams.

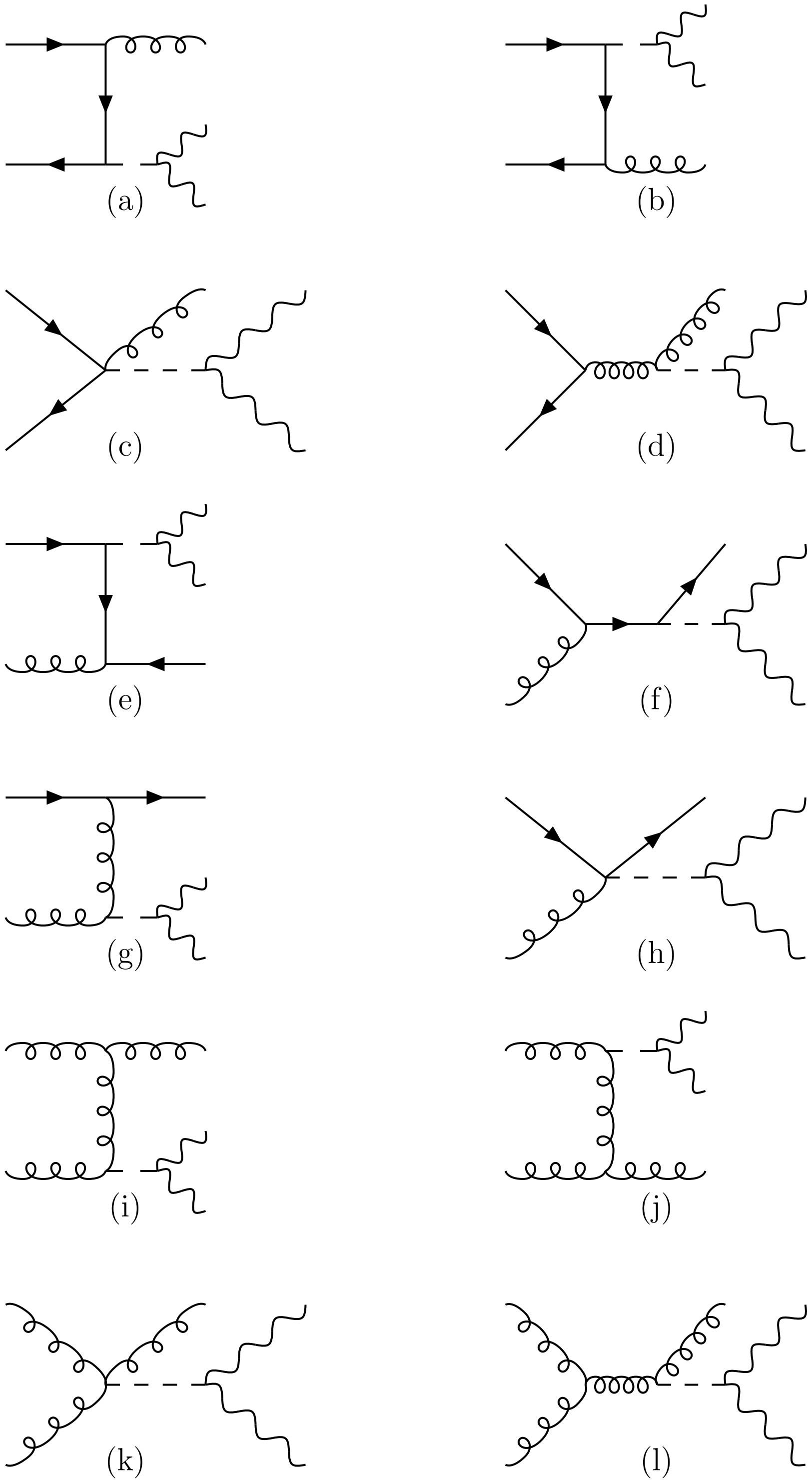


Figure 7.8: Gravity (spin-2 unparticle) mediated real emission diagrams which contribute at NLO.

## 7.2 Area of a unit sphere in $n$ dimensions

Let us label the Cartesian coordinates as $x_1, x_2, \ldots, x_n$. A sphere of radius r is defined by the equation ${x_1}^2 + {x_2}^2 + \ldots + {x_n}^2 = r^2$, introducing spherical coordinates we can write a point on the sphere in terms of its radius r and the $n-1$ angles

$$\begin{aligned}
x_n &= r\sin\theta_1 \sin\theta_2 \ldots \sin\theta_{n-2}\sin\theta_{n-1} && (7.1)\\
x_{n-1} &= r\sin\theta_1 \sin\theta_2 \ldots \sin\theta_{n-2}\cos\theta_{n-1} && (7.2)\\
x_{n-2} &= r\sin\theta_1 \sin\theta_2 \ldots \cos\theta_{n-2} && (7.3)\\
\vdots &= \qquad \vdots && (7.4)\\
x_3 &= r\sin\theta_1 \sin\theta_2 \cos\theta_3 && (7.5)\\
x_2 &= r\sin\theta_1 \cos\theta_2 && (7.6)\\
x_1 &= r\cos\theta_1 && (7.7)
\end{aligned}$$

We have, thus, for the volume element

$$d^n x = dx_1 dx_2 \ldots dx_n = J dr d\theta_1 d\theta_2 \ldots d\theta_{n-1} \tag{7.8}$$

Jacobian $J$ is given by determinant of matrix $\mathcal{J}_{ij} = \partial x_i / \partial\theta_j$, where $\theta_n = r$.

$$\begin{aligned}
\mathcal{J}_{ii} &= r\sin\theta_1 \ldots \sin\theta_{i-1}(-\sin\theta_i) && i < n && (7.9)\\
\mathcal{J}_{ij} &= 0 && i < j < n && (7.10)\\
\mathcal{J}_{in} &= \frac{x_i}{r} && && (7.11)
\end{aligned}$$

$$J = \begin{vmatrix}
\mathcal{J}_{11} & 0 & 0 & \ldots & 0 & 0 & \mathcal{J}_{1n}\\
\bullet & \mathcal{J}_{22} & 0 & \ldots & 0 & 0 & \mathcal{J}_{2n}\\
\bullet & \bullet & \mathcal{J}_{33} & \ldots & 0 & 0 & \mathcal{J}_{3n}\\
\ldots & \ldots & \ldots & \ldots & \ldots & \ldots & \ldots\\
\ldots & \ldots & \ldots & \ldots & \ldots & \ldots & \ldots\\
\bullet & \bullet & \bullet & \bullet & \bullet & \mathcal{J}_{n-1,n-1} & \mathcal{J}_{n-1,n}\\
\bullet & \bullet & \bullet & \bullet & \bullet & \mathcal{J}_{n-1,n} & \mathcal{J}_{n,n}
\end{vmatrix} \tag{7.12}$$

We have denoted the entries which do not bother us by $\bullet$. To simplify the structure let us do elementary operations on the rows. Multiply last row with $-\mathcal{J}_{in}/\mathcal{J}_{nn}$ and add to the $i^{th}$, this will annihilate the last entry in $i^{th}$ row. $\mathcal{J}_{ii}$ gets modified to

$$\begin{aligned}
\mathcal{J}_{ii} \to \hat{\mathcal{J}}_{ii} &= \mathcal{J}_{ni}\frac{-\mathcal{J}_{in}}{\mathcal{J}_{nn}} + \mathcal{J}_{ii}\\
&= -r\sin\theta_1 \ldots \sin\theta_{i-1}\frac{1}{\sin\theta_i}
\end{aligned}$$

Now we have cast the determinant in a triangular form and it can be easily evaluated as a product of diagonal entries,

$$J = \prod_{i=1}^{n-1} \hat{\mathcal{J}}_{ii} \tag{7.13}$$

$$J = r^{n-1} \sin^{n-2}\theta_1 \sin^{n-3}\theta_2 \ldots \sin^2\theta_{n-3} \sin\theta_{n-2}. \tag{7.14}$$

Area of a sphere of radius $r$ is thus

$$\int r^{n-1} \sin^{n-2}\theta_1 \sin^{n-3}\theta_2 \ldots \sin^2\theta_{n-3} \sin\theta_{n-2} d\theta_1 \ldots d\theta_{n-1}$$

To determine the integration limits, let us put $n = 3$ to get to familiar 3- dimensions. This identifies $\theta_1$ with the polar angle $\theta$ which ranges from 0 to $\pi$, and $\theta_{n-1}$ with the azimuthal angle, and this ranges between 0 and $2\pi$.

## 7.3 Dilogarithm and its properties

Here we very briefly discuss the dilog function $Li_2(z)$ which is defined as [87]

$$Li_2(z) = -\int_0^z dt \frac{\log(1-t)}{t} \tag{7.15}$$

and it has a series expansion as

$$Li_2(z) = \sum_{n=1}^{\infty} \frac{z^n}{n^2} \quad |z| \leq 1. \tag{7.16}$$

$Li_2(z)$ has a brach cut on the +ive real axis with branch point $z = 1$.

$$\text{Duplication} \tag{7.17}$$

$$Li_2(z) + Li_2(-z) = \frac{1}{2} Li_2(z^2) \tag{7.18}$$

$$\text{Inversion} \tag{7.19}$$

$$Li_2(-z) + Li_2\left(-\frac{1}{z}\right) = 2Li_2(-1) - \frac{1}{2}\log^2(z) \tag{7.20}$$

$$Li_2(z) + Li_2(1-z) = Li_2(1) - \log(z)\log(1-z) \tag{7.21}$$

$$Li_2(z) + Li_2\left[\frac{-z}{1-z}\right] = -\frac{1}{2}\log^2(1-z) \tag{7.22}$$

Below we give some useful identities after Abel.

$$\begin{aligned} Li_2\left[\frac{x}{1-x}\frac{y}{1-y}\right] &= Li_2\left[\frac{x}{1-y}\right] + Li_2\left[\frac{y}{1-x}\right] \\ &\quad -Li_2(x) - Li_2(y) - \log(1-x)\log(1-y) \end{aligned} \tag{7.23}$$

$$\begin{aligned} Li_2\left[\frac{x}{1-x}\frac{y}{1-y}\right] &= Li_2\left[\frac{x}{1-y}\right] + Li_2\left[\frac{y}{1-x}\right] + Li_2\left[\frac{-x}{1-x}\right] + Li_2\left[\frac{-y}{1-y}\right] \\ &\quad +\frac{1}{2}\log^2\left(\frac{1-x}{1-y}\right). \end{aligned} \tag{7.24}$$

$$\begin{aligned} Li_2(xy) = Li_2(x) + Li_2(y) &+ Li_2\left[-x\frac{1-y}{1-x}\right] + Li_2\left[-y\frac{1-x}{1-y}\right] \\ &+\frac{1}{2}\log^2\left[\frac{1-x}{1-y}\right] \end{aligned} \tag{7.25}$$

We can determine $Li_2(1)$and$Li_2(-1)$ easily using duplication and inversion identities. Substituting $z = -1 + i\epsilon$ we obtain

$$Li_2(1) = -2Li_2(-1) \tag{7.26}$$

and

$$2Li_2(1) = 2Li_2(-1) - \frac{1}{2}\log^2(-1+i\epsilon) \tag{7.27}$$

These two equations give

$$\begin{aligned} Li_2(1) &= \frac{\pi^2}{6}, \\ Li_2(-1) &= -\frac{\pi^2}{12} = -\frac{1}{2}\zeta(2) \end{aligned} \tag{7.28}$$

## 7.4 Gamma function $\Gamma(x)$

Expansion of $\Gamma(x)$ near its poles is

$$\Gamma(\epsilon) = \frac{1}{\epsilon} - \gamma_E + \mathcal{O}(\epsilon) \tag{7.29}$$

Another useful result is

$$\Gamma(1+\epsilon) = e^{-\gamma_E\epsilon}\exp\left(\sum_2^\infty \frac{(-1)^k\zeta(k)\epsilon^k}{k}\right), \qquad |\epsilon| < 1 \tag{7.30}$$

where Euler's gamma has a value

$$\gamma_E = 0.5772. \tag{7.31}$$

## 7.5 Casimir invariants of SU(N) algebra

$SU(N)$ algebra is generated by $N \times N$ traceless Hermitian matrices. There are $N^2 - 1$ such independent matrices. The operator

$$T^2 = \sum_{i=1}^{N^2-1} T^i T^i \tag{7.32}$$

is an invariant of the algebra as it commutes with all other generators. Thus it is proportional to the identity matrix. Let us denote by $C_F$ and $C_A$ the values it takes in fundamental $(F)$ and adjoint $(A)$ representations respectively:

$$\sum_{i=1}^{N^2-1} T_r^i T_r^i = C_r \cdot \mathbf{1}, \tag{7.33}$$

where $r = F, A$. The Casimir invariants $C_F$ and $C_A$ are given by

$$C_F = \frac{N^2-1}{2N}, \qquad C_A = N. \tag{7.34}$$

Another useful quantity which appears frequently in NLO QCD calculations is $T_F$. It appear in the following relation:

$$\mathrm{Tr}(T_F^i T_F^j) = T_F \delta^{ij}, \tag{7.35}$$

and

$$T_F = \frac{1}{2}. \tag{7.36}$$

## 7.6 Integrals

Below we give the scalar integrals which appear in the calculation of loop integrals. Results are given in $4+\epsilon$ dimensions. The
1. The two point integral $B_0(p)$

$$\int \frac{d^n l}{(2\pi)^n} \frac{1}{l^2 \left(l+p\right)^2} = -i \left(-p^2\right)^{\frac{\epsilon}{2}} \frac{1}{(4\pi)^{\frac{\epsilon}{2}+2}} \frac{2}{\epsilon} \frac{\Gamma\left(1-\frac{\epsilon}{2}\right)\Gamma^2\left(1+\frac{\epsilon}{2}\right)}{\left(1+\epsilon\right)\Gamma\left(1+\epsilon\right)} \tag{7.37}$$


Figure 7.9: Scalar diagrams. All the momenta are going into the diagrams

2. The three point integral $C_0(p,k)$; $p^2 = k^2 = 0,\ q^2 \neq 0$ (see Fig. 7.9(b)).

$$\int \frac{d^n l}{(2\pi)^n} \frac{1}{l^2 (l+p)^2 (l+p+k)^2} = -i \left(-(p+k)^2\right)^{-1+\frac{\epsilon}{2}} \frac{1}{(4\pi)^{\frac{\epsilon}{2}+2}} \frac{4}{\epsilon^2} \frac{\Gamma\left(1-\frac{\epsilon}{2}\right)\Gamma^2\left(1+\frac{\epsilon}{2}\right)}{\Gamma(1+\epsilon)} \tag{7.38}$$

3. The four point integral $D_0(p,k,q)$; $p^2 = k^2 = q^2 = r^2 = 0$ (see Fig. 7.9(a)).

$$\begin{aligned}
\int \frac{d^n l}{(2\pi)^n} \frac{1}{l^2 (l+p)^2 (l+p+k)^2 (l+p+k+q)^2} &= \frac{i}{(4\pi)^{\frac{\epsilon}{2}+2}} \frac{8}{\epsilon^2} \frac{\Gamma\left(1-\frac{\epsilon}{2}\right)\Gamma^2\left(1+\frac{\epsilon}{2}\right)}{\Gamma(1+\epsilon)} \\
&\times \frac{1}{(k+q)^2 (p+k)^2} \Bigg[ \left(-(k+q)^2\right)^{\frac{\epsilon}{2}} \left\{ 1 + \frac{\epsilon}{2} \ln\left(-\frac{(p+k)^2}{(k+q)^2}\right) + \frac{\epsilon^2}{4} Li_2\left(-\frac{(p+q)^2}{(k+q)^2}\right) \right. \\
&\left. + \frac{\epsilon^2}{8} \ln^2\left(-\frac{(p+k)^2}{(k+q)^2}\right) \right\} + \left(-(p+k)^2\right)^{\frac{\epsilon}{2}} \left\{ 1 - \frac{\epsilon}{2} \ln\left(-\frac{(p+k)^2}{(k+q)^2}\right) \right. \\
&\left. - \frac{\epsilon^2}{4} Li_2\left(-\frac{(p+q)^2}{(k+q)^2}\right) \right\} \Bigg]
\end{aligned} \tag{7.39}$$

# Bibliography


[1] P.W. Higgs, *Broken Symmetries, Massless Particles And Gauge Fields*, Phys. Lett. **12**, 132 (1964), *Spontaneous Symmetry Breakdown Without Massless Bosons*, Phys. Rev. **145**, 1156 (1966).

[2] F. Englert and R. Brout, *Broken Symmetry And The Mass Of Gauge Vector Mesons*, Phys. Rev. Lett. **13**, 321 (1964).

[3] G.S. Guralnik, C.R. Hagen and T.W. Kibble, *Global Conservation Laws And Massless Particles*, Phys. Rev. Lett. **13**, 585 (1964).

[4] N. Arkani-Hamed, S. Dimopoulos and G. R. Dvali, *The hierarchy problem and new dimensions at a millimeter*, Phys. Lett. B **429** (1998) 263 [arXiv:hep-ph/9803315].

[5] I. Antoniadis, N. Arkani-Hamed, S. Dimopoulos and G. R. Dvali, *New dimensions at a millimeter to a Fermi and superstrings at a TeV*, Phys. Lett. B **436** (1998) 257 [arXiv:hep-ph/9804398].

[6] H. Georgi, *Unparticle Physics*, Phys. Rev. Lett. **98** (2007) 221601 [arXiv:hep-ph/0703260].

[7] H. Georgi, *Another Odd Thing About Unparticle Physics*, Phys. Lett. B **650** (2007) 275 [arXiv:0704.2457 [hep-ph]].

[8] K. Cheung, W. Y. Keung and T. C. Yuan, Phys. Rev. Lett. **99** (2007) 051803 [arXiv:0704.2588 [hep-ph]].

[9] J. J. van der Bij and S. Dilcher, *HEIDI and the unparticle*, Phys. Lett. B **655**, 183 (2007) [arXiv:0707.1817 [hep-ph]].

[10] T. Banks and A. Zaks, *On The Phase Structure Of Vector-Like Gauge Theories With Massless Fermions*, Nucl. Phys. B **196** (1982) 189.

[11] G. Degrassi, *Where is the Higgs?* , arXiv:hep-ph/0102137.

[12] J. Erler, *Fundamental parameters from precision tests,* arXiv:hep-ph/0102143.

[13] D. Abbaneo *et al.* [ALEPH, DELPHI, L3 and OPAL Collaborations, LEP Electroweak Working Group, and SLD Heavy Flavor and Electroweak Groups], arXiv:hep-ex/0112021.

[14] J.R. Ellis, M.K. Gaillard and D.V. Nanopoulos, *A Phenomenological Profile Of The Higgs Boson,* Nucl. Phys. B **106**, 292 (1976).

[15] M.A. Shifman, A.I. Vainshtein, M.B. Voloshin and V.I. Zakharov, *Low-Energy Theorems For Higgs Boson Couplings To Photons*, Sov. J. Nucl. Phys. **30**, 711 (1979) [Yad. Fiz. **30**, 1368 (1979)].

[16] R.K. Ellis, I. Hinchliffe, M. Soldate and J.J. van der Bij, *Higgs Decay To Tau+ Tau-: A Possible Signature Of Intermediate Mass Higgs Bosons At The SSC*, Nucl. Phys. B **297**, 221 (1988).

[17] P. Aurenche, A. Douiri, R. Baier, M. Fontannaz and D. Schiff, *Large P(T) Double Photon Production In Hadronic Collisions: Beyond Leading Logarithm QCD Calculation*, Z. Phys. C **29**, 459 (1985).

[18] B. Bailey, J.F. Owens and J. Ohnemus, *An Order alpha-s Monte Carlo calculation of hadronic double photon production*, Phys. Rev. D **46**, 2018 (1992).

[19] B. Bailey and J.F. Owens, *An Order alpha-s two photon background study for the intermediate mass Higgs boson*, Phys. Rev. D **47**, 2735 (1993).

[20] B. Bailey and D. Graudenz, *Impact of QCD corrections on the search for the intermediate mass Higgs boson*. Phys. Rev. D **49**, 1486 (1994) [arXiv:hep-ph/9307368].

[21] C. Balazs, E.L. Berger, S. Mrenna and C.-P. Yuan, *Photon pair production with soft gluon resummation in hadronic interactions*, Phys. Rev. D **57**, 6934 (1998) [arXiv:hep-ph/9712471].

[22] C. Balazs and C.-P. Yuan, *Higgs boson production at hadron colliders with soft gluon effects. I: Backgrounds*, Phys. Rev. D **59**, 114007 (1999) [Erratum-ibid. D **63**, 059902 (1999)] [arXiv:hep-ph/9810319].

[23]

[23] T. Binoth, J.P. Guillet, E. Pilon and M. Werlen, *Beyond leading order effects in photon pair production at the Tevatron*, Phys. Rev. D **63**, 114016 (2001) [arXiv:hep-ph/0012191].

[24] T. Binoth, *Two photon background for Higgs boson searches at the LHC*, arXiv:hep-ph/0005194.

[25] Z. Bern, L. J. Dixon and C. Schmidt, *Isolating a light Higgs boson from the di-photon background at the LHC*, Phys. Rev. D **66** (2002) 074018 [arXiv:hep-ph/0206194].

[26] E. Bonvin *et al.* [WA70 Collaboration], *DOUBLE PROMPT PHOTON PRODUCTION AT HIGH TRANSVERSE MOMENTUM BY pi- ON PROTONS AT 280-GeV/c*, Z. Phys. C **41** (1989) 591.

[27] E. Bonvin *et al.* [WA70 Collaboration], *INTRINSIC TRANSVERSE MOMENTUM IN THE pi- p → gamma gamma X REACTION AT 280-GeV/c*, Phys. Lett. B **236** (1990) 523.

[28] J. Alitti *et al.* [UA2 Collaboration], *A Measurement of single and double prompt photon production at the CERN $\bar{p}p$ collider*, Phys. Lett. B **288** (1992) 386.

[29] F. Abe *et al.* [CDF Collaboration], *Measurement of the cross-section for production of two isolated prompt photons in $\bar{p}p$ collisions at $\sqrt{s} = 1.8$ TeV*, Phys. Rev. Lett. **70** (1993) 2232.

[30] Wei Chen, PhD Thesis (Univ. New-York at Stony Brook), Dec. 1997, unpublished; D0 Collaboration (P. Hanlet for the collaboration), Nucl. Phys. Proc. Suppl. **64** (1998) 78.

[31] K. m. Cheung and G. L. Landsberg, *Drell-Yan and Diphoton production at Hadron Colliders and Low Scale Gravity Model*, Phys. Rev. D **62** (2000) 076003 [arXiv:hep-ph/9909218];

[32] P. Mathews, S. Raychaudhuri and K. Sridhar, *Getting to the top with extra dimensions*, Phys. Lett. B **450** (1999) 343 [arXiv:hep-ph/9811501].

[33] P. Mathews and V. Ravindran *Angular distribution of Drell-Yan process at hadron colliders to NLO-QCD in models of TeV scale gravity*, Nucl. Phys. B **753**, 1 (2006) [arXiv:hep-ph/0507250].

[34] M. C. Kumar, P. Mathews and V. Ravindran, *PDF and scale uncertainties of various DY distributions in ADD and RS models at hadron colliders*, Eur. Phys. J. C **49**, 599 (2007) [arXiv:hep-ph/0604135].

[35] P. Mathews, V. Ravindran, K. Sridhar and W. L. van Neerven, *Next-to-leading order QCD corrections to the Drell-Yan cross section in models of TeV-scale gravity*, Nucl. Phys. B **713**, 333 (2005) [arXiv:hep-ph/0411018].

[36] P. Mathews, V. Ravindran and K. Sridhar, *NLO-QCD corrections to dilepton production in the Randall-Sundrum model*, JHEP **0510**, 031 (2005) [arXiv:hep-ph/0506158].

[37] O. J. P. Eboli, T. Han, M. B. Magro and P. G. Mercadante, *Diphoton signals for large extra dimensions at the Tevatron and CERN LHC*, Phys. Rev. D **61** (2000) 094007 [arXiv:hep-ph/9908358].

[38] D. Atwood, S. Bar-Shalom and A. Soni, Phys. Rev. D **62** (2000) 056008 [arXiv:hep-ph/9911231].

[39] P. Mathews, S. Raychaudhuri and K. Sridhar, *Testing TeV scale quantum gravity using dijet production at the Tevatron*, JHEP **0007** (2000) 008 [arXiv:hep-ph/9904232].

[40] P. Mathews, S. Raychaudhuri and K. Sridhar, *Large extra dimensions and deep-inelastic scattering at HERA*, Phys. Lett. B **455** (1999) 115 [arXiv:hep-ph/9812486].

[41] H. Georgi and S. L. Glashow, *Unity Of All Elementary Particle Forces*, Phys. Rev. Lett. **32** (1974) 438.

[42] L. Randall and R. Sundrum, *A large mass hierarchy from a small extra dimension*, Phys. Rev. Lett. **83** (1999) 3370 [arXiv:hep-ph/9905221].

[43] L. Randall and R. Sundrum, *An alternative to compactification*, Phys. Rev. Lett. **83** (1999) 4690 [arXiv:hep-th/9906064].

[44] C. Csaki, *TASI lectures on extra dimensions and branes*, arXiv:hep-ph/0404096.

[45] D. J. Kapner, T. S. Cook, E. G. Adelberger, J. H. Gundlach, B. R. Heckel, C. D. Hoyle and H. E. Swanson, *Tests of the gravitational inverse-square law below the dark-energy length scale*, Phys. Rev. Lett. **98** (2007) 021101 [arXiv:hep-ph/0611184].

[46] C. Hanhart, J. A. Pons, D. R. Phillips and S. Reddy, *The likelihood of GODs' existence: Improving the SN1987a constraint on the size of large compact dimensions*, Phys. Lett. B **509** (2001) 1 [arXiv:astro-ph/0102063].

[47] V. Krutelyov [CDF Collaboration and D0 Collaboration], *Searches for Large Extra Dimensions at the Tevatron*, arXiv:0807.0645 [hep-ex].

[48] T. Han, J. D. Lykken and R. J. Zhang, *On Kaluza-Klein states from large extra dimensions*, Phys. Rev. D **59** (1999) 105006 [arXiv:hep-ph/9811350].

[49] G. F. Giudice, R. Rattazzi and J. D. Wells, *Quantum gravity and extra dimensions at high-energy colliders*, Nucl. Phys. B **544** (1999) 3 [arXiv:hep-ph/9811291].

[50] R. Basu, D. Choudhury and H. S. Mani, Eur. Phys. J. C **61**, 461 (2009) [arXiv:0803.4110 [hep-ph]].

[51] B. Grinstein, K. A. Intriligator and I. Z. Rothstein, *Comments on Unparticles*, Phys. Lett. B **662** (2008) 367;

[52] D. J. Gross and F. Wilczek, *ULTRAVIOLET BEHAVIOR OF NON-ABELIAN GAUGE THEORIES*, Phys. Rev. Lett. **30** (1973) 1343.

[53] H. D. Politzer, *RELIABLE PERTURBATIVE RESULTS FOR STRONG INTERACTIONS?*, Phys. Rev. Lett. **30** (1973) 1346.

[54] R. P. Feynman, *Very high-energy collisions of hadrons*, Phys. Rev. Lett. **23** (1969) 1415.

[55] J. C. Collins and D. E. Soper, *The Theorems of Perturbative QCD*, Ann. Rev. Nucl. Part. Sci. **37** (1987) 383.

[56] L. N. Lipatov, *The parton model and perturbation theory*, Sov. J. Nucl. Phys. **20** (1975) 94 [Yad. Fiz. **20** (1974) 181].

[57] V. N. Gribov and L. N. Lipatov, *Deep Inelastic E P Scattering In Perturbation Theory*, Sov. J. Nucl. Phys. **15** (1972) 438 [Yad. Fiz. **15** (1972) 781].

[58] G. Altarelli and G. Parisi, *Asymptotic Freedom In Parton Language*, Nucl. Phys. B **126** (1977) 298.

[59] Y. L. Dokshitzer, *Calculation Of The Structure Functions For Deep Inelastic Scattering And E+ E- Annihilation By Perturbation Theory In Quantum Chromodynamics*, Sov. Phys. JETP **46** (1977) 641 [Zh. Eksp. Teor. Fiz. **73** (1977) 1216].

[60] G. Curci, W. Furmanski and R. Petronzio, *Evolution Of Parton Densities Beyond Leading Order: The Nonsinglet Case*, Nucl. Phys. B **175** (1980) 27.

[61] W. Furmanski and R. Petronzio, *Singlet Parton Densities Beyond Leading Order*, Phys. Lett. B **97** (1980) 437.

[62] E. G. Floratos, D. A. Ross and C. T. Sachrajda, *Higher Order Effects In Asymptotically Free Gauge Theories: The Anomalous Dimensions Of Wilson Operators*, Nucl. Phys. B **129** (1977) 66 [Erratum-ibid. B **139** (1978) 545].

[63] A. Gonzalez-Arroyo, C. Lopez and F. J. Yndurain, *Second Order Contributions To The Structure Functions In Deep Inelastic Scattering. 1. Theoretical Calculations*, Nucl. Phys. B **153** (1979) 161.

[64] E. G. Floratos, C. Kounnas and R. Lacaze, *Higher Order QCD Effects In Inclusive Annihilation And Deep Inelastic Scattering*, Nucl. Phys. B **192** (1981) 417.

[65] A. D. Martin, W. J. Stirling, R. S. Thorne and G. Watt, *Uncertainties on alpha_S in global PDF analyses*, arXiv:0905.3531 [hep-ph].

[66] T. Kinoshita, J. Math. Phys. **3** (1962) 650.

[67] T. D. Lee and M. Nauenberg, Phys. Rev. **133** (1964) B1549.

[68] H. Baer, J. Ohnemus and J. F. Owens, *A NEXT-TO-LEADING LOGARITHM CALCULATION OF DIRECT PHOTON PRODUCTION*, Phys. Rev. D **42** (1990) 61.

[69] P. Aurenche, R. Baier and M. Fontannaz, *Prompt Photon Production at Colliders*, Phys. Rev. D **42** (1990) 1440.

[70] E. L. Berger and J. w. Qiu, *Calculations Of Prompt Photon Production In QCD*, Phys. Rev. D **44** (1991) 2002.

[71] L. E. Gordon and W. Vogelsang, *Polarized and unpolarized isolated prompt photon production beyond the leading order*, Phys. Rev. D **50** (1994) 1901.

[72] S. Frixione, *Isolated photons in perturbative QCD*, Phys. Lett. B **429** (1998) 369 [arXiv:hep-ph/9801442].

[73] G. Passarino and M. J. G. Veltman, *One Loop Corrections For E+ E- Annihilation Into Mu+ Mu- In The Weinberg Modeli*, Nucl. Phys. B **160** (1979) 151.

[74] W.J.P. Beenakker, *Electroweak Corrections: Techniques and Applications*, Ph.D. thesis, Leiden University, 1989.

[75] B. Bailey, J. F. Owens and J. Ohnemus, *An Order Alpha-S Monte Carlo Calculation Of Hadronic Double Photon Production*, Phys. Rev. D **46**, 2018 (1992).

[76] F. Bloch and A. Nordsieck, *Note on the Radiation Field of the electron*, Phys. Rev. **52**, 54 (1937).

[77] L.J Bergmann, *Next-to-leading-log QCD calculation of symmetric dihadron production*, Ph.D thesis, Florida State University, 1989.

[78] B. W. Harris and J. F. Owens, Phys. Rev. D **65** (2002) 094032 [arXiv:hep-ph/0102128].

[79] W. Beenakker, H. Kuijf, W. L. van Neerven and J. Smith, *QCD Corrections to Heavy Quark Production in p anti-p Collisions*, Phys. Rev. D **40** (1989) 54.

[80] J. Smith, D. Thomas and W. L. van Neerven, *QCD CORRECTIONS TO THE REACTION p anti-p $\rightarrow$ W gamma X*, Z. Phys. C **44** (1989) 267.

[81] W. L. van Neerven, *Dimensional Regularization Of Mass And Infrared Singularities In Two Loop On-Shell Vertex Functions*, Nucl. Phys. B **268** (1986) 453.

[82] G. Mack, *All Unitary Ray Representations Of The Conformal Group SU(2,2) With Positive Energy*, Commun. Math. Phys. **55** (1977) 1.

[83] G. L. Bayatian *et al.* [CMS Collaboration], *CMS technical design report, volume II: Physics performance*, J. Phys. G **34** (2007) 995.

[84] A. D. Martin, R. G. Roberts, W. J. Stirling and R. S. Thorne, *NNLO global parton analysis*, Phys. Lett. B **531** (2002) 216 [arXiv:hep-ph/0201127].

[85] J. Pumplin *et al.*, *New generation of parton distributions with uncertainties from global QCD analysis*, JHEP **0207** (2002) 012.

[86] ATLAS Collaboration, *ATLAS detector and physics performance. Technical design report.* Vol. 2 (1999), CERN-LHCC-99-15.

[87] L. Lewin, Structural Properties of Polylogarithms, Mathematical Surveys and Monographs, Volume 37; American Mathematical Society.